ISTANBUL TECHNICAL UNIVERSITY ★ GRADUATE SCHOOL OF SCIENCE
ENGINEERING AND TECHNOLOGY

INVESTIGATION OF THE EFFECT OF DIFFERENT MODAL ANALYSIS METHODS ON FLUTTER SPEED CALCULATION

M.Sc. THESIS

Bilgehan ŞEREF

Department of Aeronautical and Astronautical Engineering

Aeronautical and Astronautical Engineering Programme

JULY 2020

ISTANBUL TECHNICAL UNIVERSITY ★ GRADUATE SCHOOL OF SCIENCE
ENGINEERING AND TECHNOLOGY

INVESTIGATION OF THE EFFECT OF DIFFERENT MODAL ANALYSIS METHODS ON FLUTTER SPEED CALCULATION

M.Sc. THESIS

Bilgehan ŞEREF
(511171102)

Department of Aeronautical and Astronautical Engineering

Aeronautical and Astronautical Engineering Programme

Thesis Advisor: Prof. Dr. Vedat Ziya DOĞAN

JULY 2020

İSTANBUL TEKNİK ÜNİVERSİTESİ ★ FEN BİLİMLERİ ENSTİTÜSÜ

FARKLI MODAL ANALİZ YÖNTEMLERİNİN ÇIRPINMA HIZI HESABI ÜZERİNDEKİ ETKİSİNİN İNCELENMESİ

YÜKSEK LİSANS TEZİ

Bilgehan ŞEREF
(511171102)

Uçak ve Uzay Mühendisliği Anabilim Dalı

Uçak ve Uzay Mühendisliği Programı

Tez Danışmanı: Prof. Dr. Vedat Ziya DOĞAN

TEMMUZ 2020

Bilgehan ŞEREF, a M.Sc. student of ITU Graduate School of Science Engineering and Technology 511171102 successfully defended the thesis entitled “INVESTIGATION OF THE EFFECT OF DIFFERENT MODAL ANALYSIS METHODS ON FLUTTER SPEED CALCULATION”, which he/she prepared after fulfilling the requirements specified in the associated legislations, before the jury whose signatures are below.

Thesis Advisor :	**Prof. Dr. Vedat Ziya DOĞAN** Istanbul Technical University	....
Jury Members :	**Prof. Dr. Ata MUĞAN** Istanbul Technical University	....
	Prof. Dr. Erol UZAL Istanbul University	....

Date of Submission : **15 June 2020**
Date of Defense : **16 July 2020**

To my wife,

FOREWORD

I would like to express my deep gratitude to my supervisor Prof. Dr. Vedat Ziya Doğan for the inspiration, confidence and endless support he gave me throughout this study. I will never forget the support that he provided me during my hard times.

I would like to thank my colleague Sedat Özöztürk at Turkish Aerospace for his invaluable experience and endless patience in aeroelasticity.

I am very grateful to my dear wife Anna for her endless trust, support and endless motivation she has provided me. I couldn't have done any of this without her.

July 2020

Bilgehan ŞEREF
Aeronautical Engineer

TABLE OF CONTENTS

Page

ABBREVIATIONS

AR	: Aspect Ratio
TR	: Thickness Ratio
FEM	: Finite Element Method
AGARD	: Advisory Group for Aerospace Research and Development
NACA	: National Advisory Committee for Aeronautics
MSC	: MacNeal-Schwendler Corporation

SYMBOLS

a	: Non-dimensional distance between elastic axis and half chord
b	: Half chord length
c	: Chord length
$\mathbf{b_R}$	: Half chord distance of reference station
h	: Plunge displacement
θ	: Rotation displacement
$\mathbf{X}_\theta$	: Static unbalance
$\mathbf{G_y}$	: Elasticity modulus in spanwise direction
EI	: Bending rigidity
g	: Damping term
$\mathbf{g}_\omega$	: Damping term for bending motion
$\mathbf{g}_\theta$	: Damping term for torsional motion
$\mathbf{E_y}$	: Shear modulus in spanwise direction
GJ	: Torsional rigidity
$\mathbf{I_p}$	: Polar moment of inertia
$\mathbf{k_h}$	: Bending stiffness
$\mathbf{k}_\theta$	: Torsion stiffness
T	: Kinetic energy
P	: Potential energy
$\mathbf{V_C}$	: Velocity of center of gravity of airfoil
$\mathbf{I_C}$	: Mass moment of inertia of airfoil
$\mathbf{I_P}$	: Mass moment of inertia about reference point P
m	: Mass of the airfoil per unit span
M	: Pitching moment about reference point P
L	: Lift
k	: Reduced frequency
μ	: Mass ratio
r	: Radius of gyration
$\mathbf{w_h}$	: Natural bending frequency
$\mathbf{w}_\theta$	: Natural torsion frequency
$\mathbf{M}_\infty$	: Mach number
ρ_∞	: Density of air
$\mathbf{U_F}$	: Flutter speed
$\mathbf{c}_\infty$	: Speed of sound
$\mathbf{k}_\beta$	: Stiffness of the control surface
σ	: Ratio of the natural frequencies
t	: Time
$\mathbf{m}_\beta$	: Mass of the control surface per unit span

$\mathbf{S}_\beta$	: Control surface's static mass moment about the hinge line
$\mathbf{S}_\alpha$	: Airfoil's static mass moment about the elastic axis
H	: Moment about the hinge line
$\mathbf{I}_\beta$	: Mass moment of inertia of the control surface
β	: Control surface motion of airfoil
α	: Pitch motion of airfoil
$\mathbf{X}_\alpha$	: Non-dimensional distance between the elastic axis and the center of mass
$\mathbf{X}_\beta$	: Non-dimensional distance between the hinge line and the center of mass of the control surface
$\mathbf{T}_\mathbf{i}$	: Functions of the distance between the hinge line and the mid-chord and the distance between the mid-chord and the elastic axis
$\mathbf{r}_\beta$	: Radius of gyration about the hinge line
$\mathbf{r}_\alpha$	: Radius of gyration about the reference point P
$\mathbf{k}_\beta$	: Angular stiffness of aileron section
$\mathbf{k}_\alpha$	: Stiffness of typical wing section in pitch direction
$\mathbf{k}_\mathbf{h}$	: Stiffness of typical wing section in plunge direction
E	: Modulus of elasticity
G	: Shear modulus of elasticity
J	: Polar moment of inertia
A	: Cross section area of the structure
w(y,t)	: Vertical movement of three dimensional structure
θ**(y,t)**	: Twist movement of three dimensional structure
$\mathbf{M}_\mathbf{j}$	: Generalized mass equations
Ξ	: Generalized force equations
$\mathbf{F}_{\mathbf{D.V.}}$	: Viscous damping force
$\mathbf{W}_{\mathbf{D.V.}}$	: Work done by viscous damping
$\mathbf{f}_\mathbf{w}$	: Bending mode shape function
$\mathbf{f}_\theta$	: Torsion mode shape function
Z	: Complex unknown value
S(y)	: Shear force
T	: Torque
q	: Shear flow
ν	: Shear flow distribution
$\mathbf{C}^{\theta\theta}$	: Torsion influence function
$\mathbf{C}^{\mathbf{ZZ}}$	: Bending influence function
$\widetilde{\mathbf{q}}^\mathbf{e}$	: Local coordinates
$\mathbf{q}^\mathbf{e}$	: Global coordinates
$\vec{\mathbf{V}}$	: Displacement vector

LIST OF TABLES

Page

LIST OF FIGURES

INVESTIGATION OF THE EFFECT OF DIFFERENT MODAL ANALYSIS METHODS ON FLUTTER SPEED CALCULATION

SUMMARY

The flexibility of the structure is of great importance in the development of modern aircraft today. Aeroelastic effects became more important in the design process by increasing the flexibility in the structure. For this reason, the flutter condition, which is a major aeroelastic problem in modern aviation, has a great importance in the certification process. For this reason, efforts to find the flutter speed are taken into consideration from the very beginning of the design phase. Moreover, the fact that the aircraft has an aeroelasticly stable structure from the very beginning of the design prevents possible problems during the design phases of the design, thus saving time and cost. Considering all these processes, determining the speed of flutter in the concept design phase is of great importance.

In the first stage of the thesis, in order to evaluate the flutter speed in the concept design stage, the k method and the classic flutter method were used to find the flutter speed of the model, which represents the structure in two dimensions. While using these two methods, aerodynamic loads were obtained using the formulas developed by Theodorsen. Analytical method has been developed for two dimensional two degree of freedom and two dimensional three degree of freedom models. These methods to be used in the design phase have saved significant time in calculations using the MATLAB commercial program. These developed analytical methods have been proved to give consistent results by applying on the problems from the literature.

In the next stage of the thesis, MATLAB code was developed to be used to find the flutter speed of three-dimensional structures. In this analytical analysis method, formulas developed by Theodorsen using standard strip theory were used to calculate aerodynamic loads. The natural bending frequency, bending mode shape function, natural torsion frequency and torsion mode shape function of the structure required for three-dimensional structures were obtained from formulas developed for beam models with a constant cross section in the literature. The models we obtained from the literature that we used to make comparisons have different flutter speed according to both standard strip theory and double lattice method. The developed MATLAB codes were applied on the models from the literature and the results were compared and it was seen that the results of these models were almost the same with the flutter speeds obtained using the standard strip theory. However, it has been observed that there is a difference between the flutter speeds obtained by using the double lattice method and the flutter speeds we have obtained. The reason for this is that MATLAB codes use standard strip theory. As a result, developed MATLAB codes have been proved to give consistent results.

In the last stage of the thesis, three different methods are explained for the modal analysis of the structure, which is required to be used in the three-dimensional

analytical aeroelastic analysis method. Aeroelastic analysis of the weakened AGARD 445.6 wing model was made using the MSC FlightLoads and Dynamics module and MSC NASTRAN commercial software programs. This commercial software program uses double lattice method to calculate aerodynamic loads. The results obtained by using commercial software were compared with the test results of the AGARD 445.6 wing model in the wind tunnel. The results were observed to be very close to each other. As a result, the results obtained from MSC FlightLoads and Dynamics module and MSC NASTRAN commercial software program have been proved to be consistent with real results. Different modal analysis methods are applied on the structure with a constant cross section and the structure where both the height and width of the cross section change with linear ratio. These data are used in MATLAB codes developed for three-dimensional aeroelastic analysis and the flutter speeds of these two different structures were obtained. By using MSC FlightLoads and Dynamics module and MSC NASTRAN commercial software program, the flutter speeds of these two different structures were obtained. The results obtained from MATLAB codes and the commercial software program were compared. As a result of the comparison, it was observed that the flutter speeds obtained from MATLAB codes were lower than the flutter speeds obtained from commercial software. As a result, it was seen that the MATLAB code using the standard strip theory gives more conservative results than the real values. Flutter speed results obtained by using the mode analysis results made by using Euler-Bernoulli beam theory and Tymoshenko beam theory in MATLAB code. These results were found to be more consistent than the results of the flutter speeds obtained by using the mode analysis results using the discrete mass system method in the MATLAB code.

FARKLI MODAL ANALİZ YÖNTEMLERİNİN ÇIRPINMA HIZI HESABI ÜZERİNDEKİ ETKİSİNİN İNCELENMESİ

ÖZET

Günümüzde modern hava araçlarının gelişmesinde yapının esnekliğinin büyük bir önemi vardır. Yapıdaki esnekliğin arttırılmasıyla aeroelastik etkiler tasarım sürecinde daha büyük bir öneme sahip olmuştur. Bu yüzden modern havacılıkta büyük bir aeroelastik problem olan çırpınma durumu sertifikasyon sürecinde büyük bir öneme sahiptir. Böylece çırpınma hızını bulma çalışmaları tasarım fazının en başından dikkate alınır. Ayrıca uçağın tasarımın en başından itibaren aeroelastik olarak kararlı bir yapıya sahip olması tasarımın ileriki aşamalarında olası problemleri engelleyerek zamandan ve maliyetten tasarruf edilmesini sağlar. Bütün bu süreçler göz önüne alınırsa, konsept tasarım fazında çırpınma hızının belirlenmesi büyük önem arz eder. Çünkü flutter hızı hesabının tasarım fazındaki etkisi önemli boyutlandırma çalışmaları açısından önemlidir. Modern havacılıkta hava aracının sağladığı güven ve hava aracının hafif olması önemli iki kriterdir. Hava aracının bu kriterleri sağlaması tasarımın ilk safhalarından son safhalarına kadar tasarımı etkileyen parametrelerin tasarım sürecine olan etkisi dikkate alınarak başarılır. Bu parametrelerin ve bu parametrelerin flutter hızı hesabı üzerindeki etkileri bu tezde incelenmiştir.

Tez çalışmasının ilk aşamasında konsept tasarım aşamasında yapının çırpınma hızını değerlendirmek için yapıyı iki boyutlu iki serbestlik dereceli ve iki boyutlu üç serbestlik dereceli olarak temsil eden ve akabinde bu iki boyutlu modelin çırpınma hızını bulmak için k methodu ve klasik çırpınma metodu kullanılmıştır. İki boyutlu, iki serbestlik dereceli yapılar için literatür araştırması sonucu elde edilen klasik yöntem ve k metodu açıklanmıştır. Bu iki metod kullanılırken aerodinamik yükler Theodorsen'in geliştirdiği formüller kullanılarak elde edilmiştir. İki boyutlu , üç serbestlik dereceli yapılar için literatür araştırması sonucu elde edilen k metodu açıklanmıştır. Aynı şekilde bu metodda kullanılan aerodinamik yük hesabında Theodorsen'in geliştirdiği formüller kullanılıyor. Theodorsen, aerodinamik yüklerin hesabında standart strip teoriyi kullanmıştır. İki boyutlu iki serbestlik dereceli ve iki boyutlu üç serbestlik dereceli modeller için analitik yöntem geliştirilmiştir. Tasarım fazında kullanılmak üzere bu yöntemler MATLAB ticari yazılım programı kullanılarak hesaplamalarda zamandan ciddi tasarruf elde edilmiştir. Geliştirilen bu analitik yöntemler literatürden gelen problemler üzerinde uygulanarak tutarlı sonuçlar verdiği ispatlanmıştır. Detay tasarım fazına geçmeden önce yapının flutter hızını hesaplamak için kullanılabilecek araç bu şekilde elde edilmiştir.

Tezin ikinci aşamasında üç boyutlu yapıların flutter hızı hesabı için geliştilen metod literatürden elde edilerek tezin bu aşamasında detaylı olarak incelenmiştir. İncelenen bu metod literatürden alınan farklı boyutlardaki modellerin flutter hızını hesaplamak için MATLAB kodu kullanılarak tool geliştirilmiştir. Flutter hızı hesaplanacak olan modeller kalınlık oranı ve en-boy oranının değiştirilmesiyle elde edilen 9 farklı modelden oluşmaktadır. Böylece yapının boyutlarını temsil eden

farklı parametrelerdeki değişimlerin flutter hızına olan etkisi de gözlemlenebilir. Modelin doğal frekans değerini ve mod şekillerini elde etmek için kullanılan mod analizi yöntemi, problemi aldığımız literatür kaynağından alınarak incelenmiştir. Bu method literatürde sabit ölçülere sahip dikdörtgensel kesitli yapılar için sıkça kullanılır. MATLAB ticari yazılımında kullandığımız üç boyutlu flutter hesabında kullanılan aerodinamik yükler Theodorsen'in geliştirdiği fonksiyonlar kullanılarak hesaplanmıştır. Theodorsen'in bu fonksiyonlarında standart strip teori kullanılmıştır. Doğrulama için kullandığımız literatür kaynağında ise modellerin flutter hızı hesabında kullanılmak üzere iki farklı metod incelenmiştir. Bu metodlar standart stip teori ve double lattice metodudur. Double lattice metod günümüzde aerodinamik yüklerin hesabında kullanılan ticari yazılım programlarında sıkça kullanılmaktadır. Bu iki metod aerodinamik yüklerin hesabında kullanılmaktadır. Geliştirilen MATLAB kodu farklı ölçülere sahip modeller üzerinde uygulanmıştır ve literatür sonuçları ile karşılaştırılmıştır. Sonuçların karlaştırılmasıyla MATLAB kodundan elde edilen sonuçlar ile standart strip teoriyi kullanan literatür sonuçlarının neredeyse aynı olduğu görülmüştür. Fakat MATLAB kodundan elde edilen sonuçlar ile double lattice metodunu kullanan literatür sonuçlarının farklı olduğu anlaşılmıştır. Çünkü aerodinamik yük hesabında kullanılan metodların flutter hızı sonuçlarında ciddi etkileri vardır. Tezin son kısmında bu konu üzerinde daha detaylı durulmuştur. Tezin bu aşamasında sadece MATLAB kodunu geliştirmek için faydalanmış olduğumuz yöntemin ve bu yöntemin aerodinamik yük hesabında kullandığı yöntemin literatür sonuçları ile tutarlı olup olmadığı araştırılmıştır. Tezin bu bölümünde ayrıca yapının mod analizini yapmak için kullanılan yöntemin flutter hızı sonuçlarına etkisi incelenmemiştir. Tezin son aşamasında bu konu detaylı şekilde ele alınmıştır. Bu bölümde elde edilen sonuçlar geliştirilen MATLAB kodunun tutarlı olduğunu ispatlamıştır. Ancak aerodinamik yüklerin hesabında kullanılan metodların flutter hızı sonucu üzerindeki etkiside ciddi şekilde gözlenmiştir.

Tezin son aşamasında üç boyutlu analitik analiz yönteminde kullanılmak üzere gerekli olan yapının mod analizi için üç farklı yöntem detaylı olarak açıklanmıştır. "MSC FlightLoads and Dynamics" modülü ve MSC NASTRAN ticari yazılım programları kullanılarak zayıflatılmış AGARD 445.6 kanat modelinin aeroelastik analizleri yapılmıştır. Bu model literatürde sıkça kullanılmaktadır. Bu ticari yazılım programı aerodinamik yüklerin hesabında double lattice metodu kullanmaktadır. Ticari yazılım programı aynı model sonlu elemanlar yöntemi temel alınarak çırpınma hızı hesaplanmıştır. Ticari yazılım kullanarak elde ettiğimiz sonuçları zayıflatılmış AGARD 445.6 kanat modelinin rüzgar tünelinde yapılan test sonuçları ile karşılaştırılmıştır. Sonuçların birbirine çok yakın olduğu gözlemlenmiştir. Sonuç olarak "MSC FlightLoads and Dynamics" modülü ve MSC NASTRAN ticari yazılım programından elde edilen sonuçların gerçek sonuçlara göre tutarlı olduğu ispatlanmıştır. Farklı mod analizi yöntemleri, sabit kesite sahip olan yapının ve kesitinin hem yüksekliğinin hem de genişliğinin doğrusal oranla değiştiği yapısal modeller üzerinde uygulanmıştır. Elde edilen bu veriler üç boyutlu aeroelastik analiz için geliştirilen MATLAB kodlarında kullanılmıştır ve bu iki farklı yapının çırpınma hızları elde edilmiştir. Ayrıca MSC FlightLoads and Dynamics modülü ve MSC NASTRAN ticari yazılım programı kullanılarak bu iki farklı yapının çırpınma hızları elde edilmiştir. MATLAB kodlarından elde edilen sonuçlar ile ticari yazılım programından elde edilen sonuçlar karşılaştırılmıştır. Karşılaştırmanın sonucunda MATLAB kodlarından elde edilen çırpınma hızlarının ticari yazılımdan elde edilen çırpınma hızlarından daha düşük olduğu görülmüştür. Bunun sonucunda standart strip teoriyi kullanan MATLAB kodunun gerçek değerlere göre daha konservatif sonuçlar verdiği görülmüştür. Euler-Bernoulli kiriş teorisi ve Timoshenko kiriş teorisi kullanılarak yapılan mod analiz sonuçlarının MATLAB kodunda kullanılmasıyla elde edilen çırpınma hızı sonuçlarının ayrık sistem metodu kullanılarak yapılan mod analizi sonuçlarının MATLAB kodunda kullanılmasıyla elde edilen çırpınma hızı sonuçlarına göre daha tutarlı olduğu görülmüştür. Böylelikle farklı mod analizi yöntemlerinin çırpınma hızı üzerindeki etkisi ve bu farklı mod analiz yöntemlerinin kendi içindeki doğruluk değerlendirmesi yapılmıştır.

xxx

1. INTRODUCTION

1.1 Purpose of Thesis

Reaching the ideal model in aviation has an important place in technology development. Before reaching the ideal model, a simple model is created to ensure the validity of the basic aeroelastic principles. Later, in order to increase the reliability of this design, aeroelastic analysis methods are applied and the design is made more ideal. These aeroelastic analysis methods apply the analysis and conclusion on the structural, aerodynamic and inertial behavior of the aircraft structure. The most important of these three behaviors of the structure is accepted as aerodynamic behavior. Because during the aeroelastic analysis of the structure, transient or unsteady aerodynamic loads due to the deformation of the structure have a key importance. In this thesis, before reaching the ideal model, a tool has been developed to be used in aeroelastic analysis of two-dimensional and three-dimensional structures. In aeroelastic analysis, the vibrational characteristic of the structure is of great importance. The different modal analysis methods developed to find this vibrational characteristic have been analytically introduced. In addition, the finite element method (FEM) has great advantages in terms of both time and reliability in finding the vibration characteristics of the structure. The use of Finite element method together with methods that calculate aerodynamic loads such as double lattice method has caused it to be an indispensable tool in the industry at the preliminary design and flight availability stages. The accuracy and reliability of the analysis performed by applying FEM in the thesis was proved by comparing it with the test results. The different vibration modal analysis methods used to find the vibration characteristic have been integrated into the three-dimensional analytical flutter rate analysis method, and its effect on the results has been desired.

1.2 Literature Review

Unsteady aerodynamics has made progress on two issues in history.First, the loads caused by impulsive motion were calculated. The first research of a two dimensional structure in this area in incompressible flow was done by Wagner [1]. R. T. Jones [2] continued this research. Unsteady-lift functions of the wings with finite aspect ratio were obtained by adjusting aerodynamic inertia and angle of attack. In finite wing, it was observed that there is less starting lift than infinite wing. However, it was observed that the final lift was largely small. The similarity of the distribution of the lift on the wing to the final distribution on the wing was observed. Curves indicating the lift changes caused by sudden change in angle of attack and continuous oscillation state were found. As a result of examining these curves, lift calculation is made easier under different conditions. As a result of these examinations, vertical acceleration of the wing caused by gust can be calculated.

Lomax [3] conducted research on the unsteady lift problems of two dimensional and three dimensional structures. For two- and three-dimensional wing models, the problem of transient lift is considered as the boundary value problem in classical wave equations. As in the case of steady state, the Kirchhoff formula enables the analysis to become an analysis of the sources.

Another area where unsteady earodynamics has made progress is the calculation of the loads of a harmonic oscillating structure. The aerodynamic loads of the structure, which makes simple harmonic oscillation in incompressible flow, were calculated by Theodorsen [4]. Aerodynamic loads were found for the 2-dimensional 2 degree of freedom airfoil or 2-dimensional 3 degree of freedom combination of airfoil-aileron. The Bessel functions used to find these loads are resolved. The theory of potential flow and Kutta conditions can be considered the same as the wing section theory, which is related to the steady case. The process of finding aerodynamic loads including potential flow and Kutta condition has been completed. The solution was found using the parameter k, which is defined as reduced frequency. The flutter speed is expressed in terms of functions consisting of the ratio of the frequency values of the airfoil-aileron combinations where the flutter state occurs. At the end of these processes, frequency-flutter velocity graphics are obtained. These graphics make a visual contribution to the interpretation of the flutter speed.

Watkins [5] developed the solution method by recovering the Kernel function used in aerodimaic calculations from singularity. The result of the integral equation used for finite wing models in subsonic flow is obtained. This equation establishes a relationship between downwash distribution and lift. This solution method is applicable for models with different shapes of leading and trailing edges. In addition, this solution method can be applied to control surfaces such as the tail of the aircraft.

The Kernel function removed from singularities was used by Rowe [6] in structures with a control surface. The method has been developed to find unstable loading caused by the oscillations of the control surfaces in the trailing edge area of the wing structure in the subsonic flow. This method can be applied for the wing with control surface throughout the span or for the wing with control surface at intervals on the span. The downwash integral equation in this method achieves its final form by separating the singular and non-singular terms. A method has been developed to eliminate discontinuities in the kinematic downwash distribution. Assumption has been made to include local velocities due to airfoil thickness in boundary conditions. As a result of these processes, it was observed that the results of pressure distribution on different control surface models were consistent by comparing theoretical and experimental data.

Another method that uses the finite element method model of the structure and used to calculate aerodynamic loads was developed by Albano and Rodden [7]. The aerodynamic surface is created by combining many lifting elements. These lifting elements refer to acceleration-potential doublets and the linearized formulation is achieved by using acceleration-potential doublets on the aerodynamic surface. Using the Kernel function, velocity caused by unit force is found. The load affecting each element in the double lattice method is found by providing normal velocity boundary condition at many points of the aerodynamic surface. The lifting elements on the aerodynamic surface are positioned to provide the Kutta condition. This method is very easy to use on complex problems.

In aeroelastic analysis, the assumption that the structure makes simple harmonic motion is quite common. The reason for this situation is that this analysis technique predicts flutter boundaries very well. Theodorsen and Garrick [8], and Smilg and Wasserman [9] are pioneers of these commonly used methods. Smilg and Wasserman has also integrated artificial structural damping into this method and used it in three dimensional structures.

Due to U-f flutter analysis methods, which cannot provide sufficient information for stable and subcritical flutter cases, methods using convolution techniques were used [10], [11]. The difference between true damping solution of flutter equation and structural damping solution is examined. If the unsteady aerodynamic system can be expressed in terms of a p variable that expresses a complex number, the damping solution can be obtained. For a system with harmonic motion, it is possible to determine the damping value in case of increasing or decreasing amplitude of aerodynamic forces. But in this case, aerodynamic loads must be given in reduced frequency k.

The natural modes of the aerodynamic structure at any speed are determined. It was observed that the damping value obtained in the critical mode increased up to 85 percent of the critical speed and then dropped to zero when it came very close to the flutter speed [12]. Stability increases sharply in non-critical mode. When the system response caused by forced excitation and normal mode responses were compared, it was seen that the system response caused by forced excitation showed the approach to the flutter state earlier. Therefore, the examination of the system response caused by forced excitation was found to be more accurate.

1.3 Scope of Thesis

In the first stage of the thesis, aeroelastic analysis of two dimensional structures with two degree of freedom and two dimensional structures with three degree of freedom was investigated. In aeroelastic analysis, the calculation of flutter speed is emphasized. For this, two different methods are used, which are frequently used in the literature. MATLAB code has been generated to apply these two methods in two dimensional structures. The validity of the MATLAB codes generated was tested on two problems obtained from the literature.

In the second stage of the thesis, the method used in the literature to calculate the flutter speed calculation of 3D structures is explained. MATLAB code has been generated to use this described method on models of different sizes. In the method used in the literature, standard strip theory is used to calculate aerodynamic loads. The modal analysis results required for the use of the structure in the calculation of the flutter speed were obtained as stated in the literature source to be used for validation. The flutter analysis tool generated in MATLAB was used on different models used in the literature and the results were compared. In the literature, these models have two different results. In the literature, the results obtained using the standard strip theory and the results obtained with the double lattice method were compared with the results obtained using the tool generated in MATLAB.

In the last stage of the thesis, three different modal analysis methods are used to use in flutter calculation. These methods are explained in detail. Finally, MATLAB code including these modal analysis methods has been generated.Generated MATLAB code and MSC PATRAN / NASTRAN commercial software, which has been proven by calculation of flutter speed on the AGARD wing, is used to calculate the flutter speed of two different models and the results are compared with each other.

2. SUBSONIC FLUTTER ANALYSIS OF A TYPICAL WING SECTION

2.1 Mathematical Modeling Of a 2 Degree Of Freedom Typical Section

In this section, we will examine how to calculate the flutter in a linear system.First we need to simplify the model we will work on.Two-dimensional, spring-mounted, rigid models were used to analyze the flutter. Figure 2.1 shows this structure.Physical simplicity is the reason why these structures are still used today. This model can represent an elastic, finite wing model that we can use in our tests, as well as the airfoil section of an airplane wing.If the model represents the model we will use in tests in the wind tunnel, the springs will reflect the bending and torsional stiffness of the wing structure and the reference point will represent the elastic axis.

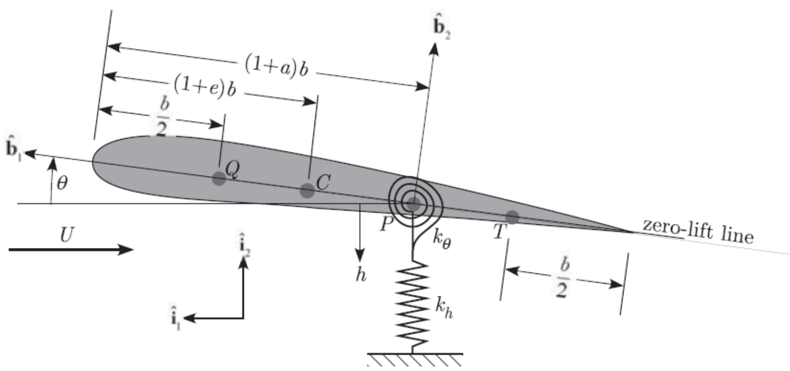

Figure 2.1 : Typical section of the wing with pitch and plunge spring restraints[21].

In such models, the points P, C, Q, and T represent respectively, the reference point where the pitching displacement (h) is measured, the center of mass, the aerodynamic center and the 3 quarter of the veter length.The dimensionless s parameter which indicates the location of the center of gravity is between -1 and 1 $(-1 \leq e \leq 1)$.The dimensionless a parameter representing the location of the reference center is also between -1 and 1 $(-1 \leq a \leq 1)$. If the value of e and a is negative, the distance of the reference axis and center of gravity from the edge of the attack is shown, if it is positive, the distance from the edge of the trailing edge is shown.The k_h and k_θ values shown in the figure 2.1 are the spring stiffness coefficients in the h and θ directions of the springs.

2.2 Equations Of Motion Of The 2 Degree Of Freedom Typical Section

Lagrange's equation can be used while obtaining the motion equation of the 2 degree of freedom system. Generalized coordinates to be used in this equation are given below.

$$q_1 = h \quad \text{and} \quad q_2 = \theta$$

Lagrange's equation;

$$\frac{d}{dt}\left(\frac{\partial T}{\partial \dot{q}_i}\right) - \frac{\partial T}{\partial q_i} + \frac{\partial P}{\partial q_i} = \Theta_i \qquad i = 1,2 \tag{2.1}$$

which T and P are kinetic energy and potential energy, respectively. From equation 2.1 for 2 degree of freedom , 2 Lagrange equations can be obtained;

$$\frac{d}{dt}\left(\frac{\partial T}{\partial \dot{h}}\right) - \frac{\partial T}{\partial h} + \frac{\partial P}{\partial h} = \Theta_h \tag{2.2}$$

$$\frac{d}{dt}\left(\frac{\partial T}{\partial \dot{\theta}}\right) - \frac{\partial T}{\partial \theta} + \frac{\partial P}{\partial \theta} = \Theta_\theta \tag{2.3}$$

The kinetic and potential energy of the typical wing airfoil section in the center of gravity is obtained as follows;

$$T = \frac{1}{2}mV_C^2 + \frac{1}{2}I_C\dot{\theta}^2 \tag{2.4}$$

which V_C and I_C are velocity of the center of the gravity and mass moment of inertia, respectively.

$$V_C = \dot{h} - b(a-e)\dot{\theta}$$

$$V_C^2 = \dot{h}^2 - 2\dot{h}b(a-e)\dot{\theta} + b^2(e-a)^2\dot{\theta}^2$$

$$T = \frac{1}{2}m\left(\dot{h}^2 - 2\dot{h}b(a-e)\dot{\theta} + b^2(e-a)^2\dot{\theta}^2\right)^2 + \frac{1}{2}I_C\dot{\theta}^2 \tag{2.5}$$

$$T = \frac{1}{2}m\dot{h}^2 + \frac{1}{2}\left(mb^2(a-e)^2 + I_C\right)\dot{\theta}^2 - m\dot{h}\ddot{\theta}b(a-e) \tag{2.6}$$

where; $mb^2(a-e)^2 + I_C = I_P$ (mass moment of inertia about reference point)

$$T = \frac{1}{2}m\dot{h}^2 + \frac{1}{2}I_P\dot{\theta}^2 - m\dot{h}\ddot{\theta}b(a-e) \tag{2.7}$$

$$P = \frac{1}{2}k_h h^2 + \frac{1}{2}k_\theta \theta^2 \tag{2.8}$$

The virtual work caused by aerodynamic pressure on a two-dimensional plate is calculated as follows.

$$\begin{aligned}\delta W = Q_h\delta h + Q_\theta\delta\theta &= \iint p\delta w dx = \int p(-\delta h - x\delta\theta)dx \\ &= \delta h\left(-\int p dx\right) + \delta\theta\left(-\int p x dx\right) \\ &= \delta h\,(-L) + \delta\theta\,(M_y)\end{aligned} \tag{2.9}$$

From equation 2.9

$$\Theta_h = -L \text{ and } \Theta_\theta = M \tag{2.10}$$

From equation 2.10, 2.2, and 2.3

$$\begin{aligned}&\frac{d}{dt}\left(\frac{\partial T}{\partial \dot{h}}\right) = m\ddot{h} - mb(a-e)\ddot{\theta} \quad , \quad \frac{\partial T}{\partial h} = 0 \quad , \quad \frac{\partial P}{\partial h} = k_h h \\ &\frac{d}{dt}\left(\frac{\partial T}{\partial \dot{\theta}}\right) = I_P\ddot{\theta} - mb(a-e)\ddot{h} \quad , \quad \frac{\partial T}{\partial \theta} = 0 \quad , \quad \frac{\partial P}{\partial \theta} = k_\theta \theta\end{aligned} \tag{2.11}$$

From equation 2.2, 2.3 , and 2.11, equations of motion of typical wing section;

$$
\begin{aligned}
m\ddot{h} + mbx_\theta\ddot{\theta} + k_h h &= -L \\
mbx_\theta\ddot{h} + I_P\ddot{\theta} + k_\theta\theta &= M
\end{aligned}
\tag{2.12}
$$

2.3 Solution of the Equations of Motion of 2 Degree of Freedom Model Using Subsonic Aerodynamics Based On Classical Flutter Analysis

Normally, analysis is not done only through the solution of generalized equations of motion as described in section 2.2. The solution method is based on simple harmonic motion. Therefore, equations of motion are solved using this basis. Classic flutter analysis for an arbitrary flight condition cannot provide modal damping.Therefore, classical flutter analysis can only provide a measure of flutter stability at the stability limit. This is a major disadvantage of classical flutter analysis. However, for a certain level of accuracy, only unsteady air loads are needed to solve the problem if compared with an arbitrary movement. This feature is a serious advantage of classical flutter analysis.

In the case of simple harmonic motion, the state of unsteady air loads on the lifting surface have to be taken into account to demonstrate classical flutter analysis. Due to the smallness of these oscillation movements, a linear aerodynamic theory should be used to determine unsteady air loads. These theories use the linear potential flow theory, which accepts the assumption that the disturbance due to movement and thickness of the wing structure is less than the free-stream flow.To demonstrate this, the typical section of the two-dimensional lifting surface, which is shown in figure 2.1, which makes rotational and translational movements simultaneously, is reviewed again.Since the motion is accepted as simple harmonic, its representation is as follows ;

$$
\begin{aligned}
h(t) &= \overline{h}\, exp(iwt) \\
\theta(t) &= \overline{\theta}\, exp(iwt)
\end{aligned}
\tag{2.13}
$$

where w is the frequency of the motion. Although h and θ movements have the same frequency, their phases are different.To take this mathematically into account, the amplitude of $\overline{\theta}$ must be taken as a real number and the amplitude of $\overline{h}$ as a complex number.Due to the use of linear aerodynamic theory, the lifting force(L) obtained and the pitching moment(M) about P ;

$$M = M_{\frac{1}{4}} + b\left(\frac{1}{2} + a\right)L \tag{2.14}$$

$$\begin{aligned} L(t) &= \overline{L}\, exp(iwt) \\ M(t) &= \overline{M}\, exp(iwt) \end{aligned} \tag{2.15}$$

According to linear aerodynamic theory, lifting force and pitching moment can be written as follows depending on the reduced frequency and Mach number.

$$\begin{aligned} \overline{L} &= -\pi\rho_\infty b^3 w^2 \left[l_h(k,\, M_\infty)\frac{\overline{h}}{b} + l_\theta(k,\, M_\infty)\overline{\theta} \right] \\ \overline{M} &= \pi\rho_\infty b^4 w^2 \left[m_h(k,\, M_\infty)\frac{\overline{h}}{b} + m_\theta(k,\, M_\infty)\overline{\theta} \right] \end{aligned} \tag{2.16}$$

The compressibility effects of the coefficients are shown by their dependence on the Mach number(M_∞). Reduced frequency (k) is specific to unsteady flows. The dimensionless reduced frequency(k) value is a value ranging from 0 to 1 depending on the flow and flight conditions. It should be known that any aerodynamic coefficient can be written as a complex number according to the dimensionless k and M_∞ value. The fact that the lift and pitching moment are complex number reflect the phase relations according to the pitch angle.The rate of occurrence of flutter varies according to the values of reduced frequency(k) and Mach numbers(M_∞) and this should be found by performing iteration.

Substituting equation 2.13 and equation 2.15 into the equations 2.12, a pair of equations for the amplitudes of h and θ in the form can be obtained.

$$\begin{aligned} -w^2 m\overline{h} - w^2 mbx_\theta\overline{\theta} + mw_h^2\overline{h} &= -\overline{L} \\ -w^2 mbx_\theta\overline{h} - w^2 I_P\overline{\theta} + I_P w_\theta^2\overline{\theta} &= \overline{M} \end{aligned} \tag{2.17}$$

Substituting equation 2.16 into equation 2.17 and rearranging, then linear, homogeneous equations can be obtained for $\overline{h}$ and $\overline{\theta}$, given by

$$\left\{\frac{m}{\pi\rho_\infty b^2}\left[1-\left(\frac{w_h}{w}\right)^2\right]+l_h(k,M_\infty)\right\}\frac{\overline{h}}{b}+\left[\frac{mx_\theta}{\pi\rho_\infty b^2}+l_\theta(k,M_\infty)\right]\overline{\theta}=0$$
$$\left[\frac{mx_\theta}{\pi\rho_\infty b^2}+m_h(k,M_\infty)\right]\frac{\overline{h}}{b}+\left\{\frac{I_P}{\pi\rho_\infty b^4}\left[1-\left(\frac{w_\theta}{w}\right)^2\right]+m_\theta(k,M_\infty)\right\}\overline{\theta}=0 \tag{2.18}$$

These equations can be simplified using the following dimensionless parameters.

$$\mu=\frac{m}{\pi\rho_\infty b^2} \qquad \text{(mass ratio)}$$
$$r=\sqrt{\frac{I_P}{mb^2}} \qquad \text{(mass radius of gyration about P)} \tag{2.19}$$

Then equation 2.18 became as follow;

$$\left\{\mu\left[1-\left(\frac{w_h}{w}\right)^2\right]+l_h(k,M_\infty)\right\}\frac{\overline{h}}{b}+\left[\mu+l_\theta(k,M_\infty)\right]\overline{\theta}=0$$
$$\left[\mu x_\theta+m_h(k,M_\infty)\right]\frac{\overline{h}}{b}+\left\{\mu r^2\left[1-\left(\frac{w_\theta}{w}\right)^2\right]+m_\theta(k,M_\infty)\right\}\overline{\theta}=0 \tag{2.20}$$

As a next step, mathematical equations are solved for flight conditions involving simple harmonic motion. As a result, the flutter boundary is found. In cases where m,e,a,I_P,w_h,w_θ, and b parameters are known, unknown $\overline{h},\overline{\theta},w,\rho_\infty,M_\infty$, and k values provide an understanding of motion and flight conditions. To get the solution of equation 2.20, which is homogeneous and linear, the determinant of the matrix, which is the coefficients of $\frac{\overline{h}}{b}$ and $\overline{\theta}$, must be 0. As a result of this step, the following situation is obtained.

$$\begin{vmatrix} \mu\left[1-\sigma^2\left(\frac{w_\theta}{w}\right)^2\right]+l_h & \mu x_\theta+l_\theta \\ \mu x_\theta+m_h & \mu r^2\left[1-\left(\frac{w_\theta}{w}\right)^2\right]+m_\theta \end{vmatrix}=0 \tag{2.21}$$

where $\sigma=\left(\frac{w_h}{w_\theta}\right)^2$.

Equation 2.21 is called flutter determinant.The σ parameter has been added to use the $\left(\frac{w_\theta}{w}\right)$ parameter. So the determinant takes us to a quadratic polynomial of $\lambda=\left(\frac{w_\theta}{w}\right)^2$.

2.3.1 Solution of the Flutter Determinant

In case of flight condition at the flutter boundary, there are 4 unknowns in the flutter determinant.These unknowns are $\left(\frac{w_\theta}{w}\right)$, $\mu=\frac{m}{(\pi\rho_\infty b^2)}$, M_∞, and $k=\frac{bw}{U}$, respectively.By equating this determinant to zero, a second degree polynomial characteristic equation is obtained.Since the aerodynamic coefficients are complex numbers, this complex equation represents two real equations. In order to get the solution, both real and imaginary parts must be equal to 0. For this, 2 of the 4 unknown must be determined. The following method describes this method that solves the flutter limit.

1. set ρ_∞ parameter for a fixed altitude.
2. The initial value is defined for M_∞, it can be taken as zero.
3. A series of k values are defined, and can be selected from 0.001 to 1.
4. l_h, l_θ, m_h, and m_θ values are calculated for each k value.
5. The flutter determinant is solved for each value of k.
6. The expression obtained as a result of the determinant has $\left(\frac{w_\theta}{w}\right)^2$ value that makes both the real and the non-real part zero.Also, after plotting both real and non-real parts according to $\frac{1}{k}$, the k value that intersects both curves can be taken as the wanted value.
7. Flutter speed and $M_\infty = \frac{U_F}{c_\infty}$ value can be calculated.
8. Steps from step 3 to step 7 are repeated until the M_∞ value converges to the M_∞ value for μ initially calculated.
9. The whole procedure is repeated from the beginning for different μ values to calculate the critical flutter speeds at the other altitudes.

2.4 Solution of the Equations of Motion of 2 Degree of Freedom Model Using Subsonic Aerodynamics Based On K-Method

After Theodore Theodorsen's analysis for the flutter problem, various schemes are prepared to reach the flutter determinant roots and determine the stability conditions.Later, Scanlan and Rosenbaum offered an overview of such techniques introduced in the 1940s [13].The use of a parameter representing the structural damping effect in flutter analysis was quite common.As a result, observations have shown that the energy lost in each cycle during simple harmonic oscillation is proportional to the square of the amplitude but independent of frequency. It was understood that this behavior could be represented by a damping force proportional to displacement and also rapidly in the same phase. If structural damping effects are added to the equations of motion in 2 degree of freedom systems, the following equations are obtained.

$$\begin{aligned} m\left(\ddot{h}+bx_\theta\ddot{\theta}\right)+k_h h &= -L+D_h \\ I_P\ddot{\theta}+mbx_\theta\ddot{h}+k_\theta\theta &= M+D_\theta \end{aligned} \tag{2.22}$$

Structural damping terms;

$$\begin{aligned} D_h = \overline{D}_h exp(iwt) &= -ig_h m w_h^2 \overline{h} exp(iwt) \\ D_\theta = \overline{D}_\theta exp(iwt) &= ig_\theta I_P w_\theta^2 \overline{\theta} exp(iwt) \end{aligned} \tag{2.23}$$

and equation 2.20 became ;

$$\begin{aligned} \left\{\mu\left[1-\left(\frac{w_h}{w}\right)^2(1+ig_h)\right]+l_h\right\}\frac{\overline{h}}{b}+(\mu x_\theta+l_\theta)\overline{\theta} &= 0 \\ (\mu x_\theta+m_h)\frac{\overline{h}}{b}+\left\{\mu r^2\left[1-\left(\frac{w_\theta}{w}\right)^2(1+ig_\theta)\right]+m_\theta\right\}\overline{\theta} &= 0 \end{aligned} \tag{2.24}$$

The g_h and g_θ damping coefficients can have values ranging from 0.01 to 0.05 depending on the structural condition. Old analysts predetermined the coefficients to get results closer to more real results. In 1948, Scanlan and Rosenbaum proposed the idea of the structural damping coefficients to be accepted together with frequency as an unknown.As a result, subscripts under g are removed and new parameter is introduced as below.

$$Z=\left(\frac{w_\theta}{w}\right)^2(1+ig) \tag{2.25}$$

consequently, if we apply this parameter to equation 2.24 and then get the flutter determinant, we get the following result.

$$\begin{vmatrix} \mu\left(1-\sigma^2 Z\right)+l_h & \mu x_\theta+l_\theta \\ \mu x_\theta+m_h & \mu r^2(1-Z)+m_\theta \end{vmatrix}=0 \tag{2.26}$$

This equation is quadratic in Z. By solving this equation, the following Z value is obtained.

$$Z_{1,2} = \left(\frac{w_\theta}{w_{1,2}}\right)^2 (1 + ig_{1,2}) \tag{2.27}$$

The method used to solve equation 2.26 is similar to the method used to solve equation 2.21. There are some differences between these 2 methods. The most important difference between them is the solution of this equation, 2 real results are obtained and these two real roots are drawn according to the reduced speed $\frac{1}{k}$ and the results are evaluated. From the graphs according to the airspeed of the damping coefficients, the flutter boundary is obtained at the points where one of the damping coefficients is equal to zero. This method is often known as the U-g method. In this method, since simple harmonic motion is always performed, g_1 and g_2 values obtained for each k value are considered as damping coefficients that provide motion at frequencies w_1 and w_2. These damping coefficients are actually not real. They are only artificial parameters that provide the desired movement. Frequency plots versus airspeed in combination with damping are often used to explain the physical condition that causes instability. With the increase of airspeed, interaction in the roots is used to observe the transfer of energy from one mode to another. Thanks to these observations, the instability can be delayed. For any reduced frequency value, motion modes can be obtained by placing the relevant eigenvalues w_i and g_i into the motion equations of the respective eigenvectors.

In addition, the aerodynamic coefficients obtained using the Theodorsen's theory to be used in the flutter speed calculation of 2 degree of freedom systems are given below.

$$l_h = 1 - \frac{2iC(k)}{k} \tag{2.28}$$

$$l_\theta = -a - \frac{i}{k} - \frac{2iC(k)\left(\frac{1}{2} - a\right)}{k} - \frac{2C(k)}{k^2} \tag{2.29}$$

$$m_h = -a + \frac{2iC(k)\left(\frac{1}{2} + a\right)}{k} \tag{2.30}$$

$$m_\theta = \frac{1}{8} + a^2 - \frac{i\left(\frac{1}{2}-a\right)}{k} + \frac{2C(k)\left(\frac{1}{2}+a\right)}{k^2} + \frac{2iC(k)\left(\frac{1}{4}-a^2\right)}{k} \tag{2.31}$$

2.5 Mathematical Modeling of 3 Degree of Freedom Typical Section of 2 Dimensional Wing Model

The typical sectional model is represented as a 2-dimensional wing mounted in the wind tunnel, which is vertically and angularly suitable, or by mounting the beam representing a 3-dimensional model on the side wall of the wind tunnel. As shown in the figure 2.3, typical section is actually the section of the wing in three-quarter. The vertical and angular displacement of the typical section results from the bending and torsion movement of the wing, respectively.

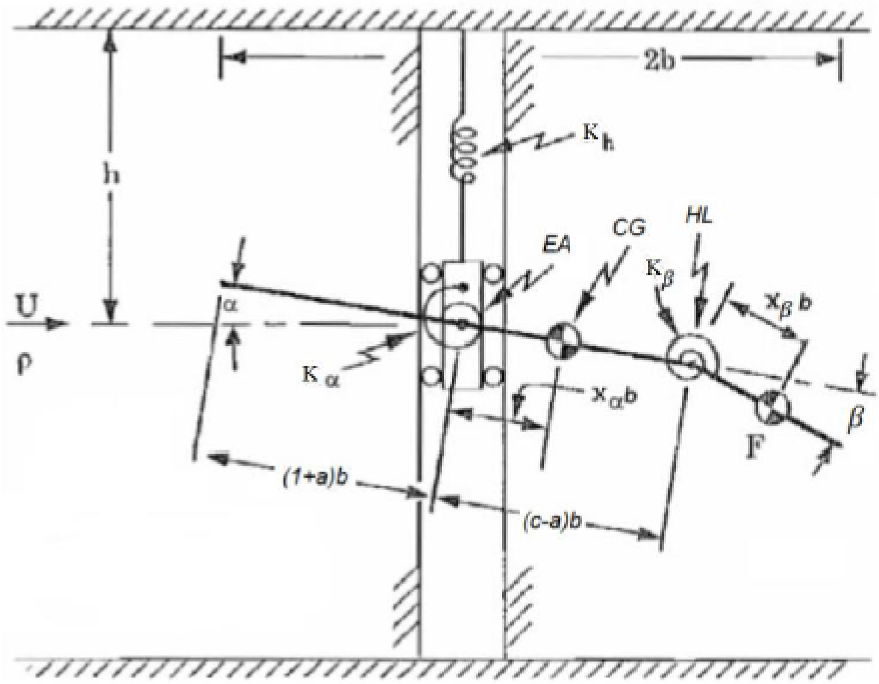

Figure 2.2 : 3 Degree of Freedom Typical Wing Section Of 2 Dimensional Wing Model[14].

In Figure 2.2, b is the half veter length, a gives the ratio of the distance between the center line and the elastic axis to b, x_α is the ratio of the distance between the center of gravity and the elastic axis to the length of b, h is the vertical displacement of the elastic axis in the vertical direction. α is the angle between the air flow direction of the

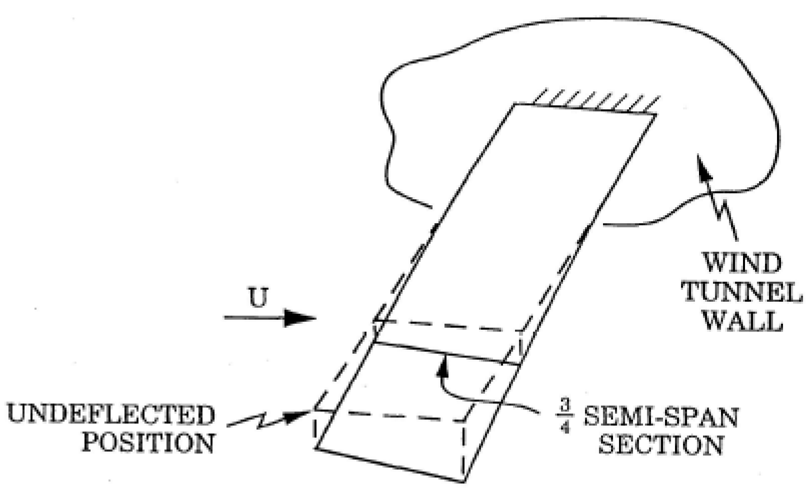

Figure 2.3 : Cantilever Wing Model mounted on Side Wall of Wind Tunnel[16].

elastic veter axis, k_h and k_α are the spring stiffness in the plunge and pitch directions, respectively. Also in figure 2.2, β shows the movement of the control surface, x_β is the spring constant in this direction of movement, c is the distance between the point $z = 0$ and the hinge line, F is the center of gravity of the control surface, x_β is the distance between the center of gravity of the control surface and the hinge line.

2.6 Mathematical Equations and Solutions for 3 Degree of Freedom Model in Incompressible Subsonic Flow

The equation of motion of the model described in section 2.5 are given below.

$$\begin{aligned} m\ddot{h} + m_\alpha b x_\alpha \ddot{\alpha} + m_\beta b x_\beta \ddot{\beta} + K_h h &= -L \\ m_\alpha b x_\alpha \ddot{h} + I_\alpha \ddot{\alpha} + \left\{(c-a) b m_\beta b x_\beta + I_\beta\right\} \ddot{\beta} + K_\alpha \alpha &= M \\ m_\beta b x_\beta \ddot{h} + \left\{(c-a) b m_\beta b x_\beta + I_\beta\right\} \ddot{\alpha} + I_\beta \ddot{\beta} + K_\beta \beta &= H \end{aligned} \tag{2.32}$$

control surface's static mass moment about the hinge line and airfoil's static mass moment about the elastic axis, respectively;

$$\begin{aligned} S_\beta &= m_\beta b c_\beta \\ S_\alpha &= m_\alpha b c_\alpha \end{aligned} \tag{2.33}$$

substituting equation 2.6 into equation 2.32, Then ;

$$
\begin{aligned}
m\ddot{h}+S_{\alpha}\ddot{\alpha}+S_{\beta}\ddot{\beta}+K_{h}h&=-L\\
S_{\alpha}\ddot{h}+I_{\alpha}\ddot{\alpha}+\left\{(c-a)bS_{\beta}+I_{\beta}\right\}\ddot{\beta}+K_{\alpha}\alpha&=M\\
S_{\beta}\ddot{h}+\left\{(c-a)bS_{\beta}+I_{\beta}\right\}\ddot{\alpha}+I_{\beta}\ddot{\beta}+K_{\beta}\beta&=H
\end{aligned}
\tag{2.34}
$$

where;

I_{β}; Mass moment of inertia of the control surface

H; Moment about the hinge line

β and H are formulated as follows, since the motion of the control surface is also considered simple harmonic motion.

$$\beta=\overline{\beta}exp(iwt) \tag{2.35}$$

$$H=\overline{H}exp(iwt) \tag{2.36}$$

The lift and moment on the elastic axis of the typical wing section with simple harmonic motion and unit span length and the moment on the hinge line of the control surface are described in the literature as follows.

$$
\begin{aligned}
L=\rho_{\infty}b^{2}&\left[\pi\ddot{h}+\pi U\dot{\alpha}-\pi ba\ddot{\alpha}-UT_{4}\dot{\beta}-T_{1}b\ddot{\beta}\right]\\
&+2\pi\rho_{\infty}UbC(k)\left[U\alpha+\dot{h}+b\left(\frac{1}{2}-a\right)\dot{\alpha}+\frac{T_{10}U\beta}{\pi}+\frac{bT_{11}\dot{\beta}}{2\pi}\right]
\end{aligned}
\tag{2.37}
$$

$$M=\rho_\infty b^2\left\{\pi ba\ddot{h}-\pi Ub\left(\frac{1}{2}-a\right)\dot{\alpha}-\pi b^2\left(\frac{1}{8}+a^2\right)\ddot{\alpha}-(T_4+T_{10})U^2\beta\right.$$
$$\left.-\left[T_1-T_8-(c-a)T_4+\frac{T_{11}}{2}\right]Ub\dot{\beta}+[T_7+(c-a)T_1]b^2\ddot{\beta}\right\} \tag{2.38}$$
$$+2\pi\rho_\infty Ub^2\left(a+\frac{1}{2}\right)C(k)\left[U\alpha+\dot{h}+b\left(\frac{1}{2}-a\right)\dot{\alpha}+\frac{T_{10}U\beta}{\pi}+\frac{bT_{11}\dot{\beta}}{2\pi}\right]$$

$$H=\rho_\infty b^2\left\{T_1b\ddot{h}-\left[-2T_9-T_1+T_4\left(a-\frac{1}{2}\right)\right]Ub\dot{\alpha}-2T_{13}b^2\ddot{\alpha}-\frac{U^2\left(T_5-T_4T_{10}\right)\beta}{\pi}\right.$$
$$\left.+\frac{UbT_4T_{10}\dot{\beta}}{2\pi}+\frac{T_4b^2\ddot{\beta}}{\pi}\right\}-\rho_\infty Ub^2T_{12}C(k)\left[U\alpha+\dot{h}+b\left(\frac{1}{2}-a\right)\dot{\alpha}+\frac{T_{10}U\beta}{\pi}+\frac{bT_{11}\dot{\beta}}{2\pi}\right] \tag{2.39}$$

substituting equation 2.13, equation 2.35, and 2.36 into equations 2.37, 2.38 2.39, we can obtain equations ;

$$L=\left\{\rho_\infty b^2\left[-w^2\pi\overline{h}+iw\pi U\overline{\alpha}+w^2\pi ba\overline{\alpha}-iwUT_4\overline{\beta}+w^2T_1b\overline{\beta}\right]\right.$$
$$\left.+2\pi\rho_\infty UbC(k)\left[U\overline{\alpha}+iw\overline{h}+iwb\left(\frac{1}{2}-a\right)\overline{\alpha}+\frac{T_{10}U\overline{\beta}}{\pi}+iw\frac{bT_{11}\overline{\beta}}{2\pi}\right]\right\}exp(iwt) \tag{2.40}$$

$$M=\left\{\rho_\infty b^2\left\{-w^2\pi ba\overline{h}-iw\pi Ub\left(\frac{1}{2}-a\right)\overline{\alpha}+w^2\pi b^2\left(\frac{1}{8}+a^2\right)\overline{\alpha}-(T_4+T_{10})U^2\overline{\beta}\right.\right.$$
$$\left.-iw\left[T_1-T_8-(c-a)T_4+\frac{T_{11}}{2}\right]Ub\overline{\beta}-w^2[T_7+(c-a)T_1]b^2\overline{\beta}\right\}$$
$$\left.+2\pi\rho_\infty Ub^2\left(a+\frac{1}{2}\right)C(k)\left[U\overline{\alpha}+iw\overline{h}+iwb\left(\frac{1}{2}-a\right)\overline{\alpha}+\frac{T_{10}U\overline{\beta}}{\pi}+iw\frac{bT_{11}\overline{\beta}}{2\pi}\right]\right\}exp(iwt) \tag{2.41}$$

$$H=\left\{\rho_\infty b^2\left\{-w^2T_1b\overline{h}-iw\left[-2T_9-T_1+T_4\left(a-\frac{1}{2}\right)\right]Ub\overline{\alpha}+2w^2T_{13}b^2\overline{\alpha}\right.\right.$$
$$\left.-\frac{U^2\left(T_5-T_4T;_{10}\right)\overline{\beta}}{\pi}+iw\frac{UbT_4T_{11}\overline{\beta}}{2\pi}-w^2\frac{T_3b^2\overline{\beta}}{\pi}\right\}$$
$$\left.-\rho_\infty Ub^2T_{12}C(k)\left[U\overline{\alpha}+iw\overline{h}+iwb\left(\frac{1}{2}-a\right)\overline{\alpha}+\frac{T_{10}U\overline{\beta}}{\pi}+iw\frac{bT_{11}\overline{\beta}}{2\pi}\right]\right\}exp(iwt) \tag{2.42}$$

Where, $U=\dfrac{bw}{k}$, then;

$$L=\left\{\left(-bw^2\right)\rho_\infty b^2\left[\frac{-w^2\pi\overline{h}+iw\pi\frac{bw}{k}\overline{\alpha}+w^2\pi ba\overline{\alpha}-iw\frac{bw}{k}T_4\overline{\beta}+w^2T_1b\overline{\beta}}{-bw^2}\right]\right.$$
$$\left.+(bw)\,2\pi\rho_\infty\frac{bw}{k}bC(k)\left[\frac{\frac{bw}{k}\overline{\alpha}+iw\overline{h}+iwb\left(\frac{1}{2}-a\right)\overline{\alpha}+\frac{T_{10}bw\overline{\beta}}{\pi k}+iw\frac{bT_{11}\overline{\beta}}{2\pi}}{bw}\right]\right\} \tag{2.43}$$

$$M=\left[\left(b^2w^2\right)\rho_\infty b^2\left[\frac{-w^2\pi ba\overline{h}+iw\pi\frac{bw}{k}b\left(\frac{1}{2}-a\right)\overline{\alpha}+w^2\pi b^2\left(\frac{1}{8}+a^2\right)\overline{\alpha}}{b^2w^2}\right.\right.$$
$$\left.+\frac{-\left(T_4+T_{10}\right)\left(\frac{bw}{k}\right)^2\overline{\beta}-iw\left[T_1-T_8-(c-a)T_4+\frac{T_{11}}{2}\right]\frac{bw}{k}b\overline{\beta}-w^2\left[T_7+(c-a)T_1\right]b^2\overline{\beta}}{b^2w^2}\right]$$
$$\left.+(bw)\,2\pi\rho_\infty\frac{bw}{k}b^2\left(a+\frac{1}{2}\right)C(k)\left[\frac{\frac{bw}{k}\overline{\alpha}+iw\overline{h}+iwb\left(\frac{1}{2}-a\right)\overline{\alpha}+\frac{T_{10}bw\overline{\beta}}{\pi k}+iw\frac{bT_{11}\overline{\beta}}{w\pi}}{bw}\right]\right\}exp(iwt) \tag{2.44}$$

$$H=\left\{\left(\pi b^2w^2\right)\rho_\infty b^2\left\{\frac{iw^2T_1b\overline{h}-iw\left[-2T_9-T_1+T_4\left(a-\frac{1}{2}\right)\right]\frac{bw}{k}b\overline{\alpha}+w^22T_{13}b^2\overline{\alpha}}{\pi b^2w^2}\right.\right.$$
$$\left.+\frac{\frac{-(bw)^2(T_5-T_4T_{10})\overline{\beta}}{\pi k^2}+iw\frac{b^2wT_4T_{11}\overline{\beta}}{2\pi k}-w^2\frac{T_3b^2\overline{\beta}}{\pi}}{\pi b^2w^2}\right\}$$
$$\left.-(\pi bw)\rho_\infty\frac{bw}{k}b^2T_{12}C(k)\left[\frac{\frac{bw}{k}\overline{\alpha}+iw\overline{h}+iwb\left(\frac{1}{2}-a\right)\overline{\alpha}+\frac{T_{10}bw\overline{\beta}}{\pi k}+iw\frac{bT_{11}\overline{\beta}}{2\pi}}{\pi bw}\right]\right\}exp(iwt) \tag{2.45}$$

Equation 2.43, equation 2.44, and equation 2.45 can be rearranged as shown below.

$$\begin{aligned}L=&-\pi\rho_\infty b^3w^2\left\{\frac{1}{b}\overline{h}-i\frac{1}{h}\overline{\alpha}-a\overline{\alpha}+i\frac{1}{\pi k}T_4\overline{\beta}-\frac{1}{\pi}T_1\overline{\beta}\right.\\&\left.-2\frac{1}{k}C(k)\left[\frac{1}{k}\overline{\alpha}+i\frac{1}{b}\overline{h}+i\left(\frac{1}{2}-a\right)\overline{\alpha}+\frac{T_{10}\overline{\beta}}{\pi k}+i\frac{T_{11}\overline{\beta}}{2\pi}\right]\right\}exp(iwt)\end{aligned} \tag{2.46}$$

$$\begin{aligned}M=&\pi\rho_\infty b^4w^2\left\{-a\frac{1}{b}\overline{h}-i\frac{1}{k}\left(\frac{1}{2}-a\right)\overline{\alpha}+\left(\frac{1}{8}+a^2\right)\overline{\alpha}-(T_4+T_{10})\frac{1}{\pi k^2}\overline{\beta}\right.\\&-i\left[T_1-T_8-(c-a)T_4+\frac{T_{11}}{2}\right]\frac{1}{\pi k}\overline{\beta}-\frac{1}{\pi}\left[T_7+(c-a)T_1\right]\overline{\beta}\\&\left.+2\frac{1}{k}\left(\frac{1}{2}+a\right)C(k)\left[\frac{1}{k}\overline{\alpha}+i\frac{1}{b}\overline{h}+i\left(\frac{1}{2}-a\right)\overline{\alpha}+\frac{T_{10}\overline{\beta}}{\pi k}+i\frac{T_{11}\overline{\beta}}{2\pi}\right]\right\}exp(iwt)\end{aligned} \tag{2.47}$$

$$
\begin{aligned}
H =& \pi\rho_\infty b^4 W^2 \left\{ \left\{ -\frac{T_1}{\pi b}\overline{h} - i\left[-2T_9 - T_1 + T_4\left(a-\frac{1}{2}\right)\right]\frac{1}{\pi k}\overline{\alpha} + 2\frac{1}{\pi}T_{13}\overline{\alpha} \right.\right.\\
&\left. -\frac{1}{\pi^2 k^2}\left(T_5 - T_4 T_{10}\right)\overline{\beta} + i\frac{1}{2\pi^2 k}T_4 T_{11}\overline{\beta} - \frac{T_3\overline{\beta}}{\pi^2} \right\}\\
&\left. -\pi\rho_\infty b^4 w^2 \frac{1}{k}T_{12}C(k)\left[\frac{1}{\pi k}\overline{\alpha} + i\frac{1}{\pi b}\overline{h} + i\frac{1}{\pi}\left(\frac{1}{2}-a\right)\overline{\alpha} + T_{10}\frac{1}{\pi^2 k}\overline{\beta} + i\frac{T_{11}\overline{\beta}}{2\pi^2}\right]\right\} exp(iwt)
\end{aligned}
\tag{2.48}
$$

Final form of Equation 2.46, equation 2.47, and equation 2.48 ;

$$
\begin{aligned}
L =& -\pi\rho_\infty b^3 w^2 \left\{ \left(1 - \frac{2iC(k)}{k}\right)\frac{\overline{h}}{b} + \left(-a - \frac{i\left(1+(1-2a)\,C(k)\right)}{k} - \frac{2C(k)}{k^2}\right)\overline{\alpha} \right.\\
&\left. + \left(-\frac{T_1}{\pi} + \frac{iT_4}{\pi k} - \frac{iT_{11}C(k)}{\pi k} - \frac{2T_{10}C(k)}{\pi k^2}\right)\overline{\beta} \right\} exp(iwt)
\end{aligned}
\tag{2.49}
$$

$$
\begin{aligned}
M =& \pi\rho_\infty b^4 w^2 \left\{ \left[-a + \frac{i\,(2a+1)\,C(k)}{k}\right]\frac{\overline{h}}{b} + \left[\frac{1}{8} + a^2 + \frac{(2a+1)\,C(k)}{k^2} \right.\right.\\
&\left. - \frac{i\left(\frac{1}{2}-a\right)\left(1-(2a+1)\,C(k)\right)}{k}\right]\overline{\alpha} + \left[-\frac{T_4 + T_{10} - (2a+1)\,T_{10}C(k)}{\pi k} \right.\\
&\left.\left. - \frac{T_7 + (c-a)\,T_1}{\pi} - \frac{i\left(T_8 - T_1 + (c-a)T_4 - \frac{1}{2}T_{11} + \left(\frac{1}{2}+a\right)T_{11}C(k)\right)}{\pi k}\right]\overline{\beta} \right\} exp(iwt)
\end{aligned}
\tag{2.50}
$$

$$H = \pi\rho_\infty b^4 w^2 \left\{ \left(-\frac{T_1}{\pi} - \frac{iT_{12}C(k)}{\pi k} \right) \frac{\overline{h}}{b} + \left(\frac{i\left(2T_9 + T_1 + \left(\frac{1}{2} - a\right)(T_4 - T_{12}C(k))\right)}{\pi k} \right. \right.$$

$$\left. + \frac{2T_{13}}{\pi} - \frac{T_{12}C(k)}{\pi k^2} \right) \overline{\alpha} + \left(-\frac{T_3}{\pi^2} + \frac{iT_4T_{11}}{2\pi^2 k} - \frac{iT_{11}T_{12}C(k)}{2\pi^2 k} - \frac{(T_5 - T_4T_{10})}{\pi^2 k^2} \right.$$

$$\left. \left. - \frac{T_{10}T_{12}C(k)}{\pi^2 k^2} \right) \overline{\beta} \right\} exp(iwt) \tag{2.51}$$

We can write the Equation 2.49, equation 2.50, and equation 2.51 in terms of aerodynamic coefficients as follows;

$$L = -\pi\rho_\infty b^3 w^2 \left[L_h \frac{\overline{h}}{b} + L_\alpha \overline{\alpha} + L_\beta \overline{\beta} \right] exp(iwt) \tag{2.52}$$

$$M = \pi\rho_\infty b^4 w^2 \left[M_h \frac{\overline{h}}{b} + M_\alpha \overline{\alpha} + M_\beta \overline{\beta} \right] exp(iwt)) \tag{2.53}$$

$$H = \pi\rho_\infty b^4 w^2 \left[H_h \frac{\overline{h}}{b} + H_\alpha \overline{\alpha} + H_\beta \overline{\beta} \right] exp(iwt) \tag{2.54}$$

the aerodynamic coefficients in these equations are as follows

$$L_h = 1 - \frac{2iC(k)}{k} \tag{2.55}$$

$$L_\alpha = -a - \frac{i(1 + (1 - 2a)C(k))}{k} - \frac{2C(k)}{k^2} \tag{2.56}$$

$$M_h = -a + \frac{i(2a + 1)C(k)}{k} \tag{2.57}$$

$$M_\alpha = \frac{1}{8} + a^2 - \frac{i\left(\frac{1}{2} - a\right)(1-(2a+1)C(k))}{k} + \frac{(2a+1)C(k)}{k^2} \tag{2.58}$$

$$L_\beta = -\frac{T_1}{\pi} + \frac{iT_4}{\pi k} - \frac{iT_{11}C(k)}{\pi k} - \frac{2T_{10}C(k)}{\pi k^2} \tag{2.59}$$

$$M_\beta = -\frac{T_7 + (c-a)T_1}{\pi} - \frac{i\left(T_8 - T_1 + (c-a)T_4 - \left(\frac{1}{2}\right)T_{11}C(k)\right)}{\pi k} \tag{2.60}$$

$$H_h = \left(-\frac{T_1}{\pi} - \frac{iT12C(k)}{\pi k}\right) \tag{2.61}$$

$$H_\alpha = \frac{2T_{13}}{\pi} + \frac{i\left(2T_9 + T_1 + \left(\frac{1}{2} - a\right)(T_4 - T_{12}C(k))\right)}{\pi k} - \frac{T_{12}C(k)}{\pi k^2} \tag{2.62}$$

$$H_\beta = -\frac{T_3}{\pi^2} + \frac{iT_4T_{11}}{2\pi^2 k} - \frac{iT_{11}T_{12}C(k)}{2\pi^2 k} - \frac{(T_5 - T_4T_{10})}{\pi^2 k^2} - \frac{T_{10}T_{12}C(k)}{\pi^2 k^2} \tag{2.63}$$

The terms T_i are functions of the distance between the hinge line and the midchord, and the distance between the midchord and the elastic axis [14];

$$\begin{aligned}
T_1 &= -\frac{1}{3}\sqrt{1-c^2}\left(2+c^2\right) + c\left(cos^{-1}c\right) \\
T_2 &= c\left(1-c^2\right) - \sqrt{1-c^2}\left(1+c^2\right)cos^{-1}c + c\left(cos^{-1}c\right)^2 \\
T_3 &= -\left(\frac{1}{8}+c^2\right)\left(cos^{-1}c\right)^2 + \frac{1}{4}c\sqrt{1-c^2}cos^{-1}c\left(7+2c^2\right) - \frac{1}{8}\left(1-c^2\right)\left(5c^2+4\right) \\
T_4 &= -cos^{-1}c + c\sqrt{1-c^2} \\
T_5 &= -\left(1-c^2\right) - \left(cos^{-1}c\right)^2 + 2c\sqrt{1-c^2}cos^{-1}c \\
T_6 &= T_2 \\
T_7 &= -\left(\frac{1}{8}+c^2\right)cos^{-1}c + \frac{1}{8}c\sqrt{1-c^2}\left(7+2c^2\right) \\
T_8 &= -\frac{1}{3}\sqrt{1-c^2}\left(2c^2+1\right) + c\left(cos^{-1}c\right)
\end{aligned}$$

$$
\begin{aligned}
T_9 &= \frac{1}{2}\left(\frac{1}{3}\sqrt{1-c^2}+aT_4\right)\\
T_{10} &= \sqrt{1-c^2}+cos^{-1}c\\
T_{11} &= cos^{-1}c\,(1-2c)+\sqrt{1-c^2}\,(2-c)\\
T_{12} &= \sqrt{1-c^2}\,(2+c)-cos^{-1}c\,(2c+1)\\
T_{13} &= \frac{1}{2}\left(-T_7-(c-a)\,T_1\right)\\
T_{14} &= \frac{1}{16}+\frac{1}{2}ac
\end{aligned}
\tag{2.64}
$$

if we rewrite the equations of motion, we reach the following equations;

$$mb\frac{\ddot{h}}{b}+S_\alpha\ddot{\alpha}+S_\beta\ddot{\beta}+bK_h\frac{h}{b}+L=0 \tag{2.65}$$

$$S_\alpha\frac{\ddot{h}}{b}+\frac{I_\alpha}{b}\alpha+\frac{\left((c-a)\,bS_\beta+I_\beta\right)}{b}\ddot{\beta}+\frac{K_\alpha}{b}\alpha-\frac{M}{b}=0 \tag{2.66}$$

$$S_\beta\frac{\ddot{h}}{b}+\frac{(c-a)\,bS_\beta+I_\beta}{b}\ddot{\alpha}+\frac{I_\beta}{b}\ddot{\beta}+\frac{K_\beta}{b}\beta-\frac{H}{b}=0 \tag{2.67}$$

If we write the equation 2.65, equation 2.66, and equation 2.67 in a matrix form where structural damping is neglected, we obtain the matrix equation below.

$$
\begin{aligned}
&\begin{bmatrix} mb & S_\alpha & S_\beta \\ S_\alpha & \frac{I_\alpha}{b} & \frac{(c-a)bS_\beta+I_\beta}{b} \\ S_\beta & \frac{(c-a)bS_\beta+I_\beta}{b} & \frac{I_\beta}{b} \end{bmatrix}
\begin{bmatrix} \frac{\ddot{h}}{b} \\ \ddot{\alpha} \\ \ddot{\beta} \end{bmatrix}
+\begin{bmatrix} bK_h & 0 & 0 \\ 0 & \frac{K_\alpha}{b} & 0 \\ 0 & 0 & \frac{K_\beta}{b} \end{bmatrix}
\begin{bmatrix} \frac{h}{b} \\ \alpha \\ \beta \end{bmatrix}\\
&-\pi\rho_\infty b^3 w^2 \begin{bmatrix} L_h & L_\alpha & L_\beta \\ M_h & M_\alpha & M_\beta \\ H_h & H_\alpha & H_\beta \end{bmatrix}
\begin{bmatrix} \overline{\frac{h}{b}} \\ \overline{\alpha} \\ \overline{\beta} \end{bmatrix}=0
\end{aligned}
\tag{2.68}
$$

Then;

$$[M]\,[\ddot{q}]+[K]\,[q]-\pi\rho_\infty b^3 w^2\,[A(k)]\,[\overline{q}]=0 \tag{2.69}$$

where $[M]$, $[K]$, $[A]$, $[q]$;

$$[M] = \begin{bmatrix} mb & S_\alpha & S_\beta \\ S_\alpha & \dfrac{I_\alpha}{b} & \dfrac{(c-a)bS_\beta + I_\beta}{b} \\ S_\beta & \dfrac{(c-a)bS_\beta + I_\beta}{b} & \dfrac{I_\beta}{b} \end{bmatrix} \tag{2.70}$$

$$[K] = \begin{bmatrix} bK_h & 0 & 0 \\ 0 & \dfrac{K_\alpha}{b} & 0 \\ 0 & 0 & \dfrac{K_\beta}{b} \end{bmatrix} \tag{2.71}$$

$$[q] = \begin{bmatrix} \dfrac{h}{b} \\ \alpha \\ \beta \end{bmatrix} \tag{2.72}$$

$$[A] = \begin{bmatrix} L_h & L_\alpha & L_\beta \\ M_h & M_\alpha & M_\beta \\ H_h & H_\alpha & H_\beta \end{bmatrix} \tag{2.73}$$

2.7 Solution of the 3 Degree of Freedom Model Equation Using Subsonic Aerodynamics Based on K-Method

To find the flutter boundaries of an aeroelastic system, equations of motion must be solved. Generally, structural damping is derived from the real part of the eigenvalue value obtained by solving the equations of motion given in matrix form. If the real part is negative, the motion means stable. If the movement is positive, it is understood that the movement is not stable. In k-method, structural damping is used in the system's equations of motion. In this method, equations of motion are brought into a simple form and eigenvalues are used to solve the flutter boundary. These eigenvalues contain structural damping values. Structural damping values are obtained from Eigenvalues. The point where the structural damping values change from negative to positive indicates the flutter boundary. This zero point is used to find flutter speed and frequency. Adding the structural damping coefficient to equation 2.77, the following equation is reached.

$$[M]\,[\ddot{q}] + (1+ig)\,[K]\,[q] - \pi\rho_\infty b^3 w^2\,[A(k)]\,[\overline{q}] = 0 \tag{2.74}$$

Motion in degree of freedoms of flight is simple harmonic motion. Then, equation 2.74 is converted to form as shown below.

$$-w^2\,[M]\,[\overline{q}] + (1+ig)\,[K]\,[\overline{q}] - \pi\rho_\infty b^3 w^2\,[A(k)]\,[\overline{q}] = 0 \tag{2.75}$$

After simplifying equation 2.75 by dividing by $-w^2$, equation below is obtained.

$$\left[[M]\,\pi\rho_\infty b^3\,[A(k)] - \frac{(1+ig)\,w_h^2}{w^2}\,[K]\right][\overline{q}] = 0 \tag{2.76}$$

where eigenvalue $= \dfrac{(1+ig)\,w_h^2}{w^2}$ and $g = \dfrac{Im(\lambda)}{Re(\lambda)}$,

After multiplying equation 2.76 with $\dfrac{1}{\pi\rho_\infty b^3}$, equation below is obtained.

$$\left\{\begin{bmatrix} \frac{mb}{\pi\rho_\infty b^3} & \frac{S_\alpha}{\pi\rho_\infty b^3} & \frac{S_\beta}{\pi\rho_\infty b^3} \\ \frac{S_\alpha}{\pi\rho_\infty b^3} & \frac{I_\alpha}{\pi\rho_\infty b^4} & \frac{(c-a)bS_\beta + I_\beta}{\pi\rho_\infty b^4} \\ \frac{S_\beta}{\pi\rho_\infty b^3} & \frac{(c-a)bS_\beta + I_\beta}{\pi\rho_\infty b^4} & \frac{I_\beta}{\pi\rho_\infty b^4} \end{bmatrix} + \begin{bmatrix} L_h & L_\alpha & L_\beta \\ M_h & M_\alpha & M_\beta \\ H_h & H_\alpha & H_\beta \end{bmatrix}\right.$$

$$\left. -\lambda \begin{bmatrix} \frac{K_h}{w_h^2\pi\rho_\infty b^2} & 0 & 0 \\ 0 & \frac{K_\alpha}{w_h^2\pi\rho_\infty b^4} & 0 \\ 0 & 0 & \frac{K_\alpha}{w_h^2\pi\rho_\infty b^4} \end{bmatrix}\right\} \begin{bmatrix} \frac{\overline{h}}{b} \\ \overline{\alpha} \\ \overline{\beta} \end{bmatrix} = 0 \tag{2.77}$$

Where;

$r_\alpha^2 = \frac{I_\alpha}{mb^2}$ which is the radius of gyration about the reference point

$\mu = \frac{m}{\rho_\infty \pi b^2}$ which is mass ratio

$r_\beta^2 = \frac{I_\beta}{m_\beta b^2}$ which is the radius of gyration about the hinge line

$K_h = mw_h^2$ which is the stiffness of typical wing section in plunge direction

$K_\alpha = I_\alpha w_\alpha^2$ which is the stiffness of typical wing section in pitch direction

$K_\beta = I_\beta w_\beta^2$ which is the angular stiffness of aileron section

(2.78)

after rearranging equation 2.77 with parameters from equation 4.4.2.4 , equations of motion associated with the k-method is obtained as follow.

$$\left\{ \begin{bmatrix} \mu & \mu X_\alpha & \frac{m_\beta}{m}\mu X_\beta \\ \mu X_\alpha & \mu r_\alpha^2 & \frac{m_\beta}{m}\mu\left((c-a)X_\beta + r_\beta^2\right) \\ \frac{m_\beta}{m}\mu X_\beta & \frac{m_\beta}{m}\mu\left((c-a)X_\beta + r_\beta^2\right) & \frac{m_\beta}{m}\mu r_\beta^2 \end{bmatrix} + \begin{bmatrix} L_h & L_\alpha & L_\beta \\ M_h & M_\alpha & M_\beta \\ H_h & H_\alpha & H_\beta \end{bmatrix} \right.$$

$$\left. -\lambda \begin{bmatrix} \mu & 0 & 0 \\ 0 & \frac{w_\alpha^2}{w_h^2}\mu r_\alpha^2 & 0 \\ 0 & 0 & \frac{w_\beta^2}{w_h^2}\frac{m_\beta}{m}\mu r_\beta^2 \end{bmatrix} \right\} \begin{bmatrix} \frac{\overline{h}}{b} \\ \overline{\alpha} \\ \overline{\beta} \end{bmatrix} = 0 \tag{2.79}$$

After simplifying equation 2.79 , equation below is obtained.

$$\left(\left[\overline{M}\right] + \left[\overline{A}\right] - \lambda \left[\overline{K}\right] \left[\overline{q}\right] \right) = 0 \tag{2.80}$$

Where,

$$\left[\overline{M}\right] = \begin{bmatrix} \mu & \mu X_\alpha & \frac{m_\beta}{m}\mu X_\beta \\ \mu X_\alpha & \mu r_\alpha^2 & \frac{m_\beta}{m}\mu\left((c-a)X_\beta + r_\beta^2\right) \\ \frac{m_\beta}{m}\mu X_\beta & \frac{m_\beta}{m}\mu\left((c-a)X_\beta + r_\beta^2\right) & \frac{m_\beta}{m}\mu r_\beta^2 \end{bmatrix} \tag{2.81}$$

$$\left[\overline{K}\right] = \begin{bmatrix} \mu & 0 & 0 \\ 0 & \frac{w_\alpha^2}{w_h^2}\mu r_\alpha^2 & 0 \\ 0 & 0 & \frac{w_\beta^2}{w_h^2}\frac{m_\beta}{m}\mu r_\beta^2 \end{bmatrix} \tag{2.82}$$

$$\left[\overline{A}(k)\right] = [A(k)] \tag{2.83}$$

2.7.1 Solution of The K-Method for Three Degree of Freedom System

We used the classic version of the aeroelastic system in a 2 degree of freedom system. In this system, in addition to our reduced frequency $k = \frac{bw}{U}$ value, structural damping (g) is also included. ”g” is a commonly used symbol in flutter limit calculations.

Adding the structural damping symbol to this solution is somewhat artificial. In real conditions, eigenvalues found in the solution of the flutter determinant in flight conditions allow structural damping to reach zero. Consequently, structural damping in a stable system is negative. In general, graphs containing the structural damping value drawn against the air speed are used in the flutter speed calculation. As a result, it is often referred to as this V-g chart. If equation 2.80 is rearranged, new equation of motion will be as follows.

$$\left[\left[\overline{K}\right]^{-1}\left(\left[\overline{M}\right]+\left[\overline{A}(k)\right]\right)-[I]\,\lambda\right][\overline{q}]=0 \tag{2.84}$$

The following steps should be followed to find the critical flutter speed from this equation.

1. A series of k values are defined, and can be selected from 0.001 to 1.
2. Aerodynamic coefficients $\left[\overline{A}(k)\right]$ are calculated for each k value.
3. Equation should be solved for each k values to determine eigenvalues.
4. Frequencies and damping coefficients are determined from these eigenvalues.
5. The corresponding speed can be determined as $U_i = \dfrac{bw_i}{k}$
6. U-w and U-g graphics are drawn for each mode.
7. Using the graphs, the flutter speed is found at the point where the damping passes from negative to positive.

MATLAB will be used to reduce solution time using the steps described above. To obtain eigenvalues from the flutter determinant, ”*eig*” command will be used.

2.8 Code Validation for Flutter Analysis

Flutter analysis methods of two dimensional, two degree of freedom and two dimensional, three degree of freedom systems presented in this chapter are aimed to be verified through examples by using MATLAB program. These Matlab codes save serious time in finding the flutter speed using the classic method and the k method. First example is given by Y.C.Fung [15].

2.8.1 Case 1

This example represents a two dimensional and two degree of freedom system. Values representing a two degree of freedom and a two dimensional incompressible system are given below. The values in this example represent the dimensionless parameters shown in the figure 2.1.The elastic axis located on the mid-chord line, and the mass distribution is symmetrical.Find flutter speed and frequency by using classical flutter method and k method.

$$b = 30ft, \qquad r_\alpha^2 = 0.6222$$

$$m = 269\ slugs\ per\ foot, \qquad w_h^2 = 0.775, \qquad w_\alpha^2 = 2.41$$

Solution;

Because the elastic axis is in the mid chord and the mass distribution is symmetrical;

$$a = 0, \;\; e = 0, \;\; x_\theta = 0$$

In this case;

$$\mu = \frac{m}{\pi \rho b^2} = 40$$

$$\rho = 0.002378\ slugs\ per\ foot$$

Classic Flutter Method; The aerodynamic coefficients obtained from Theodorsen's theory will be used both in the classical flutter method and in the k method as mentioned earlier. As a priority, the problem will be solved with the classical flutter method. The solution to this problem starts with the calculation of the Theodorsen's function from the k values (reduced frequency) we determined. After determining the value of this function,with a (determine the locations of the point P in figure ref fig: 2D typical section), k and these determined theodorsen's function values, aerodynamic coefficients are obtained.These values are used in the flutter determinant. When the determinant is opened, a complex expression occurs due to the structure of the Theodorsen's function. Therefore, both the real and the imaginary part must be equal to zero for the solution of this complex expression. Aerodynamic coefficients depend on the Theodorsen's function as known, and since this function depends on the value of k (reduced frequency), the result of the flutter determinant depends on the μ, k, w, x_θ, σ, r values. μ, r, x_θ, σ values were defined at the beginning of the problem. So for a given k (reduced frequency) value, there is a frequency value that makes both the real part and the imaginary part of the equation zero.As a result, the flutter frequency of the system can be calculated in w_θ using the classic flutter method.

Flutter speed calculated by using MATLAB code is shown as below;

$$U_{flutter}(flutter\ speed) = 161.5373 \text{ ft/sn}$$

K Method; Problem above calculated with classic flutter method can be calculated by k method also. K method was introduced in section 2.4 . Equation 2.24 is matris form of equations of motion. New parameter is introduced as $Z = \left(\frac{w_\theta}{w}\right)^2 (1+ig)$.

$$\left\{\mu\left[1-\left(\frac{w_h}{w}\right)^2(1+ig_h)\right]+l_h\right\}\frac{\overline{h}}{b}+(\mu x_\theta+l_\theta)\,\overline{\theta}=0$$
$$(\mu x_\theta+m_h)\frac{\overline{h}}{b}+\left\{\mu r^2\left[1-\left(\frac{w_\theta}{w}\right)^2(1+ig_\theta)\right]+m_\theta\right\}\overline{\theta}=0$$

If we apply this parameter to equation above and then get the flutter determinant, we get the following result.

$$\begin{vmatrix} \mu\left(1-\sigma^2 Z\right)+l_h & \mu x_\theta+l_\theta \\ \mu x_\theta+m_h & \mu r^2(1-Z)+m_\theta \end{vmatrix}=0$$

When flutter determinant is being solved by using MATLAB code to find flutter speed, Steps introduced below is used;

1. Eigenvalue parameter is given as $\lambda = \left(\frac{w_\theta}{w}\right)^2 (1+ig)$

2. eigenvalue problem should been solved for each $k = \frac{bw}{U}$ (reduced frequency) value.

3. parameters shown below should been found to find damping parameter (g) for each k (reduced frequency) value.

$$reel(\lambda) = \left(\frac{w_\theta}{w}\right)^2, \quad Imaginer(\lambda) = \left(\frac{w_\theta}{w}\right)^2 g$$
$$g(\text{damping parameter}) = \frac{Imaginer(\lambda)}{reel(\lambda)} \tag{2.85}$$

4. to find flutter speed equation below is used for each value of k(reduced frequency).

$$U = \left(\frac{bw_\theta}{1}\right)\left(\frac{1}{k}\right)\left(\frac{w}{w_\theta}\right) \tag{2.86}$$

5. g (damping parameter) vs. U (speed) plot should been created.

6. The point where g (damping parameter) is equal to zero shows place where U (speed) is equal to $U_{flutter}$ (flutter speed).

7. And point found at step 6 gives flutter frequency $w_{flutter}$ from reduced frequency equation $(k_{flutter} = \frac{bw_{flutter}}{U_{flutter}})$

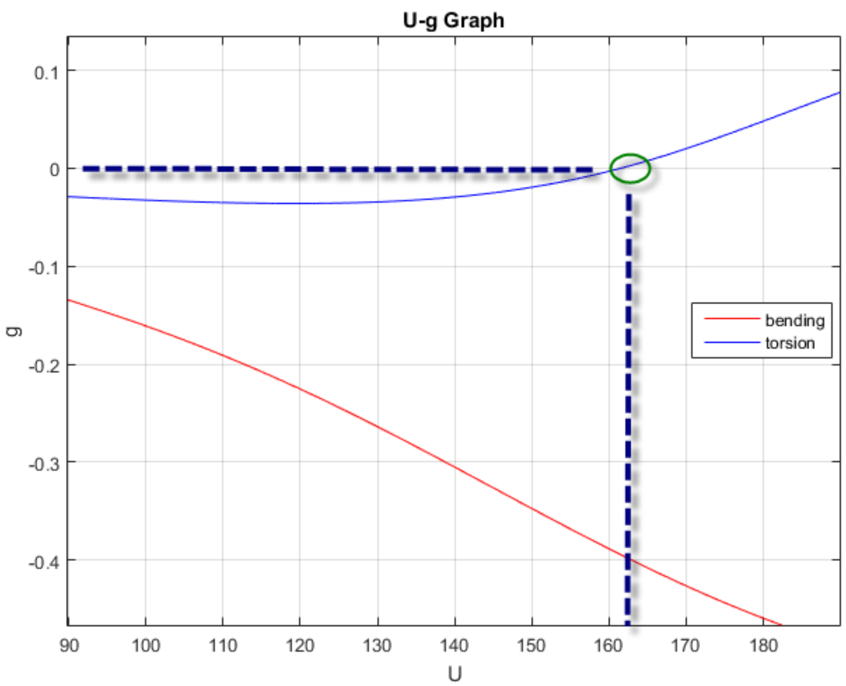

Figure 2.4 : Damping vs. speed plot of the 2DoF typical section (k-method).

After following the steps described above, the graph 2.4 was obtained. The area enclosed in the green circle in this graph shows where the damping parameter passes 0. The place corresponding to the point where the damping is 0 represents the flutter speed. To see the speed value at this point more clearly, after zooming on the graph, the following graph is obtained.

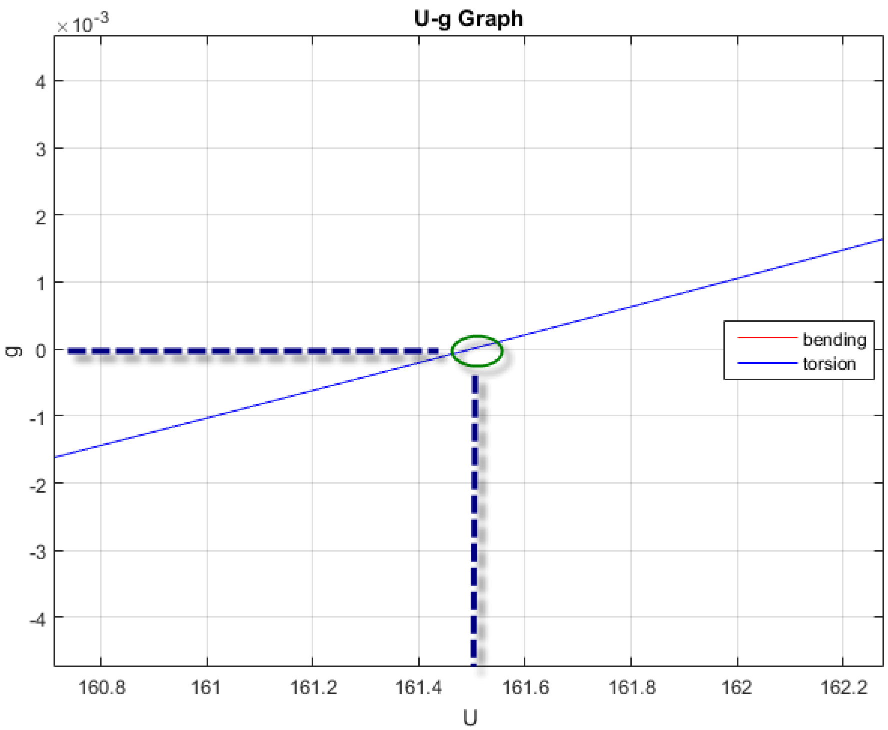

Figure 2.5 : Damping vs. speed plot of the 2DoF typical section (k-method).

As seen from the graph, the flutter speed is approximately 161.5 ft/sn.

The result of this proplem is 162 ft/sn. in the book "an introduction to the theory of aeroelasticity" [15] which we use as a reference in this problem.

Table 2.1 : Table comparing the results obtained with the reference results.

	from reference book	classic flutter method	k-method
Flutter Speed (ft/sn)	162	161.5373	161.5

The argument we obtained from this example; The results table 2.1 obtained by applying both the classic flutter method and the k method are almost perfect with the results given in the reference book.

2.8.2 Case 2

the inference we obtained from this example; The results obtained by applying both the classic flutter method and the k method are almost same with the results given in the reference book.the second example is an example taken from reference [16]. This example represents a 2 dimensional and 3 degree of freedom system. Values representing a three degree of freedom and a two dimensional incompressible system are given below. The values in this example represent the dimensionless parameters shown in the figure 2.2.

$$
\begin{array}{llll}
a = -0.4, & x_\alpha = 0.2 & c = 0.6 & \\
\mu = 40\ , & \dfrac{m_\beta}{m} = 0.2, & r_\alpha^2 = 0.25 & \\
r_\beta^2 = 0.05, & x_\beta = 0.0125, & \dfrac{w_h}{w_\alpha} = 0.5 & \dfrac{w_h}{w_\beta} = 0.2108
\end{array}
$$

K Method; This problem is solved by using the k method described in section 2.7. The steps used to solve this problem are similar to the steps used in the previous k method.The eigenvalue values of the flutter determinant of the 3 degree of freedom system are found using the MATLAB code. This flutter determinant used was given in section 2.7;

$$\left(\left[\overline{M}\right] + \left[\overline{A}\right] - \lambda \left[\overline{K}\right] \left[\overline{q}\right]\right) = 0$$

When flutter determinant is being solved by using MATLAB code to find flutter speed,Steps introduced below is used

1. Eigenvalue parameter is given as $\lambda = \left(\frac{w_h}{w}\right)^2 (1 + ig)$
2. eigenvalue problem should been solved for each $k = \dfrac{bw}{U}$ (reduced frequency) value.

3. parameters shown below should been found to find damping parameter (g) for each k (reduced frequency) value.

$$reel(\lambda) = \left(\frac{w_h}{w}\right)^2, \quad Imaginer(\lambda) = \left(\frac{w_h}{w}\right)^2 g$$
$$g(\text{damping parameter}) = \frac{Imaginer(\lambda)}{reel(\lambda)} \tag{2.87}$$

4. Dimensionless air speed ;

$$U_{dimensionless} = \frac{U}{bw_h} \tag{2.88}$$

5. reel part of square root of eigenvalue (λ) found in step 2 is calculated as shown below;

$$\sqrt{reel(\lambda)} = \left(\frac{w_h}{w}\right),$$

6. to find dimensionless air speed, equation below is used for each value of k(reduced frequency).

$$U_{dimensionless} = \left(\frac{1}{\frac{w_h}{w}}\right)\left(\frac{1}{k}\right) = \left(\frac{U}{bw_h}\right) \tag{2.89}$$

7. g (damping parameter) vs. $U_{dimensionless}$ plot should been created.

8. The point where g (damping parameter) is equal to zero shows place where $U_{dimensionless}$ is equal to $\dfrac{U_{flutter}}{bw_h}$.

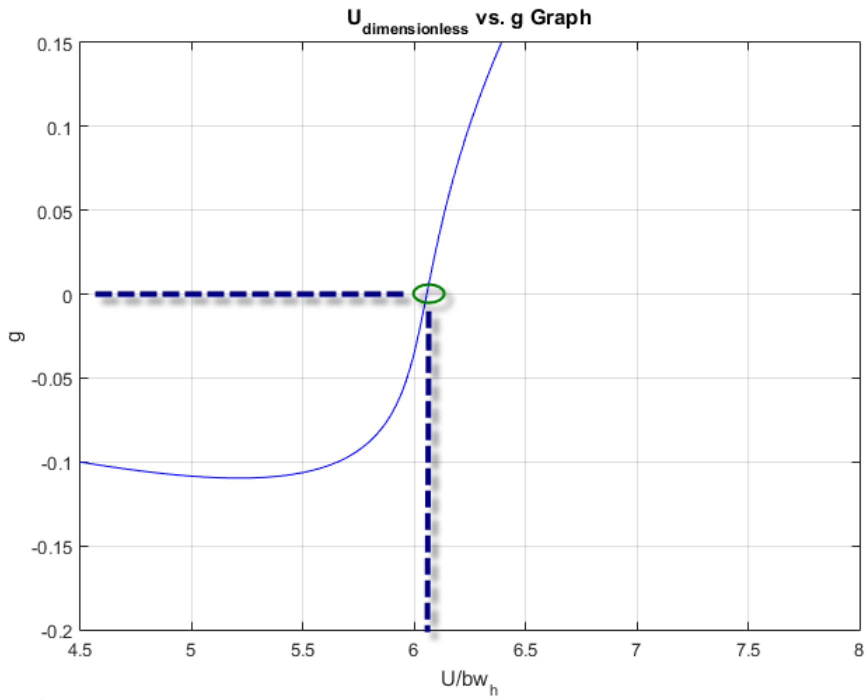

Figure 2.6 : Damping vs. dimensionless air speed plot (k-method).

After applying all these steps, the graphic in figure 2.6 is obtained from the MATLAB code.As mentioned above, the dimensionless air speed is obtained from the point coming to the region where the damping parameter is zero. On the graph, this point zone is circled in green. A vertical dashed line is drawn on the graph towards the x axis, where the dimensionless air velocity value corresponding to this point is located. in order to see the dimensionless air speed value on this x-axis more clearly, the graph is zoomed and then the following graph in figure 2.7 is obtained.

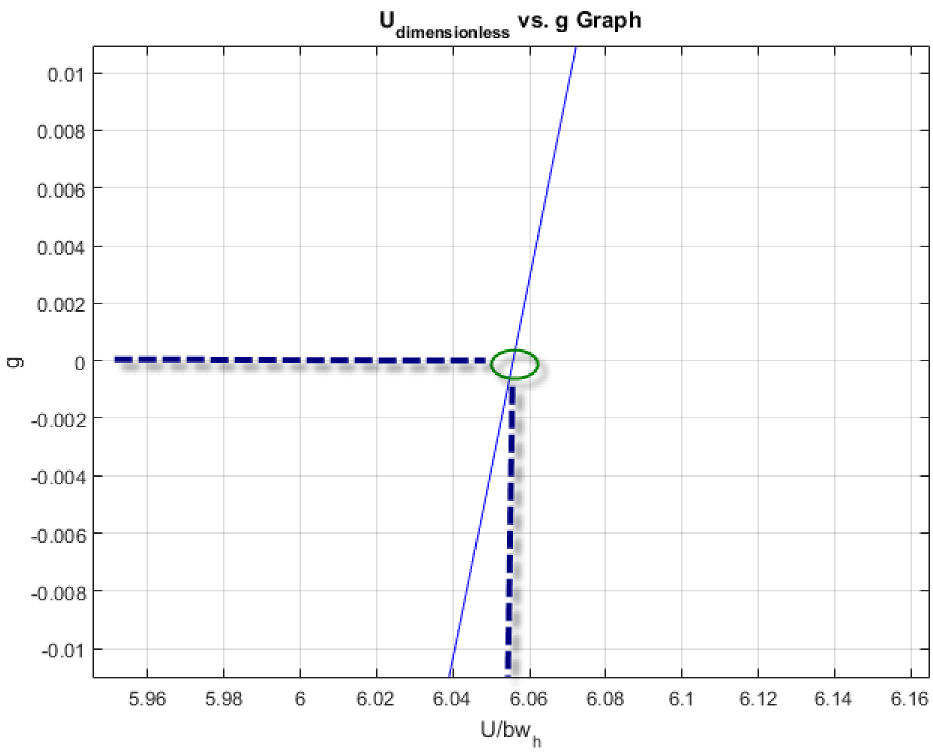

Figure 2.7 : Damping vs. dimensionless air speed plot (k-method).

As seen from the graph, the dimensionless air speed $\left(\frac{U_f}{bw_h}\right)$ is approximately 6.055

Table 2.2 : Table comparing the results obtained with the reference result.

	from reference book[16]	k-method
Flutter Speed (ft/sn)	6.05	6.055

The argument we obtained from this example; The results table 2.2 obtained by applying the k method is almost perfect with the result given in the reference book [16].

3. SUBSONIC 3 DIMENSIONAL FLUTTER ANALYSIS OF A WING STRUCTURE

3.1 Introduction

In this section, it is aimed to create an analytical solution method for the 3D wing structure. This method will be created based on the uniform cantilever wing structure. Analysis of a structure with pure bending and pure torsional modes will be shown in the 3D flutter method we found using the assumed mode shape method. This method is then applied on a sample from the literature and the results are compared with the results from the literature.

3.2 Exact Treatment of The Bending-Torsion Flutter of a Uniform Cantilever Wing

The most useful flutter analyzes are based on the assumption that the structure consists of superpositions of a number of predetermined deformation modes. This process is used on the structure having externally excited vibrations. Structures with inertial and elastic properties at a certain point and difficult to express mathematically leave the analyst in a difficult situation. Accordingly, flutter analysis of some simple wing structures that remained within the limits of linearized aerodynamic and elastic theories can be fully resolved. Such solutions are used as a comparison tool to find out whether the solutions of other structures are correct. Examples of such simple systems are the systems described in chapter 2. In addition, structures with large aspect ratio values and representative structures with flaps used by Myklestad [17] feature lumped-mass approaches. Unless too many degrees of freedom are given, it is unlikely that a real structure will get too close to reality in the flutter analysis. The exact solutions applied for uniform wings are used to compare approximate solution methods. they are unique in terms of improving distributed parameters with partial differential tests and using flutter mode shape functions along the wing. The first conclusion about this subject was

Goland [18], who dealt with the bending-torsion flutter analysis of cantilever wings with constant chord value, uniformly distributed mass and elastic properties.

It is assumed that the EI and GJ values, which express the stiffness of the wing structure in bending and torsion respectively, are deformed in a manner similar to those of the slender beam. Any section on the structure has infinite rigid value and the elastic axis is considered straight.In case the vertical movement $(w(y,t))$ and twist movement $(\theta(y,t))$ of the elastic axis of the structure are specified, the strain state of the structure is completed. The representation of the wing structure moving in the air exposed to aerodynamic force $L(y,t)$ and moment $M_y(y,t)$ is shown in the figure below.

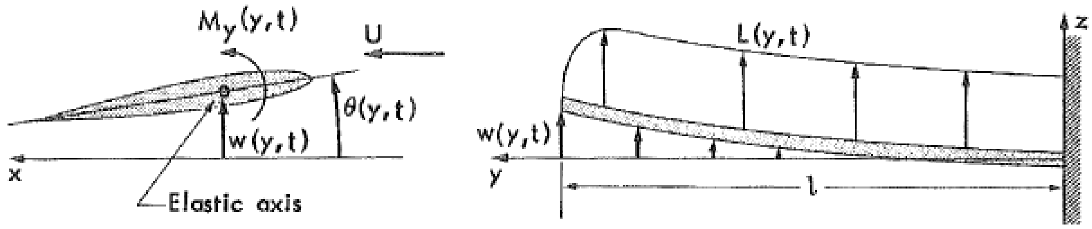

Figure 3.1 : Two views of a uniform restrained wing deforming in bending and torsion under running aerodynamic loads $L(y,t)$ and $M_y(y,t)$.

equations of motion for a wing with constant stifness and torsion stiffness values along the wing span are given below.

$$
\begin{aligned}
m\ddot{w}(y,t) - S_y\ddot{\theta}(y,t) + EI\frac{\partial^4 w(y,t)}{\partial y^4} &= L(y,t) \\
I_y\ddot{\theta}(y,t) - S_y\ddot{w}(y,t) - GJ\frac{\partial^2 \theta(y,t)}{\partial y^2} &= M_y(y,t)
\end{aligned} \tag{3.1}
$$

Superscript dots represent derivative over time t. The movement of the wing structure is assumed to be simple harmonic motion. According to this assumption, the movement in vertical and angular direction is shown as follows.

$$
\begin{aligned}
w(y,t) &= W_1(y)\cos wt + W_2(y)\sin wt \\
\theta(y,t) &= \Theta_1(y)\cos wt + \Theta_2 \sin wt
\end{aligned} \tag{3.2}
$$

Where W_1, W_2 and Θ_1, Θ_2 describe bending and twisting deformations of wing structure. It is assumed that the wing structure has a low flight speed to provide incompressible aerodynamic condition. In addition, the aspect ration is assumed to be high enough to allow the use of strip theory. The lift and moment in these conditions are given below.

$$\begin{aligned} L(y,t) &= w^2 L_w w + w L'_w \dot{w} + w^2 L_\theta + w L'_\theta \dot{\theta} \\ M(y,t) &= w^2 M_w w + w M'_w \dot{w} + w^2 M_\theta \theta + w M'_\theta \dot{\theta} \end{aligned} \tag{3.3}$$

The coefficients given in this equation are the function of air density and wing chord. At the same time, these coefficients indirectly depend on the value of k(reduced frequency). If we integrate the equation 3.2 and equation 3.3 into equation 3.1, we separate this resulting equation as those with $\cos wt$ and $\sin wt$ coefficients. Values in parentheses must be zero, since all of these attempts are zero at any point in time. so we have 4 different equations.

$$\begin{aligned} & EI\frac{d^4 W_1}{dy^4} - m w^2 W_1 - w^2 L_w W_1 - w^2 L'_w W_2 \\ & + S_y w^2 \Theta_1 - w^2 L_\theta \Theta_1 - w^2 L'_\theta \Theta_2 = 0 \end{aligned} \tag{3.4}$$

$$\begin{aligned} & w^2 L'_w W_1 + EI\frac{d^4 W_2}{dy^4} - m w^2 W_2 - w^2 L_w W_2 \\ & + w^2 L'_\theta \Theta_1 + S_y w^2 \Theta_2 - w^2 L_\theta \Theta_2 = 0 \end{aligned} \tag{3.5}$$

$$\begin{aligned} & - w^2 S_y W_1 + w^2 M_w W_1 + w^2 M'_w W_2 + GJ\frac{d^2 \Theta_1}{dy^2} \\ & + I_y w^2 \Theta_1 + w^2 M_\theta \Theta_1 + w^2 M'_\theta \Theta_2 = 0 \end{aligned} \tag{3.6}$$

$$\begin{aligned} & - w^2 M'_w W_1 - w^2 S_y W_2 + w^2 M_w W_2 - w^2 M_\theta \Theta_1 \\ & + GJ\frac{d^2 \Theta_2}{dy^2} + I_y w^2 \Theta_2 + w^2 M_\theta \Theta_2 = 0 \end{aligned} \tag{3.7}$$

Boundary conditions ;

at $y = 0$	There is no twist, bending deflection, and slope
at $y = l$	There is no torque, shear, and bending moment

Then;

$$W_1(0) = W_2(0) = \frac{dW_1(0)}{dy} = \frac{dW_2(0)}{dy} = \Theta_1(0) = \Theta_2(0) = 0 \tag{3.8}$$

$$\frac{d^2W_1(l)}{dy^2} = \frac{d^2W_2(l)}{dy^2} = \frac{d^3W_2(l)}{dy^3} = \frac{d^3W_2(l)}{dy^3} = \frac{d\Theta_1(l)}{dy} = \frac{d\Theta_2(l)}{dy} = 0 \tag{3.9}$$

In the solution of this equation, the method used in the solution of the homogeneous differential equation with a constant coefficient is used. In this equation, as already mentioned, simple harmonic motion will be based on. Then the accuracy of the calculation is increased by using the Laplace transform.The solution of the equation is started using the assumption stated below according to the known frequency and reduced frequency (k) value.

$$\begin{aligned} W_1 &= Ae^{\lambda y} \\ W_2 &= Be^{\lambda y} \\ \Theta_1 &= Ce^{\lambda y} \\ \Theta_2 &= De^{\lambda y} \end{aligned} \tag{3.10}$$

We can apply this assumption in equation 3.4, equation 3.5, equation 3.6, and equation 3.7, and write the coefficients of the unknown as different equations. In order for these equations to reach the result, the determinant of these equations, which have been turned into a matrix form, must be equal to zero. The opening of this determinant takes us to the sixth order polynomial of λ^2.

$$\begin{vmatrix} \left[\frac{EI}{w^2}\lambda^4 - m - L_w\right] & -L'_w & [S_y - L_\theta] & -L'_\theta \\ L'_w & \left[\frac{EI}{w^2}\lambda^4 - m - L_w\right] & L'_\theta & [S_y - L_\theta] \\ [M_w - S_y] & M'_w & \left[\frac{GJ}{w^2}\lambda^2 + I_y + M_\theta\right] & M'_\theta \\ -M'_w & [M_w - S_y] & -M'_\theta & \left[\frac{GJ}{w^2}\lambda^2 + I_y + M_\theta\right] \end{vmatrix} = 0 \tag{3.11}$$

All coefficients of the polynomial obtained by opening this determinant are real. This polynomial has 6 complex roots in λ^2. This λ^2 value gives the complex conjugate value of a pair λ as shown below.

$$\begin{aligned} \lambda_r &= \xi_r + i\eta_r \\ (\lambda_r)_{conjugate} &= \xi_r - i\eta_r \end{aligned} \tag{3.12}$$

For these functions to be real, there must be a $(A_r)_{conjugate}$ associated with $(\lambda_r) conjugate$. Each conjugate pair combines to form the following definition.

$$A_r e^{(\xi_r + i\eta_r)y} + (A_r)_{conjugate} e^{(\xi_r - i\eta_r)y} = e^{\xi r y}\left[a_r \cos \eta_r y + a'_r \sin \eta_r y\right] \tag{3.13}$$

Constants in this equation;

$$\begin{aligned} a_r &= A_r + (A_r)_{conjugate} \\ a'_r &= i\left[A_r - (A_r)_{conjugate}\right] \end{aligned} \tag{3.14}$$

If equation 3.12 is written in the form of equation 3.13, the following equation is obtained.

$$\begin{aligned} W_1(y) &= \sum_{r=1}^{6} e^{\xi_r y}\left[a_r \cos \eta_r y + a'_r \sin \eta_r y\right] \\ W_2(y) &= \sum_{r=1}^{6} e^{\xi_r y}\left[b_r \cos \eta_r y + b'_r \sin \eta_r y\right] \\ \Theta_1(y) &= \sum_{r=1}^{6} e^{\xi_r y}\left[c_r \cos \eta_r y + c'_r \sin \eta_r y\right] \\ \Theta_2(y) &= \sum_{r=1}^{6} e^{\xi_r y}\left[d_r \cos \eta_r y + d'_r \sin \eta_r y\right] \end{aligned} \tag{3.15}$$

36 quantities b_r, b'_r, c_r, c'_r, d_r and d'_r are associated with 12 a_r and a'_r. The following relations have emerged by substituting the solutions obtained from equation 3.12 into equations 3.4-3.7 and then finding the $\frac{B_r}{A_r}$, $\frac{C_r}{A_r}$, and $\frac{D_r}{A_r}$ ratios.

$$
\begin{aligned}
\frac{B_r}{A_r} &= \alpha_r + i\beta_r \\
\frac{(B_r)_{conjugate}}{(A_r)_{conjugate}} &= \alpha_r - i\beta_r \\
b_r &= \alpha_r a_r + \beta_r a_t' \\
b_r' &= -\beta_r a_r + \alpha_r a_r'
\end{aligned}
\tag{3.16}
$$

The a_r and a_r' constants, which must be determined according to the boundary conditions in 3.8 and 3.9 still exist. The next step is to adapt the general solution to a specific beam model. In this part there is a difference from the method created for the eigenvalue calculation of the characteristic equation of motion having free vibration. The w (frequency) and k (reduced frequency) values used in the calculation of aerodynamic coefficients should be determined in advance until one is found that satisfies the boundary conditions. The literal coefficients in the equations are given in 12 a_r and a_r'. These coefficients are used in boundary conditions. As a result, 12 real, homogeneous and simultaneous equations are obtained. All coefficients obtained are real, but the determinant obtained from here does not vanish. All these steps are repeated until the k_F and w_F value is found, which makes the determinant zero. This situation where the wing structure has this simple harmonic flutter state is considered as a critical situation and the velocity in this state is defined as the flutter speed. Flutter speed is calculated as shown below from frequency and reduced frequency which bring wing structure into critical flutter situation.

$$
U_F = \frac{b w_F}{k_F} \tag{3.17}
$$

The bending and torsion mode shapes are obtained by placing the a_r and a_r' values in equation 3.15, after this equation is placed in equation 3.2. The amount of energy initially given to the system determines the magnitude of the system's oscillation. Due to this situation one of these constants remains uncertain. Difference is observed between the vibration modes of the system and the characteristic modes of the vacuum. Since the $\frac{W_1}{W_2}$, $\frac{\Theta_1}{\Theta_2}$ and $\frac{w}{\theta}$ ratios change along the wing span, the bending and torsional movements at various stations on the wing do not pass from zero at the same time. Therefore the degrees of freedom are not in the same phase. This type of vibration seen in the system shows waves that move in deflection and twist. A system with only inertia and stiffness values that do not have damping value cannot have these waves by vibration without having external force effects. Phase between aerodynamic loads and movements cause such waves.

3.3 Aeroelastic Modes

In chapter 2, it was analyzed in detail how 2 dimensional 2 degree of freedom and 3 degree of freedom systems show vibration movement in an air flow and how flutter speed is calculated. This theory is valid in a flexible structural wing in the air flow. However, since the degree of freedom is infinite in elastic structures, in this theory the aeroelastic mode can be imagined in an infinite number. These modes completely overlap with the free vibration modes of the immobile structural wing. A wind tunnel can be designed where the air velocity is regularly increased starting from zero and the frequency and structural damping of the structural wing model is observed. At low air speed, the air absorbs the energy caused by vibration in the system and the damping rates grow with increasing air speed. As a result, with the increase of air speed, the decreasing damping value of the structure increases with approaching the flutter speed and reaches the zero value. In some cases aeroelastic modes include the movement of the entire structure of the aircraft. however, critical modes in flutter velocity analysis generally occur on certain aerodynamic surfaces. In such cases, the rest of the aircraft is neglected and the wing is modeled as a cantilever beam and the modes of this model are examined. The pure bending and pure torsion modes of this model are first examined to examine the reliability of this simplification. Important structural deformations are defined as the bending and twisting of wing structures with large aspect ratio. The lowest frequency coupled modes of the wing structure in zero air velocity modeled as cantilever beam are examined. As mentioned above, these modes are generally the lowest frequency bending and subsequent torsion modes. Studies show that pure bending and pure torsional modes cause flutter mode.

Theory of transient motion is more complex than simple harmonic motion. When calculating aeroelastic modes, flutter analysis cannot estimate the stability of the modes in terms of speed.In simple structures where strip theory can be used to calculate air load, the calculation mentioned in the previous sentence can be used.

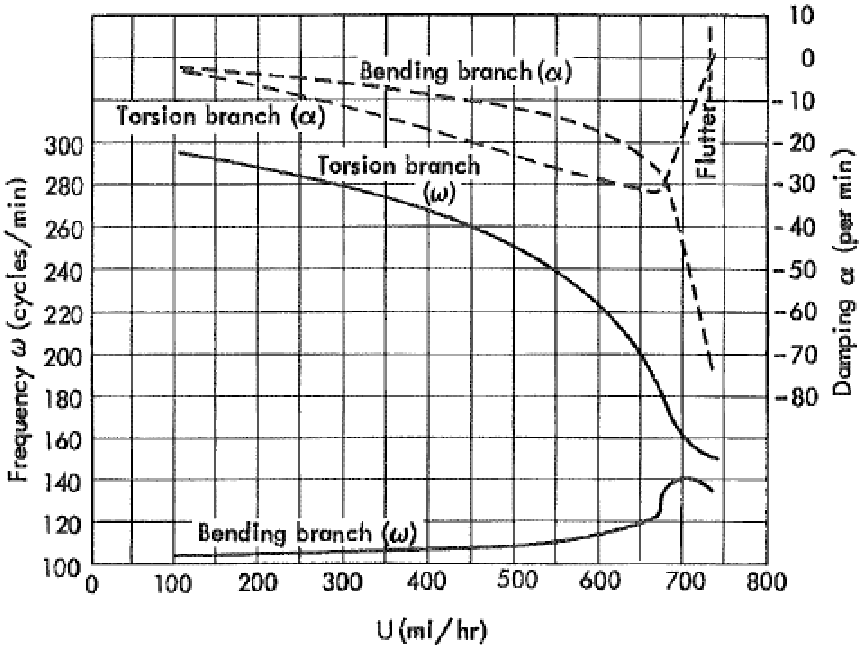

Figure 3.2 : Frequency and damping of the fundamental aeroelastic modes plotted vs. airspeed for an airplane wing with natural bending and torsional frequencies 103.5 cycles/min and 304 cycles/min[22].

Goland and Luke made this calculation for wings with a tip mass and large aspect ratio [12]. In incompressible flows, the calculation of lift and moment is calculated similar to that described in chapter 2. Elastic and inertial properties are found using pre-determined deformations shapes used in Rayleigh-Ritz method. In figure 3.4 and 3.6 , the ratio of bending frequency in vacuum to torsion frequency , which is the results of reference [12], was found again. In this section, it is only aimed to investigate the aeroelastic modes of the aircraft. In these 2 figures, the y axis has the frequency value (w), which is the real part of the time-dependent complex equation, and the damping value (α), which is the imaginary part.Flight speed (U) is given on the x axis in these figures.

$$e^{(-\alpha+iw)t} \tag{3.18}$$

The α value associated with the damping ratio of the structure is used to find the magnitude of the degree of damping of the structure.

$$\text{Damping Ratio} = \frac{\alpha}{\sqrt{\alpha^2+w^2}} \tag{3.19}$$

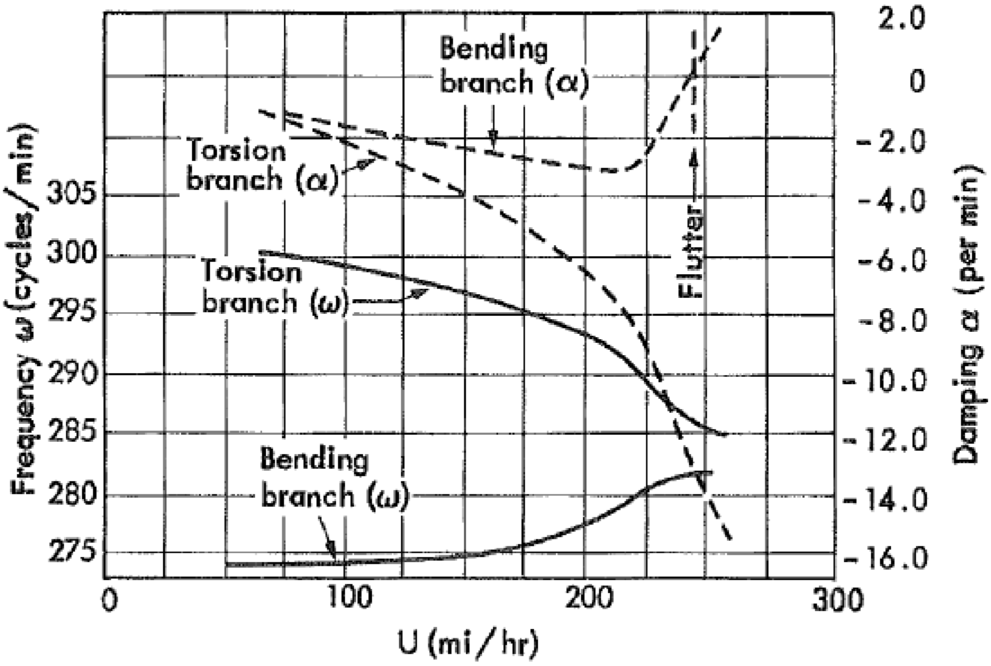

Figure 3.3 : Frequency and damping of the fundamental aeroelastic modes plotted vs. airspeed for an airplane wing with natural bending and torsional frequencies 276 cycles/min and 304 cycles/min[22].

Figure 3.4 is given for the system with natural bending frequency of 103 rpm and torsion frequency of 304 rpm. The ratio of these values is generally quite common for metal wings with skin structure. According to this figure, the first torsion mode starting from U = 0 indicates that it is a flutter mode. Both modes in the figure are a function of the air velocity and show a highly reliable damping value. As shown in the figure, the damping value of the bending branch is lower than that of the torsion branch, but the damping ratio of the bending branch is greater than that of the torsion branch until it drops to a rapid decrease in the flutter state. If we come to the frequency value of the modes, the frequency values of the bending and torsion modes start to get very different from each other as they approach the flutter condition. If we look at figure 3.6, we see a less common case where the bending frequency and torsion frequency are 276 rpm and 304 rpm, respectively. In this case, the flutter speed is lower due to the frequency resonance effect. At all air speeds, the damping value of the bending branch is lower than the damping value of the torsion branch. As can be understood from this figure, we cannot observe the transition of aeroelastic mode to flutter mode until the flow rate gets closer to the flutter speed. This indicates that an airplane can fly at close speeds before reaching the flutter speed during flight. This also explains the emergence of the bending and torsion flutter condition suddenly when it reaches the flutter speed. According to figure 3.4 and figure 3.6, if the flutter speed is exceeded 5 miles / hour, the blades are irreversibly damaged and become unusable. If a structure does not have an estimated range when investigating the flutter condition, this research should be done very precisely. Dynamic properties in an structure change with flight speed due to the compressibility of air and deformations occurring in the structure. Rigid body degrees of freedom are included in calculations to facilitate flutter calculation and save time.

3.4 Flutter Analysis by Assumed-Mode Methods

To find the flutter equation of a system, the way known as Rayleigh-Ritz method is the method obtained by using a finite number of mode shapes. For this we consider a flat structure on the xy plane and assume that the structure on this plane is quite rigid. We only get comprehensive information about stress and strain in the structure if we know the $w(x,y,t)$ value that represents the displacement of the structure according to the initial condition. Two methods are used to obtain the assumed modes used in the methods developed for approximately all flutter analysis. The first of these two methods takes advantage of the normal vibration modes, a more classic way. The second method uses primitive modes, which is a more efficient way. If the first method using the normal modes of the structure is used, the displacement statement defined below is used.

$$w(x,y,t) = \sum_{i=1}^{\infty} \phi_i(x,y)\xi_i(t) \tag{3.20}$$

This statement allows us to reach another statement below.

$$M_j\ddot{\xi}_j + M_j w_j^2 \xi_j = \Xi_j \qquad (j = 1,2,3....,\infty) \tag{3.21}$$

$\phi_j(x,y)$ and w_j used in this expression represent the mod shape and natural frequency.Below are the jth generalized mass and generalized force equations:

$$M_j = \iint_S \phi_j^2 \rho(x,y)\, dx\, dy \tag{3.22}$$

$$\Xi_j = \iint_S F_z(x,y,t)\phi_j(x,y)\,dx\,dy \tag{3.23}$$

The $F_z(x,y,t)$ unit used in the generalized force equation represents the external force for the unit xy area with the motion in the z direction. The integration process is calculated over the projection area of the entire aircraft. $F_z(x,y,t)$ used in such a calculation represents the pressure difference between the lower and upper surfaces of the structure during flight. If we formulate this difference in pressure, we will get the following definition.

$$F_z(x,y,t) = (p_L - p_U) = -\Delta p_a(x,y,t) \tag{3.24}$$

If we take an unrestrained aircraft, rigid body plunging, pitching and rolling are achieved as the first three modes.

$$\begin{aligned} \phi_1(x,y) &= 1 \\ \phi_2(x,y) &= -x \\ \phi_3(x,y) &= y \end{aligned} \tag{3.25}$$

These modes have zero natural frequency value. The generalized masses are the sum of the moment of inertia about the y axis and the moment of inertia about the x axis. Generalized forces are lift, pitching moment and rolling moment. The deformation shapes obtained using the $\gamma_i(x,y)$ function to create the flutter mode are given below.

$$w(x,y,t) = \sum_{i=1}^{n} \gamma_i(x,y) q_i(t) \tag{3.26}$$

Finally, the motion equations obtained are;

$$\sum_{j=1}^{n} m_{ij}\ddot{q}_j + \sum_{j=1}^{n} k_{ij} q_j = Q_i \qquad (i = 1,2,3,...,n) \tag{3.27}$$

Where,

$$
\begin{aligned}
Q_i &= \iint_S F_z(x,y,t)\gamma_i(x,y)\,dx\,dy = -\iint_S \Delta p_a(x,y,t)\gamma_i(x,y)\,dx\,dy \\
m_{ij} &= \iint_S \gamma_i(x,y)\gamma_j(x,y)\rho(x,y)\,dx\,dy \\
k_{ij} &= \iint_S \gamma_i(x,y) \iint_S k(x,y;\xi,\eta)\gamma_j(\xi,\eta)\,d\xi\,d\eta\,dx\,dy
\end{aligned}
\tag{3.28}
$$

The kinetic and potential energy expressions that enter the Lagrange's equations are as shown below.

$$
\begin{aligned}
T &= \frac{1}{2}\sum_{i=1}^{n}\sum_{j=1}^{n} m_{ij}\dot{q}_i\dot{q}_j \\
U_E &= \frac{1}{2}\sum_{i=1}^{n}\sum_{j=1}^{n} k_{ij}q_iq_j
\end{aligned}
\tag{3.29}
$$

We can use solid body degrees of freedom instead of γ_i values. In this case, the associated stiffness values disappear. The simple harmonic motion expression to be used in the calculation of the flutter is given below.

$$
\xi_j(t) = \overline{\xi}e^{iwt} \quad \text{or} \quad q_j(t) = \overline{q}e^{iwt} \tag{3.30}
$$

In this expression, $\overline{\xi}$ and $\overline{q}$ values are coefficients. Based on the system being linear, we get external force as follows.

$$
F_z(x,y,t) = \overline{F_z}(x,y)e^{iwt} = -\Delta\overline{p}_a(x,y)e^{iwt} \tag{3.31}
$$

Time-dependent variables in equation 3.31 are removed. $\Delta\overline{p}_a(x,y)$ is a function dependent on the amplitudes of the different modes. hence Ξ_j and Q_j depend on these amplitudes. The motion equation is a homogeneous equation depending on $\overline{\xi}$ or $\overline{q}$ and this equation leads us to the problem of algebraic eigenvalue. To obtain a result that is not equal to zero, the determinant of the coefficients must be equal to zero. This condition gives us the flutter determinant. We obtain complex numbers from the solution of the flutter determinant due to the phase difference between aerodynamic loads and motion. As explained in part 2, different parts of the structure do not move in the same phase. The flutter mode shape of the structure is given below.

$$Re\left\{\sum_{j=1}^{n}\gamma_j(x,y)\overline{q}_j\right\} \tag{3.32}$$

It can be difficult to get results from this equation. Modeling the structure that we want to apply flutter analysis like a plate can be quite efficient using the solution method obtained using modal analysis. By applying this method, we get rid of the terms elastic(k_{ij}) and inertial coupling(m_{ij}) . The same difficulties are observed in both Ξ_j and Q_j forms, regardless of the difference. The use of artificial modes is more suitable where the structure has rigid sections. The application of this method is quite common, since most of the wing structures have rigid sections. The rest of this chapter proceeds using artificial modes in calculations.

3.4.1 Bending-Torsion Flutter Analysis With Artificial Modes

If we consider the wing or tail structure whose elastic axis is perpendicular to the direction of flight, we consider the point y = 0 as the wing root and take into account the effects of rigid body degrees of freedom caused by bending and torsion in the fuselage. Deflections in bending and torsion are modeled as beam bending and torsion as we show in Figure 3.1. However, deformations are considered to occur due to overlapping of modes that do not depend each other.

$$\begin{aligned} w_B(y,t) &= \sum_{i=1}^{r} f_{w_i}(y)w_i(t) \\ Q_T(y,t) &= \sum_{i=1}^{n-r} f_{\theta_i}(y)\theta_i(t) \end{aligned} \tag{3.33}$$

If by placing the entire mass of the structure along the elastic axis of the structure and then finding the lowest modes of this system obtained, f_{w_i} mode shapes and related frequencies can be obtained. f_{θ_i} can be found in case the structure is prevented from bending by adding a rigid structure along its elastic axis. The surface deformation equation is given below.

$$w(x,y,t) = \sum_{i=1}^{r} f_{w_i}(y)w_i(t) - \sum_{i=1}^{n-r} x f_{\theta_i}(y)\theta_i(t) \tag{3.34}$$

Where;

$$\begin{aligned} \gamma_i(x,y) &= f_{w_i}(y) \qquad\qquad i = 1,2,....,r \\ \gamma_{r+1}(x,y) &= -x f_{\theta_i}(y) \qquad\qquad i = 1,2,....,(n-r) \end{aligned} \tag{3.35}$$

$q_i(t)$ represents $w_i(t)$ and $\theta_i(t)$. To find the inertial coefficients m_{ij}, only half span between 0 and l will be examined.

$$\begin{aligned} T &= \frac{1}{2}\int_0^l \int_{chord} [\dot{w}(x,y,t)]^2 \rho(x,y)\,dx\,dy \\ &= \frac{1}{2}\int_0^l \int_{chord} \left[\dot{w}_B(y,t) - x\dot{\theta}_T(y,t)\right]^2 \rho(x,y)\,dx\,dy \\ &= \int_0^l \left[\frac{1}{2}m\dot{w}_B^2 - S_y\dot{w}_B\dot{\theta}_T + \frac{1}{2}I_y\dot{\theta}_T^2\right] dy \end{aligned} \tag{3.36}$$

The $m(y)$, $S_y(y)$ and $Iy(y)$ parameters in this equation represent the mass calculated per unit span, the static unbalance and the moment of inertia about the elastic axis, respectively.

$$\begin{aligned} T = &\frac{1}{2}\sum_{i=1}^{r}\sum_{j=1}^{r} \dot{w}_i\dot{w}_j \int_0^l m f_{w_i} f_{w_j}\,dy - \sum_{i=1}^{r}\sum_{i=1}^{r}\sum_{j=1}^{(n-r)} \dot{w}_i\dot{\theta}_j \int_0^l S_y f_{w_i} f_{\theta_j}\,dy \\ &+ \frac{1}{2}\sum_{i=1}^{(n-r)}\sum_{j=1}^{(n-r)} \dot{\theta}_i\dot{\theta}_j \int_0^l I_y f_{\theta_i} f_{\theta_j}\,dy \end{aligned} \tag{3.37}$$

From the total potential energy found as a result of the examination of the elastic deformation,values of k_{ij} can be found. As we have explained so far, we only consider uncoupled bending mode and uncoupled torsion mode when trying to achieve the result. Contrary to what is predicted in this way, no important features of the analysis are lost. In this way, we can convert the kinetic energy equation to the form below.

$$T = \frac{1}{2}\dot{w}_R{}^2 \int_0^l m f_w^2\,dy - \dot{w}_R\dot{\theta}_R \int_0^l S_y f_w f_\theta\,dy + \frac{1}{2}\dot{\theta}_R{}^2 \int_0^l I_y f_\theta^2\,dy \tag{3.38}$$

Given as subscript, R indicates that these parameters are taken from reference points. Since the structure is considered as a simple beam model, potential energy is given as follows.

$$U_E = \frac{1}{2}\int_0^l EI\left[\frac{\partial^2 w_B}{\partial y^2}\right]^2 dy + \frac{1}{2}\int_0^l GJ\left[\frac{\partial \theta_T}{\partial y}\right]^2 dy$$
$$= \frac{1}{2}w_R^2\int_0^l EI\left[\frac{d^2 f_w}{dy^2}\right]^2 dy + \frac{1}{2}\theta_R^2\int_0^l GJ\left[\frac{df_\theta}{dy}\right]^2 dy \tag{3.39}$$

In order not to take the derivatives of the f_w and f_θ expressions in this given equation, we write the equation in the form below.

$$U_E = \frac{1}{2}w_w^2 W_R^2\int_0^l mf_w^2\,dy + \frac{1}{2}w_\theta^2\theta_R^2\int_0^l I_y f_\theta^2\,dy \tag{3.40}$$

These frequencies are obtained by decoupling 2 deformations occurring in the direction of bending and torsion. If we distribute the mass along the elastic axis, we can express the oscillation as follows.

$$w_B(y,t) = f_w(y)\cos w_w t \tag{3.41}$$

Based on this step, we find kinetic and potential energy as follows.

$$T_{F.V.} = \frac{1}{2}\int_0^l b\dot{w}_B^2\,dy = \frac{1}{2}w_w^2\sin^2 w_w t\int_0^l mf_w^2\,dy$$
$$U_{F.V.} = \frac{1}{2}\int_0^l EI\left[\frac{\partial^2 w_B}{\partial y^2}\right]^2 dy = \frac{1}{2}\cos^2 w_w t\int_0^l EI\left[\frac{d^2 f_w}{dy^2}\right]^2 dy \tag{3.42}$$

Since the maximum potential energy and the maximum kinetic energy are equal from the principle of energy conservation, the following statement emerges.

$$\frac{1}{2}\int_0^l EI\left[\frac{\partial^2 f_w}{\partial y^2}\right]^2 dy = \frac{1}{2}w_w^2\int_0^l mf_w^2\,dy \tag{3.43}$$

By multiplying both sides of equation 3.43 by w_R^2, the relationship between the first term of equation 3.39 and the first term of equation 3.40 is found. As can be remembered from the external force calculation, the pressure difference has a negative value. Therefore, generalized forces are found by integrating aerodynamic quantities.

$$
\begin{aligned}
Q_w &= -\int_0^l \int_{chord} \Delta p_a(x,y,t) f_w \, dx\, dy = \int_0^l L(y,t) f_w(y)\, dy \\
Q_\theta &= -\int_0^l \int_{chord} \Delta p_a(x,y,t)[-x f_\theta(y)]\, dx\, dy = \int_0^l M_y(y,t) f_\theta(y)\, dy
\end{aligned}
\tag{3.44}
$$

L in this equation represents the lift for the unit span and M represents the pitching moment parameter on the elastic axis. Structural friction have a very strong effect on flutter analysis, as Theodorsen and Garrick [8] point out. In the observations in the literature, it was stated that the amount of energy lost due to friction is proportional to the square of the amplitude of the friction, but is dependent on frequency. Based on this, a viscous damping force can be expressed as harmonic motion.

$$
F_{D.V.} = -f\frac{dx}{dt} = -f_w x_0 \cos wt = \pm f_w \sqrt{x_0^2 - x^2} \tag{3.45}
$$

The positive or negative sign in this experiment is given because the viscous damping force is opposite to the instantaneous velocity. The work done per cycle is given as follows.

$$
W_{D.V.} = \int_{t=0}^{t=2\pi/w} F_{D.V.dx} \tag{3.46}
$$

Damping force, which has the same effect as friction;

$$
F_{D.S.} = -g x_0 \cos wt = \pm g \sqrt{x_0^2 - x^2} \tag{3.47}
$$

It is quite difficult to fully explain the mechanism of friction in aerial structures mathematically. It should be known that what exactly the friction does is actually cause energy loss from the system in proportion to the amplitude and frequency. The elastic restoring force and torque of the beam acting on each dy element are expressed as follows.

$$
\begin{aligned}
dF &= -\frac{\partial^2}{\partial y^2}\left[EI\frac{\partial^2 w_B}{\partial y^2}\right] dy \\
dt &= \frac{\partial}{\partial y}\left[GJ\frac{\partial \theta_T}{\partial y}\right] dy
\end{aligned}
\tag{3.48}
$$

If we associate each of these equations with friction, we get the following equations.

$$
\begin{aligned}
dF_{D.S.} &= -ig_w \frac{\partial^2}{\partial y^2}\left[EI\frac{\partial^2 w_B}{\partial y^2}\right] dy \\
dt_{D.S.} &= ig_\theta \frac{\partial}{\partial y}\left[GJ\frac{\partial \theta_T}{\partial y}\right] dy
\end{aligned}
\tag{3.49}
$$

According to the researches in the literature, g_w and g_θ values generally vary between 0.01 and 0.03. By integrating $dF_{D.S.}$ and d$dt_{D.S.}$ into general forces in the direction of bending and twisting we obtain the following equations.

$$
\begin{aligned}
(Q_w)_{D.S} &= \int_0^l \frac{dF_{D.S.}}{dy} f_w(y)\, dy = -ig_w w_R \int_0^l \int_0^l \frac{d^2}{dy^2}\left[EI\frac{d^2 f_w}{dy^2}\right] f_w\, dy \\
(Q_w\theta_{D.S} &= \int_0^l \frac{dt_{D.S.}}{dy} f_\theta(y)\, dy = -ig_\theta \theta_R \int_0^l \int_0^l \frac{d}{dy}\left[GJ\frac{df_\theta}{dy}\right] f_\theta\, dy
\end{aligned}
\tag{3.50}
$$

After applying integration to this equation twice, we apply boundary conditions.After applying equation 3.43, the following statement is obtained.

$$
\begin{aligned}
(Q_w)_{D.S} &= -ig_w w_R \int_0^l EI\left[\frac{d^2 f_w}{dy^2}\right]^2 dy = -ig_w w_w^2 w_R \int_0^l m f_w^2\, dy \\
(Q_w\theta_{D.S} &= -ig_\theta \theta_R \int_0^l GJ\left[\frac{df_\theta}{dy}\right]^2 dy = -ig_\theta w_\theta^2 \theta_R \int_0^l I_y f_\theta^2\, dy
\end{aligned}
\tag{3.51}
$$

After these operations, we obtain the equation of motion required to perform flutter analysis by substituting the equations 3.38, 3.40, 3.44, and 3.51 into the Lagrange's equation. The two degrees of freedom in this process are w_R and θ_R, respectively. Following these operations, the following two equations of motion are obtained.

$$
\begin{aligned}
\ddot{w}_R \int_0^l m f_w^2\, dy - \ddot{\theta}_R \int_0^l S_y f_w f_\theta\, dy + w_R w_w^2 \left[1+ig_w\right] \int_0^l m f_w^2\, dy &= \int_0^l L f_w\, dy \\
\ddot{\theta}_R \int_0^l I_y f_\theta^2\, dy - \ddot{w}_R \int_0^l S_y f_w f_\theta\, dy + \theta_R w_\theta^2 \left[1+ig_\theta\right] \int_0^l I_y f_\theta^2\, dy &= \int_0^l M_y f_\theta\, dy
\end{aligned}
\tag{3.52}
$$

The lift and moment equations for a structure with simple harmonic motion in incompressible flow are given below.

$$
\begin{aligned}
L(y,t) &= \pi\rho_\infty b^3 w^2 \left\{ \frac{w_R}{b} f_w(y) L_h - \theta_R f_\theta(y) \left[L_\alpha - L_h\left(\frac{1}{2}+a\right)\right]\right\} \\
M_y(y,t) &= \pi\rho_\infty b^4 w^2 \left\{ -\frac{w_R}{b} f_w(y) \left[M_h - L_h\left(\frac{1}{2}+a\right)\right] \right. \\
&\quad \left. +\theta_R f_\theta(y) \left[M_\alpha - (M_h + L_\alpha)\left(\frac{1}{2}+a\right) + L_h\left(\frac{1}{2}+a\right)^2\right]\right\}
\end{aligned}
\tag{3.53}
$$

The parameter $b(y)$ in these equations represents the half-veter length of the wing and the $a(y)$ parameter represents the distance between the elastic axis and the midpoint of the veter. Dimensionless aerodynamic coefficients are functions of reduced frequency and mach number. As we know, we indicate the simple harmonic motion in the direction of bending and torsion as follows.

$$w_R(t) = \overline{w}_R e^{iwt}, \qquad \theta_R(t) = \overline{\theta}_R e^{iwt} \tag{3.54}$$

After substitıting equations 3.53, and 3.54 into equation 3.53, we collect the terms and divide them into $\pi\rho_\infty b_R^3 w^2 l e^{iwt}$ and $\pi\rho_\infty b_R^4 w^2 l e^{iwt}$ values, and then reach the final equations we will use in the flutter analysis.

$$\begin{aligned}&\frac{\overline{w_R}}{b_R}\left\{\frac{1}{\pi\rho_\infty b_R^2}\left[1-(1+ig_w)\left(\frac{w_w}{w_\theta}\right)^2\left(\frac{w_\theta}{w}\right)^2\right]\int_0^1 m f_w^2\,dy^* + \int_0^1\left(\frac{b}{b_R}\right)^2 L_h f_w^2\,dy^*\right\}\\ &-\overline{\theta}_R\left\{\frac{1}{\pi\rho_\infty b_R^3}\int_0^1 S_y f_w f_\theta\,dy^* + \int_0^1\left(\frac{b}{b_R}\right)^3\left[L_\alpha - L_h\left(\frac{1}{2}+a\right)\right] f_w f_\theta\,dy^*\right\} = 0\end{aligned} \tag{3.55}$$

$$\begin{aligned}&-\frac{\overline{w_R}}{b_R}\left\{\frac{1}{\pi\rho_\infty b_R^3}\int_0^1 S_y f_w f_\theta\,dy^* + \int_0^1\left(\frac{b}{b_R}\right)^3\left[M_h - L_h\left(\frac{1}{2}+a\right)\right] f_w f_\theta\,dy^*\right\}\\ &+\overline{\theta}_R\left\{\frac{1}{\pi\rho_\infty b_R^4}\left[1-(1+ig_\theta)\left(\frac{w_\theta}{w}\right)^2\right]\int_0^1 I_y f_\theta^2\,dy^*\right.\\ &\qquad\left.+\int_0^1\left(\frac{b}{b_R}\right)^4\left[M_\alpha-(M_h+L_\alpha)\left(\frac{1}{2}+a\right)+L_h\left(\frac{1}{2}+a\right)^2\right] f_\theta^2\,dy^*\right\} = 0\end{aligned} \tag{3.56}$$

$$L_h = 1 - \frac{2i}{k}C(k) \tag{3.57}$$

$$L_\alpha = \frac{1}{2} - \frac{i}{k} - \frac{2i}{k}C(k) - \frac{2}{k^2}C(k) \tag{3.58}$$

$$M_h = \frac{1}{2} \qquad \text{(for subsonic cases)} \tag{3.59}$$

$$M_\alpha = \frac{3}{8} - \frac{i}{k} \tag{3.60}$$

$$C(k) = 1 + \frac{-0.4544ik}{ik + 0.1902} \tag{3.61}$$

Integrals in these equations are the function of the reduced spanwise variable shown below.

$$y^* = \frac{y}{l} \tag{3.62}$$

We can make some changes on equation 3.55 and equation 3.56 to get the flutter determinant. First, we assume that the structural damping values used in bending and twisting situations are equal to each other [9].

$$g_w \approx g_\theta = g \tag{3.63}$$

This parameter (g) combines with other unknown $\left(\frac{w_\theta}{w}\right)$ to create complex unknown value Z shown below.

$$Z = \left(\frac{w_\theta}{w}\right)^2 [1 + ig] \tag{3.64}$$

4 coefficients of $\frac{\overline{w}_R}{b_R}$ and $\overline{\theta}_R$ in equation 3.55 and equation 3.56 form the flutter determinant used to determine the flutter speed of our system after the assumed modes are determined. In order to reach the results that do not equal to only 0 from equation 3.55 and equation 3.56, the flutter determinant that we will create from the 4 coefficients of $\frac{\overline{w}_R}{b_R}$ and $\overline{\theta}_R$ must be equal to 0.

$$\begin{vmatrix} A & B \\ C & D \end{vmatrix} = 0 \tag{3.65}$$

Where,

$$A=\left\{\frac{1}{\pi\rho_\infty b_R^2}\left[1-Z\left(\frac{w_w}{w_\theta}\right)^2\right]\int_0^1 mf_w^2\,dy^*+\int_0^1\left(\frac{b}{b_R}\right)^2 L_h f_w^2\,dy^*\right\}$$
$$B=-\left\{\frac{1}{\pi\rho_\infty b_R^3}\int_0^1 S_y f_w f_\theta\,dy^*+\int_0^1\left(\frac{b}{b_R}\right)^3\left[L_\alpha-L_h\left(\frac{1}{2}+a\right)\right]f_w f_\theta\,dy^*\right\}$$
$$C=-\left\{\frac{1}{\pi\rho_\infty b_R^3}\int_0^1 S_y f_w f_\theta\,dy^*+\int_0^1\left(\frac{b}{b_R}\right)^3\left[M_h-L_h\left(\frac{1}{2}+a\right)\right]f_w f_\theta\,dy^*\right\}$$
$$D=\left\{\frac{1}{\pi\rho_\infty b_R^4}[1-Z]\int_0^1 I_y f_\theta^2\,dy^* +\int_0^1\left(\frac{b}{b_R}\right)^4\left[M_\alpha-(M_h+L_\alpha)\left(\frac{1}{2}+a\right)+L_h\left(\frac{1}{2}+a\right)^2\right]f_\theta^2\,dy^*\right\}$$

From the static mass balance equation we can expand S_y parameter as $x_\alpha mb$ .In order to obtain the eigenvalue values of the flutter determinant given above, we must convert the determinant to $[X]-\lambda\,[Y]$ form.

$$\begin{vmatrix}X(11) & X(12)\\ X(21) & X(22)\end{vmatrix}-\lambda\begin{vmatrix}Y(11) & Y(12)\\ Y(21) & Y(22)\end{vmatrix}=0 \tag{3.66}$$

Where,

$$\lambda=Z$$
$$X(11)=\left\{\frac{1}{\pi\rho_\infty b_R^2}\int_0^1 mf_w^2\,dy^*+\int_0^1\left(\frac{b}{b_R}\right)^2 L_h f_w^2\,dy^*\right\}$$
$$X(12)=-\left\{\frac{1}{\pi\rho_\infty b_R^3}\int_0^1 x_\alpha mbf_w f_\theta\,dy^*+\int_0^1\left(\frac{b}{b_R}\right)^3\left[L_\alpha-L_h\left(\frac{1}{2}+a\right)\right]f_w f_\theta\,dy^*\right\}$$
$$X(21)=-\left\{\frac{1}{\pi\rho_\infty b_R^3}\int_0^1 x_\alpha mbf_w f_\theta\,dy^*+\int_0^1\left(\frac{b}{b_R}\right)^3\left[M_h-L_h\left(\frac{1}{2}+a\right)\right]f_w f_\theta\,dy^*\right\}$$
$$X(22)=\left\{\frac{1}{\pi\rho_\infty b_R^4}\int_0^1 I_y f_\theta^2\,dy^* +\int_0^1\left(\frac{b}{b_R}\right)^4\left[M_\alpha-(M_h+L_\alpha)\left(\frac{1}{2}+a\right)+L_h\left(\frac{1}{2}+a\right)^2\right]f_\theta^2\,dy^*\right\}$$
$$Y(11)=\left\{\frac{1}{\pi\rho_\infty b_R^2}\left(\frac{w_w}{w_\theta}\right)^2\int_0^1 mf_w^2\,dy^*\right\}$$
$$Y(12)=0$$
$$Y(21)=0$$
$$Y(22)=\left\{\frac{1}{\pi\rho_\infty b_R^4}\int_0^1 I_y f_\theta^2\,dy^*\right\}$$

We cannot directly get the flutter speed from the flutter determinant. In chapter 2, the procedure that we follow for the k method used in the flutter speed calculation of the 2D wing profile will be used. We use the different reduced frequency values used to achieve the damping value to zero, to obtain eigenvalue from the flutter determinant. For these reduced frequency values, the flutter determinant expands to a complex polynomial in Z. Since there are two degrees of freedom in our system, this polynomial can be factored using the quadratic formula.

3.5 Code Validation for 3D Flutter Analysis

We will investigate the validity and reliability of the 3D flutter analysis method by applying this method we have described in this chapter on a structure studied in the literature. The analytical calculation method required for 3D flutter analysis will be implemented using MATLAB. This analytical calculation method is an iterative process applied for different reduced frequency values in each step. The MATLAB code allows us to save time seriously when calculating the flutter speed.

Case for 3D Flutter Analysis; The created MATLAB code will be applied for a rectangular cantilevered wing, consisting of isotropic material and having a veter of 1 meter and different aspect ratio values and thickness ratio values [19]. The root of the wing is fixed on the elastic axis from all degrees of freedom. The bending stiffness EI and torsion stiffness GJ values of the wing structure are found using the formulas given below [20].

$$\begin{aligned} EI &= \frac{Ech^3}{12(1-\upsilon^2)} \\ GJ &= \frac{Ech^3}{6(1+\upsilon)}\left(1-\frac{3h}{5c}\right) \end{aligned} \tag{3.67}$$

The section height of our beam-like wing model with a rectangular cross section is represented by the h parameter. We obtain mass and the mass moment of inertia value in the torsion direction of our uniform wing model per it's rectangular cross-sectional area from the following formulas [20].

$$m = \rho_s hc \ , \qquad \mu_\theta = \frac{m}{12}\left(h^2+c^2\right) \tag{3.68}$$

The ρ_s parameter in these equations gives the density of the material forming the structure. Since the cross section of the structure is symmetrical, the elastic axis and the inertial axis coincide on the y axis, which is the symmetry axis. Therefore, the elastic center of the section coincides with the center of mass ($x_\alpha = 0$). The material properties of the structure are given below.

$$\rho_s = 2700\, kg/m^3 \qquad E = 70^9\ Pa \qquad \upsilon = 0.35 \tag{3.69}$$

In this case used in the literature, 9 different combinations formed by using 3 different aspect ratios and 3 different thickness ratio values were used.

$$AR = \frac{2l}{c} = [4,6,8] \qquad TR = \frac{h}{c} = [0.006, 0.008, 0.010] \tag{3.70}$$

The natural bending mod shape, natural bending frequency, natural torsion shape and natural torsion frequencies of our wing model with uniform beam features are obtained from the following formulas [21], [22].

$$\begin{gathered}\phi_i = \cosh(\gamma_i \frac{y}{l}) - \cos(\gamma_i \frac{y}{l}) - \left(\frac{\cosh\gamma_i + \cos\gamma_i}{\sinh\gamma_i + \sin\gamma_i}\right)\left[\sinh(\gamma_i \frac{y}{l}) - \sin(\gamma_i \frac{y}{l})\right] \\ f_{\phi_i} = \frac{\gamma_i^2}{2\pi l^2}\sqrt{\frac{EI}{m}}\ , \gamma_1 = 0.597\pi\,,\ \ \gamma_i \approx \left(1 - \frac{1}{2}\right)\pi \\ \varphi_i = \sin(\theta_i \frac{y}{l}),\ \ f_{\varphi_i} = \frac{\theta_i}{2\pi l}\sqrt{\frac{GJ}{\mu_\theta}},\ \ \theta_i = \left(i - \frac{1}{2}\right)\pi\end{gathered} \tag{3.71}$$

After doing flutter analysis for 9 different wing modifications, we get the following U (flutter speed) -g (damping) graphs for each modification.

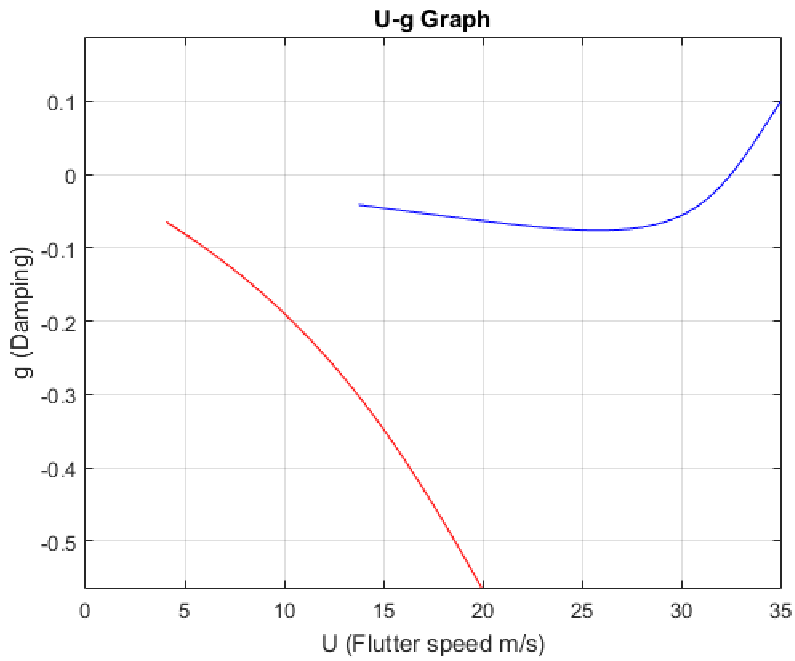

Figure 3.4 : U-g graphic for wing model having AR=4 and TR=0.006.

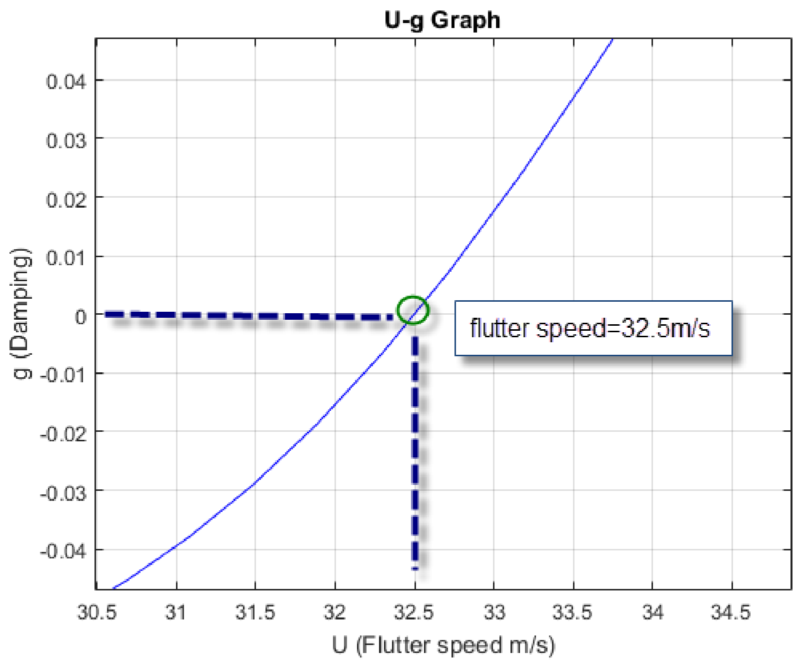

Figure 3.5 : U-g graphic for wing model having AR=4 and TR=0.006.

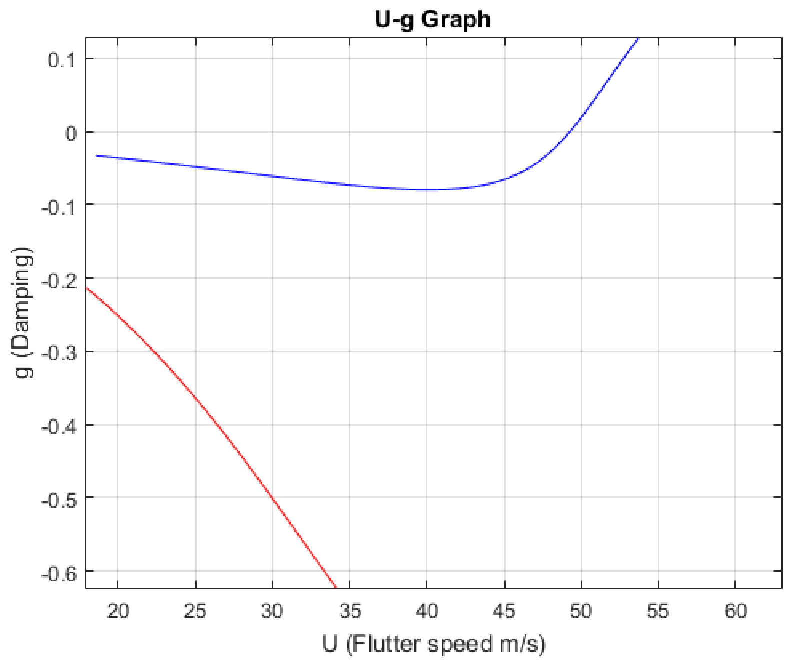

Figure 3.6 : U-g graphic for wing model having AR=4 and TR=0.008.

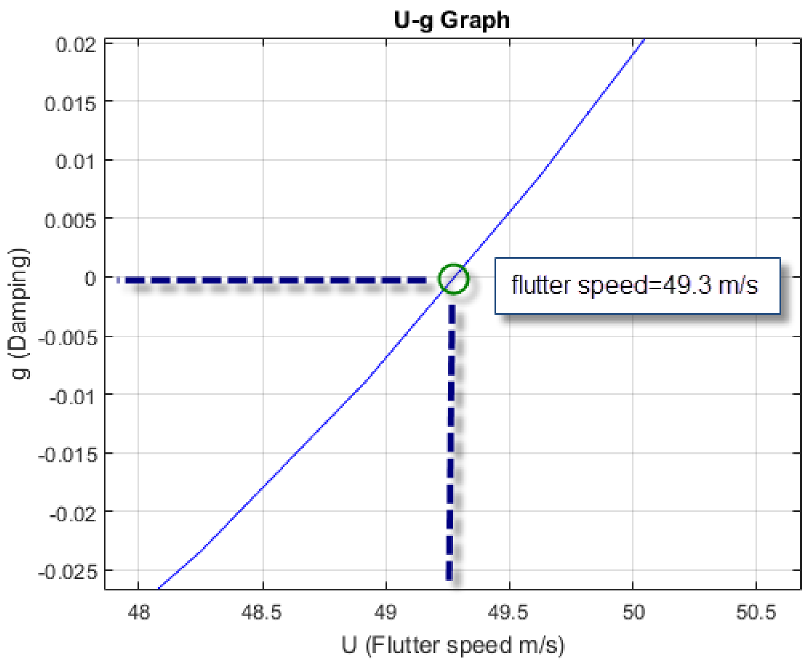

Figure 3.7 : U-g graphic for wing model having AR=4 and TR=0.008.

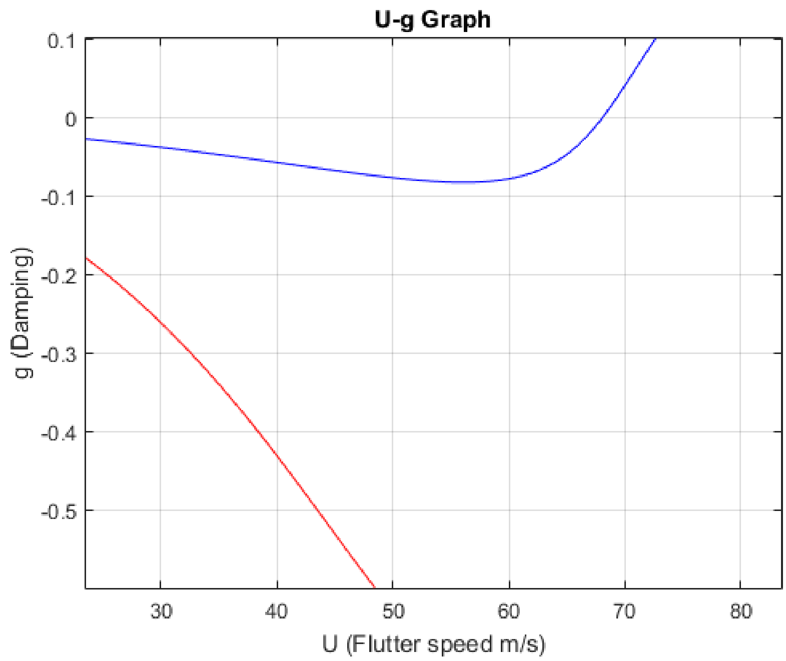

Figure 3.8 : U-g graphic for wing model having AR=4 and TR=0.01.

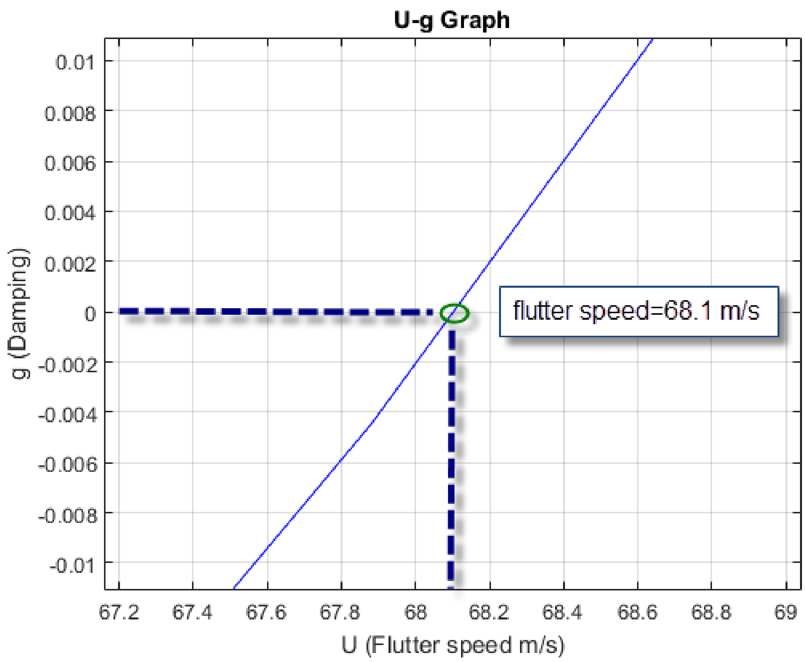

Figure 3.9 : U-g graphic for wing model having AR=4 and TR=0.01.

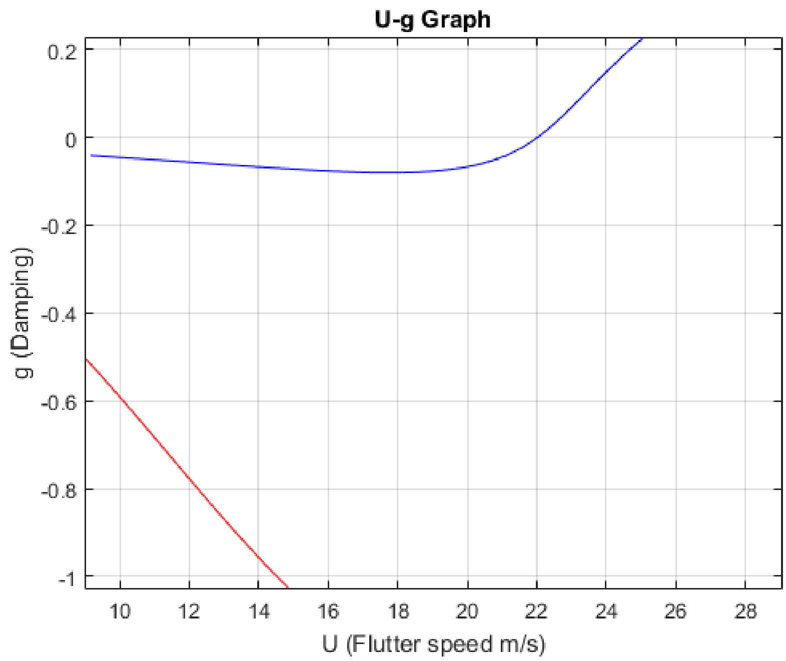

Figure 3.10 : U-g graphic for wing model having AR=6 and TR=0.006.

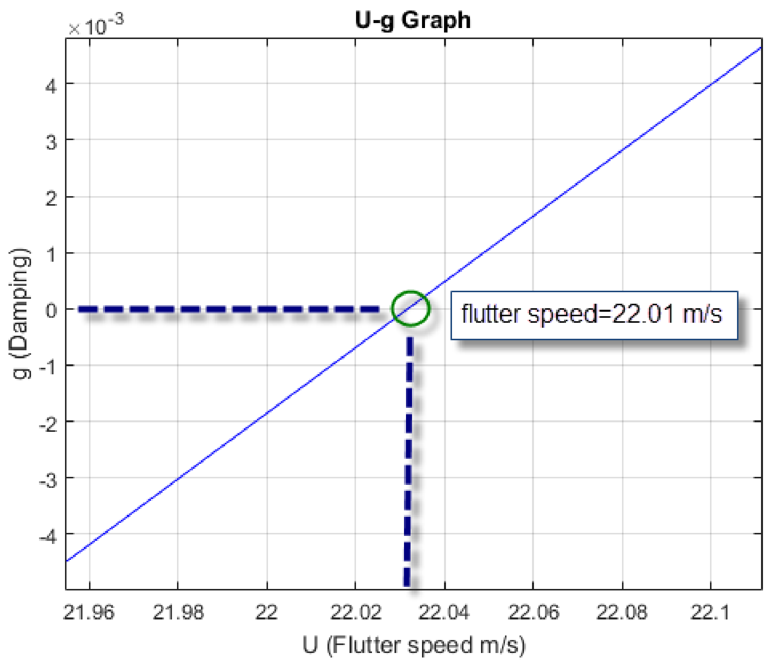

Figure 3.11 : U-g graphic for wing model having AR=6 and TR=0.006.

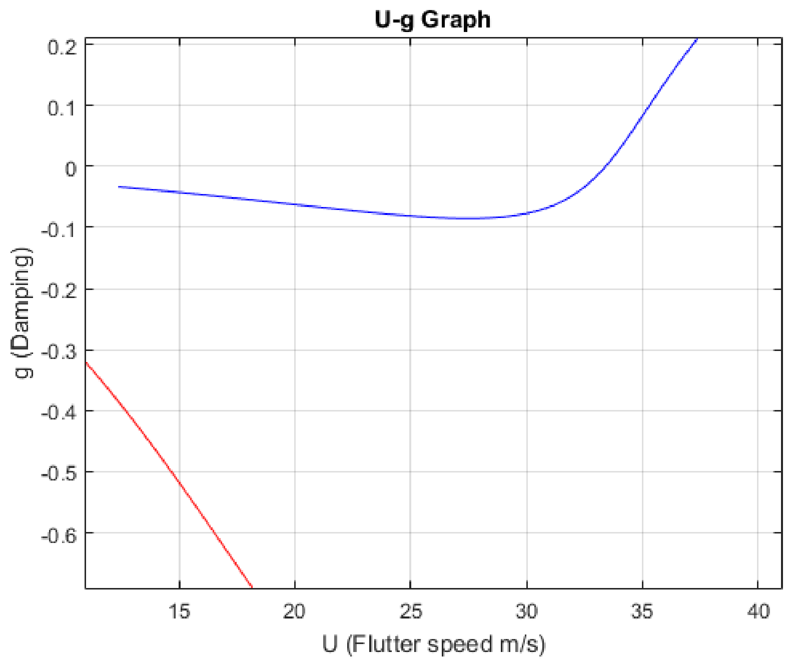

Figure 3.12 : U-g graphic for wing model having AR=6 and TR=0.008.

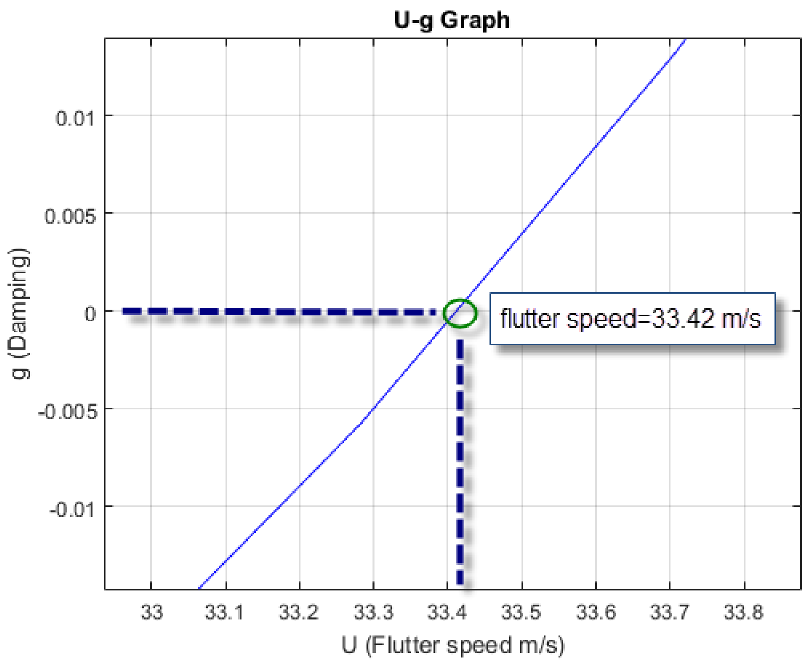

Figure 3.13 : U-g graphic for wing model having AR=6 and TR=0.008.

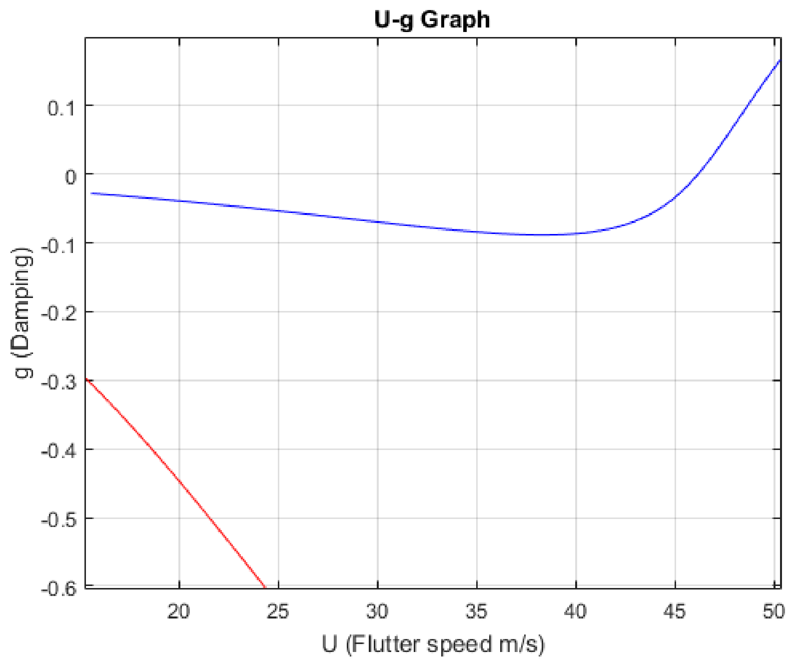

Figure 3.14 : U-g graphic for wing model having AR=6 and TR=0.01.

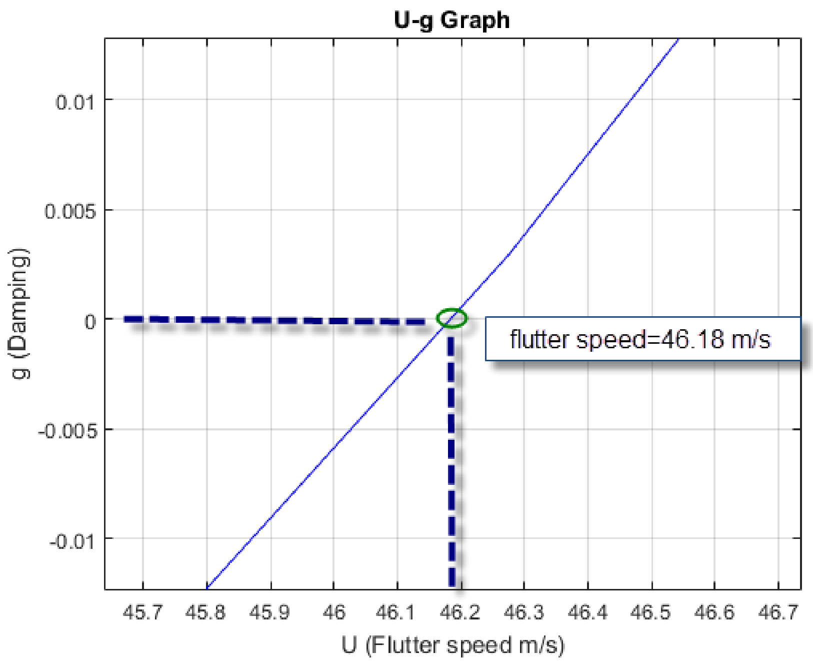

Figure 3.15 : U-g graphic for wing model having AR=6 and TR=0.01.

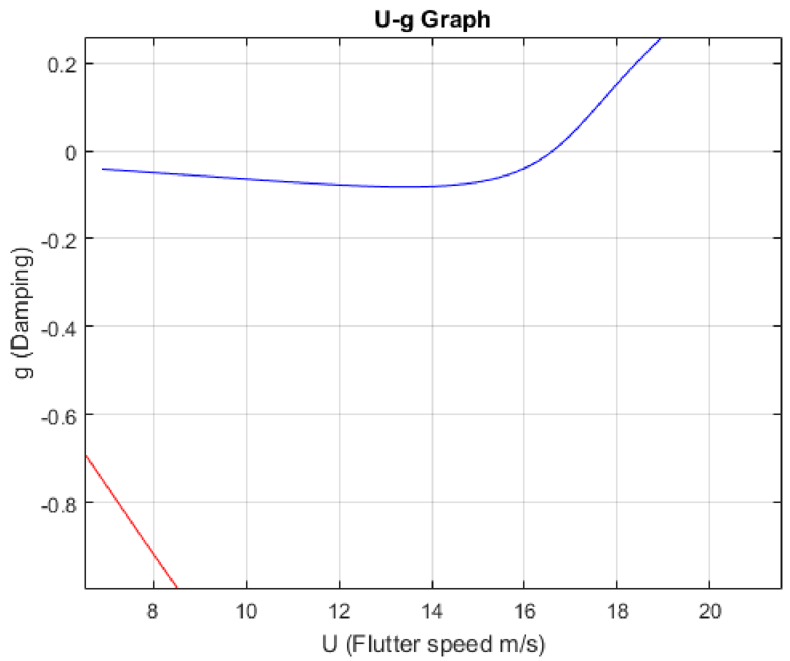

Figure 3.16 : U-g graphic for wing model having AR=8 and TR=0.006.

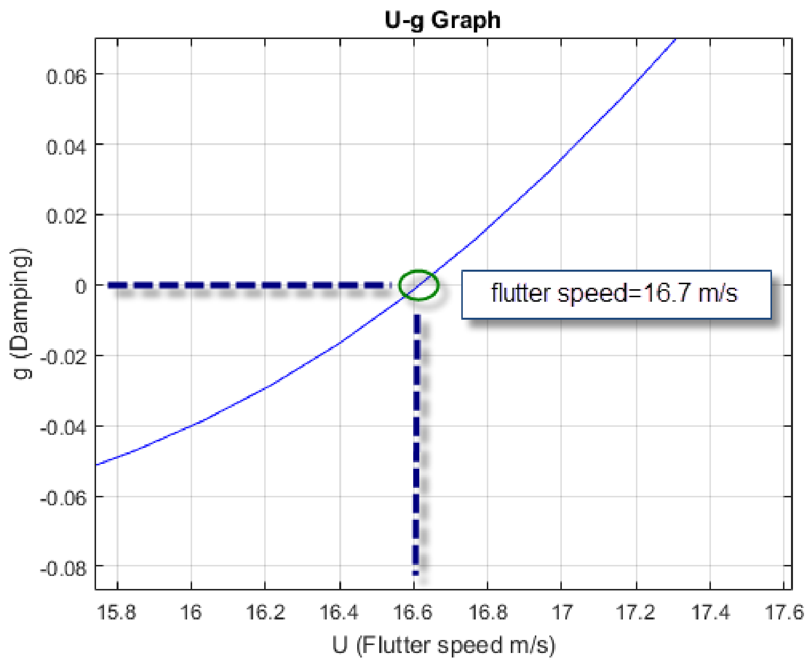

Figure 3.17 : U-g graphic for wing model having AR=8 and TR=0.006.

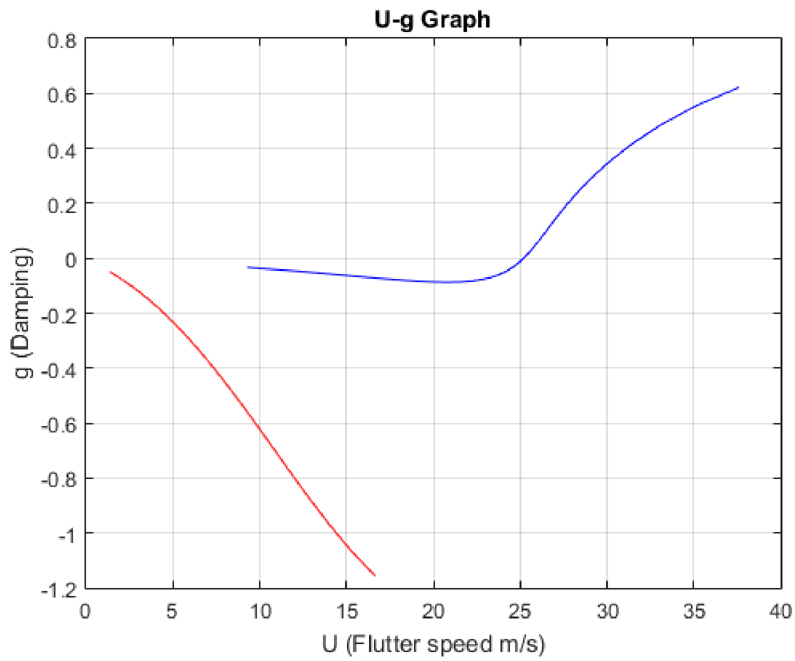

Figure 3.18 : U-g graphic for wing model having AR=8 and TR=0.008.

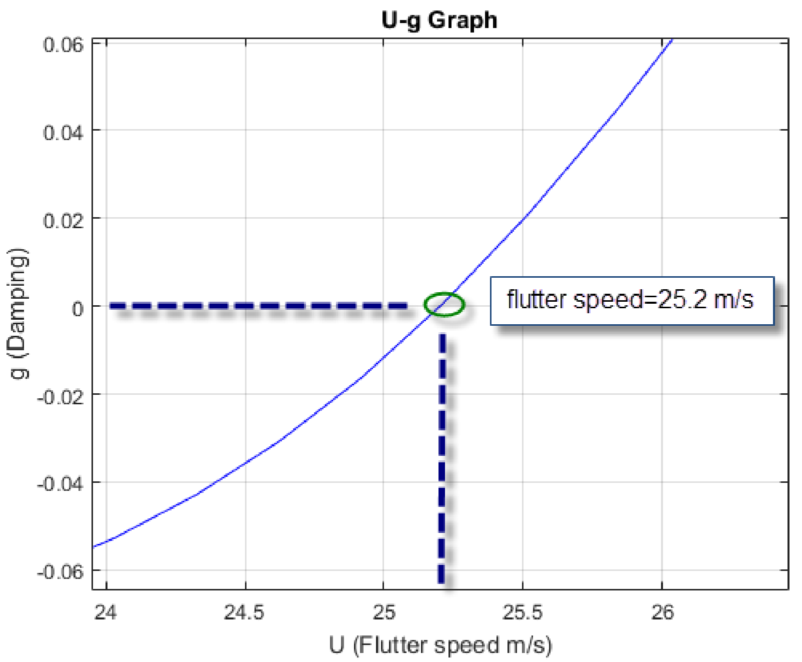

Figure 3.19 : U-g graphic for wing model having AR=8 and TR=0.008.

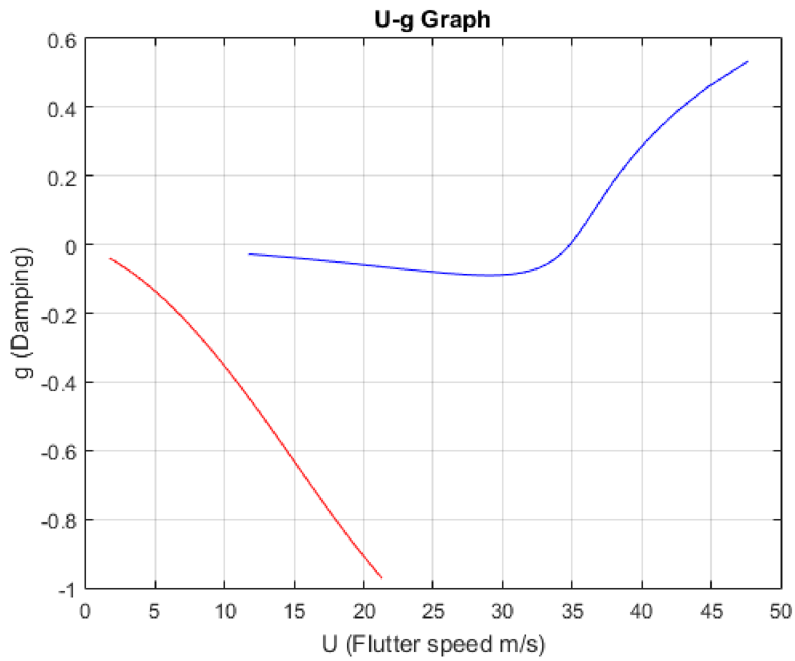

Figure 3.20 : U-g graphic for wing model having AR=8 and TR=0.01.

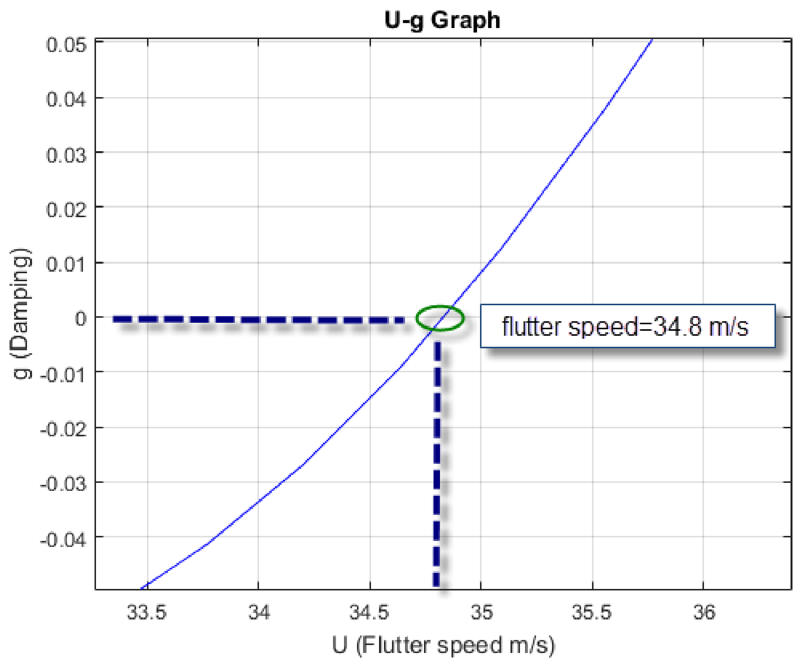

Figure 3.21 : U-g graphic for wing model having AR=8 and TR=0.01.

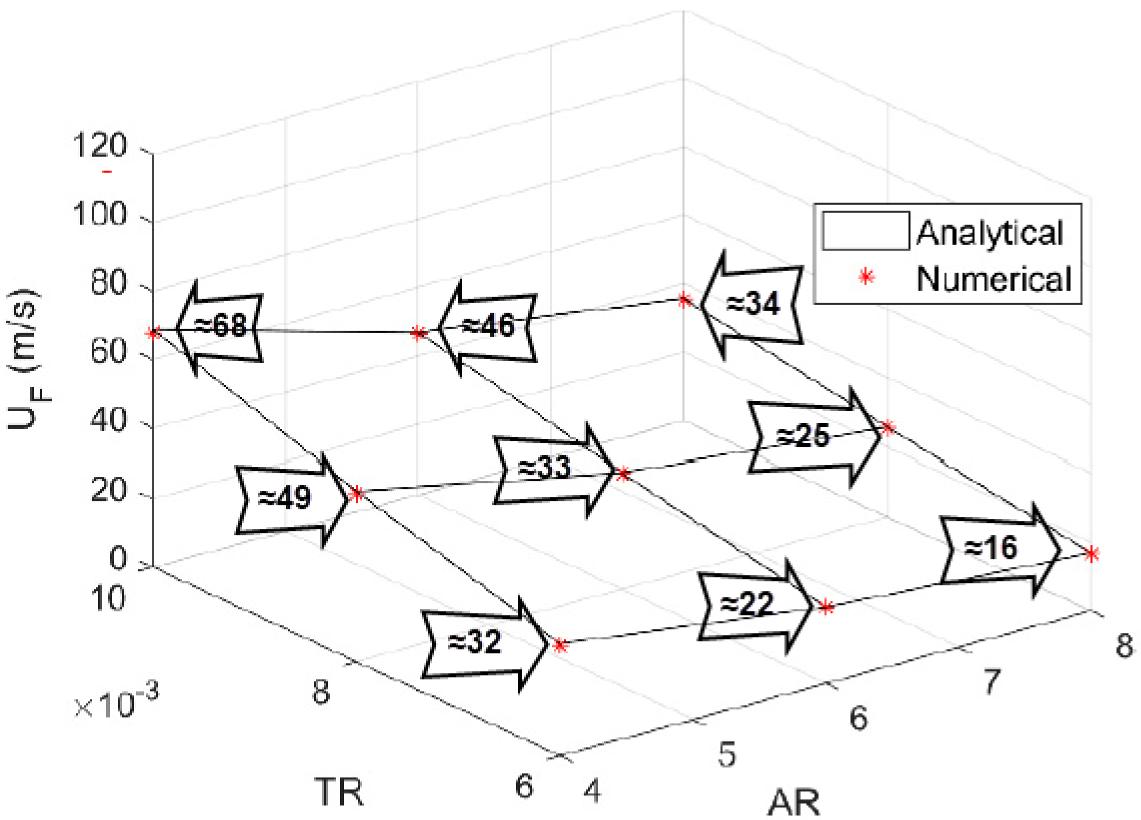

Figure 3.22 : Flutter speeds according to standard strip theory for 9 different wing modifications from reference[19].

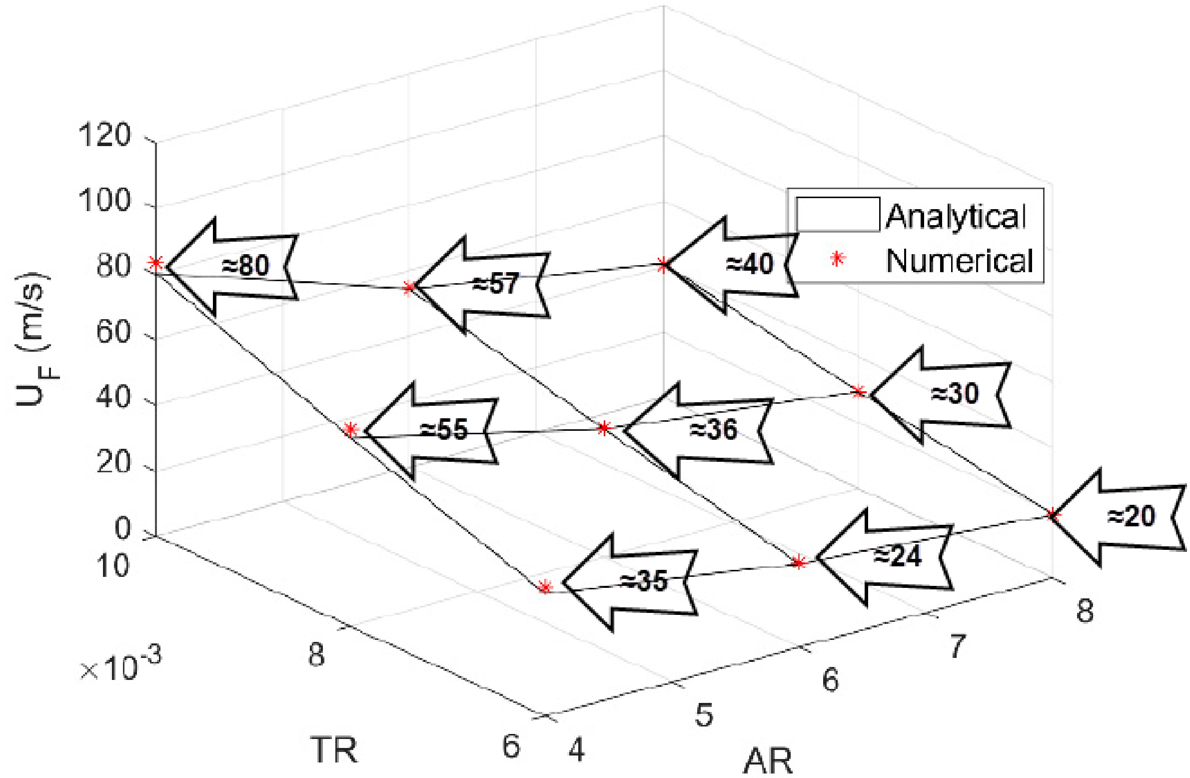

Figure 3.23 : Flutter speeds according to double lattice method for 9 different wing modifications from reference[19].

3.6 Conclusion

Using the MATLAB code developed for 3D flutter analysis on 9 different models, flutter speeds were obtained. Standard strip theory was used to calculate the aerodynamic loads used for the analytical analysis we created. Finally, in reference [19], U-g plots of flutter velocity results obtained using standard strip theory and double lattice method are given for the same models, respectively. In graph in figure 3.22, flutter speeds obtained using standard strip theory are given. Flutter speeds obtained using double lattice method are given in graph in figure 3.23. If we compare the flutter speed results we obtained with the graph in figure 3.22 containing the results obtained by using the standard strip theory of reference [19], the results are almost same. The results are almost the same because the method used for aerodynamic load calculation is the same. As can be understood from this situation, it is seen that the MATLAB code we have developed is consistent. When the results obtained in graphic in figure 3.22 are compared with our results, it is seen that there is a difference. The reason for this difference is that the flutter speed results in graph in figure 3.23 are obtained by using the double lattice method.

4. EFFECTS OF DIFFERENT METHODS OF COMPUTING NATURAL MODE SHAPES AND FREQUENCIES ON CALCULATING FLUTTER SPEED

4.1 Modal Analysis by Using Concentrated Mass Systems

4.1.1 Deformations of Slender Unswept Wings

Let's consider a wing model that is assumed to have a thin thickness on its skin and web of spars. We can model this wing model like a beam. This beam model is assumed to have no bending rigidity value. And the cross-sectional shape of the beam model representing this wing is determined by the ribs of the wing. These ribs are assumed to have infinite rigidity value. The cross-section dimensions of the beam can vary in the spanwise direction of the beam. the figure representing this beam model and the loads on it is given below.

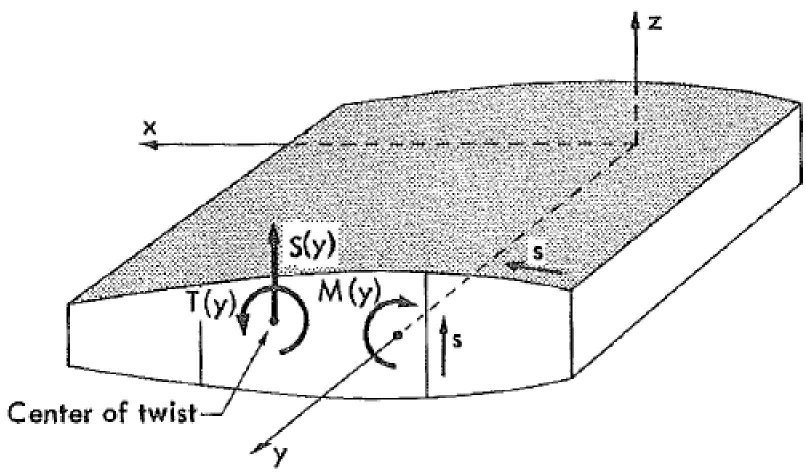

Figure 4.1 : Loaded cross section of shell beam[22].

In the beam model representing the wing structure, the y axis is formed along the length of the beam, passing through the center of the stress bearing area on each cross-section. The x and z axes go through the bending axes of the xy and yz planes, respectively. The coordinates of a point on the section are determined by the spanwise

(y) axis and tangential coordinate (s). On counterclockwise, the measured tangential coordinate is positive for the skin, and is positive for upward direction of z axis on the web of ribs. The point where shear $S(y)$ and torque $T(y)$ are applied is in the twist and shear center of the cross section. Normal stresses in the y-axis direction are represented by the σ. Shear flow, which has a positive sign in the s direction, is represented by the q sign. In this section, where we describe the modeling of the wing as a slender beam, two assumptions will be made. The first of these assumptions is that when the torque load is applied on the beam, the beam can be completely bent. This situation allows the application of the principle of St. Venant and allows the bending and torsional movements of the beam to be considered as uncoupled actions. The second of the assumptions is that the cross-section remains as the plane when beam is bending. This assumption gives us the possibility of applying bending theory.

4.1.1.1 Bending and Shearing Deformations

The wing structure consists of balanced skin elements that are exposed to normal stresses and shear flows shown in figure 4.2.

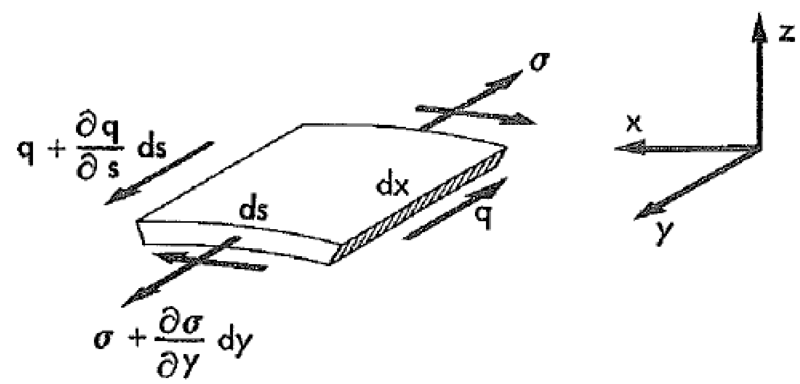

Figure 4.2 : Element of wing skin[22].

Rib structures, one of the elements that make up the wing structure, are assumed to be rigid. Therefore, normal stresses on the rib throughout the veter are neglected. The strain energy formed on the wing is found in terms of stresses on the wing as follows.

$$U = \frac{1}{2E}\int_0^l \int_{C.S.} \overline{\sigma}^2 t\, ds\, d\lambda + \frac{1}{2G}\int_0^l \int_{C.S.} \overline{q}^2 \frac{ds}{t}\, d\lambda \tag{4.1}$$

The parameter t in this equation represents the skin thickness. In this equation, the integral operation on s is done on the wing section. Again, in this equation, the integration process on λ is done throughout spanwise. First, lateral deflection $w(y)$ should be calculated from the bending moment and shear force distributed over the wing structure. In order to apply Castigliano's Theorem on this system, an additional P load must be applied where $\lambda = y$ is located. We show the total normal stress caused by the bending moment $M(\lambda)$ and the P load we have included in the system as follows.

$$\overline{\sigma}(\lambda,s) = \sigma(\lambda,s) + P\frac{\partial\overline{\sigma}}{\partial P} \tag{4.2}$$

$\sigma(\lambda,s)$ in this equation is caused by the bending moment distribution $M(\lambda)$. The $\dfrac{\partial\overline{\sigma}}{\partial P}$ parameter, which also represents the normal stress distribution in this equation, occurs when $P = 1$. Similarly, total shear flow is found as shown in the equation below.

$\overline{q}(\lambda,s) = q(\lambda,s) + P\dfrac{\partial\overline{q}}{\partial P}$(4.3)

$q(\lambda,s)$ in this equation is caused by the cut distribution $S(\lambda)$. The $\dfrac{\partial\overline{q}}{\partial P}$ parameter, which also represents the shear flow in this equation, occurs when $P = 1$. By substituting equation 4.2 and equation 4.3 into equation 4.1, the total strain energy resulting from bending moment, shear distribution and P load is given below.

$$\begin{aligned} U = &\frac{1}{2E}\int_0^l \int_{C.S.} \left[\sigma(\lambda,s) + P\frac{\partial\overline{\sigma}}{\partial P}\right]^2 t\,ds\,d\lambda \\ &+ \frac{1}{2G}\int_0^l \int_{C.S.} \left[q(\lambda,s) + P\frac{\partial\overline{q}}{\partial P}\right]^2 \frac{ds}{t}\,d\lambda \end{aligned} \tag{4.4}$$

After taking the differential of this equation on P, if we equal the value of P to zero, we get the lateral deflection given below.

$$w(y) = \frac{1}{E}\int_0^l \int_{C.S.} \sigma(\lambda,s)\frac{\partial\overline{\sigma}}{\partial P} t\,ds\,d\lambda + \frac{1}{G}\int_0^l \int_{C.S.} q(\lambda,s)\frac{\partial\overline{q}}{\partial P}\frac{ds}{t}\,d\lambda \tag{4.5}$$

The α parameter used in this equation represents bending deflection and we can determine this parameter with the help of the equation below.

$$\alpha(y) = \frac{1}{E}\int_0^l \int_{C.S.} \sigma(\lambda, s)\frac{\partial \overline{\sigma}}{\partial P} t\, ds\, d\lambda \tag{4.6}$$

If we assume that we can apply theory of beam bending, normal stresses are expressed as follows.

$$\begin{aligned} \sigma(\lambda, s) &= -\frac{M(\lambda)z}{I} \\ \frac{\partial \overline{\sigma}}{\partial P} &= \begin{cases} -\frac{y-\lambda}{I}z, & (y > \lambda), \\ 0, & (y < \lambda) \end{cases} \end{aligned} \tag{4.7}$$

The parameter I used in this equation represents the moment of inertia in the axis of the cross-section. If we substituting equation 4.7 into equation 4.6, we get the new bending deflection expression shown below.

$$\alpha(y) = \int_0^y \frac{M(\lambda)(y-\lambda)}{EI} d\lambda \tag{4.8}$$

If we take the differential of this equation twice on y, we find the relationship between the bending moment and curvature given below.

$$\alpha'' = \frac{M}{EI} \tag{4.9}$$

We can find the value of shearing deflection from the second part of equation 4.5.

$$\beta(y) = \frac{1}{G}\int_0^l \int_{C.S.} q(\lambda, s)\frac{\partial \overline{q}}{\partial P}\frac{ds}{t} d\lambda \tag{4.10}$$

We can find the shear flow distribution expression that occurs in $S = 1$ as follows.

$$q(\lambda,s) = Su(\lambda,s)$$

$$\frac{\partial\overline{q}}{\partial P} = \begin{cases} u(\lambda,s), & (y > \lambda), \\ 0, & (y < \lambda) \end{cases} \tag{4.11}$$

Expressing the shearing constant of the cross-section of the beam caused by the unit shear force in terms of shear flow is obtained by substituting equation 4.11 into equation 4.10.

$$\begin{aligned} \beta(y) &= \int_0^y \frac{Sd\lambda}{GK} \\ K &= \frac{1}{\int_{C.S.} u^2 \frac{ds}{t}} \end{aligned} \tag{4.12}$$

If the differential of equation 4.12 is taken on y, the relationship between shear and the first derivative of shear deformation is found.

$$\beta' = \frac{S}{GK} \tag{4.13}$$

4.1.1.2 Influence Functions and Coefficients

From equation 4.5, which expresses lateral deflection, we can obtain influence functions that take into account both bending and shear deformations. To get the $C^{zz}(y,\eta)$ expression, we can obtain the following equations by placing them in equation 4.5.

$$\begin{aligned} \sigma(\lambda,s) &= -\frac{\eta-\lambda}{I}z, \quad (0 < \lambda < \eta) \\ \frac{\partial\overline{\sigma}}{\partial P} &= -\frac{y-\lambda}{I}z, \quad (0 < \lambda < y) \\ q(\lambda,s) &= u(\lambda,s), \quad (0 < \lambda < \eta) \\ \frac{\partial\overline{q}}{\partial P} &= u(\lambda,s), \quad (0 < \lambda < y) \end{aligned} \tag{4.14}$$

The influence functions that take into account both bending and shear deformations after this process are given below.

$$
\begin{aligned}
C^{zz}(y,\eta) &= \int_0^y \frac{(\eta-\lambda)(y-\lambda)}{EI}\,d\lambda + \int_0^y \frac{d\lambda}{GK} \qquad (\eta \geq y) \\
C^{zz}(y,\eta) &= \int_0^\eta \frac{(\eta-\lambda)(y-\lambda)}{EI}\,d\lambda + \int_0^\eta \frac{d\lambda}{GK} \qquad (y \geq \eta)
\end{aligned}
\tag{4.15}
$$

4.1.1.3 Torsional Deformation and Influence Function

If the beam does not resist twisting when the torsion moment is applied to the beam model representing the wing model, strain energy consists of shear stresses, as can be understood from the following statement.

$$
U = \frac{1}{2G}\int_0^l \int_{C.S.} \overline{q}^2 \frac{ds}{t}\,d\lambda \tag{4.16}
$$

The twist angle of the beam is found as follows using Castigliano's theorem.

$$
\theta(y) = \frac{1}{G}\int_0^l \int C.S.q(\lambda,s)\frac{\partial \overline{q}}{\partial T}\frac{ds}{t}\,d\lambda \tag{4.17}
$$

If the torque value is equal to 1, and shear flow distribution is shown with v, the following statements are obtained.

$$
\begin{aligned}
& q(\lambda,s) = T(\lambda)v(\lambda,s) \\
& \frac{\partial \overline{q}}{\partial T} = \begin{cases} v(\lambda,s), & (y > \lambda), \\ 0, & (y < \lambda) \end{cases}
\end{aligned}
\tag{4.18}
$$

By substituting equation 4.18 into equation equation 4.17, the angle of twist value is given as follows.

$$
\theta(y) = \int_0^y \frac{T(\lambda)d\lambda}{GJ} \tag{4.19}
$$

The torsion constant in the cross section of the beam;

$$
J = \frac{1}{\int_{C.S.} v^2 \frac{ds}{t}} \tag{4.20}
$$

If the differential of equation 4.19 is taken on y, the relationship between the rate of twist and torsional moment is obtained as follows.

$$\theta' \frac{T}{GJ} \tag{4.21}$$

Figure 4.3 shows the wing structure model used to calculate the torsion influence value.

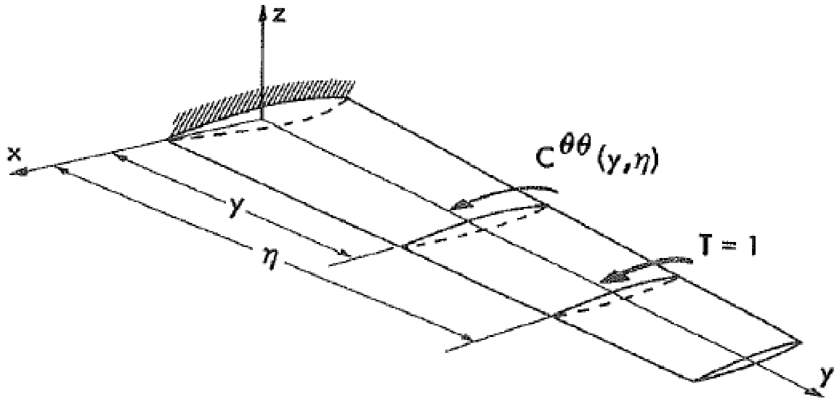

Figure 4.3 : Cantilever wing under unit torque load[22].

We can obtain the torsion influence function by using the following expressions in equation 4.17.

$$\begin{aligned} q(\lambda,s) &= v(\lambda,s) \\ \frac{\partial \bar{q}}{\partial T} &= v(\lambda,s) \end{aligned} \tag{4.22}$$

Torsion influence functions is obtained as shown below:

$$\begin{aligned} C^{\theta\theta}(y,\eta) &= \int_0^y \frac{d\lambda}{GJ} \qquad (\eta \geq y) \\ C^{\theta\theta}(y,\eta) &= \int_0^\eta \frac{d\lambda}{GJ} \qquad (y \geq \eta) \end{aligned} \tag{4.23}$$

The parameter J used in these equations represents torsion constant.

4.1.2 Integral Equation of Motion of a Slender Beam

As shown in the figure below, when distributed load and moment are applied on the restrained beam, deflection in the z-axis direction and the slope around the x-axis can be defined as follows.

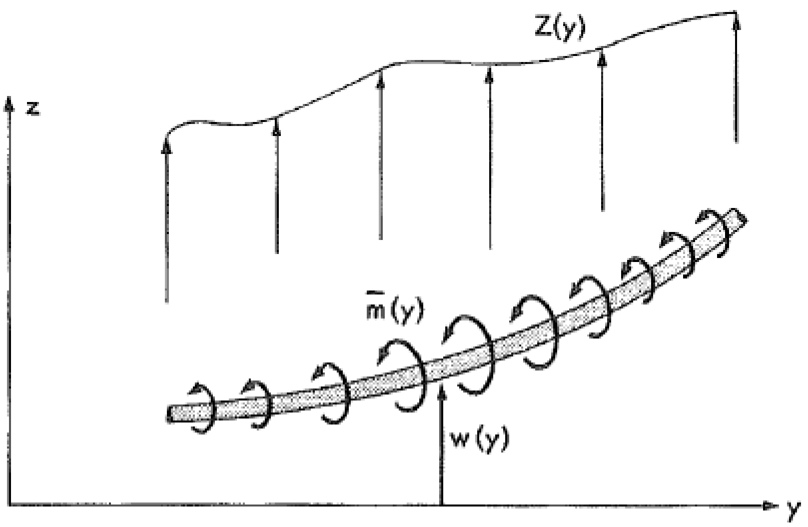

Figure 4.4 : Beam loaded by lateral load and running moment[22].

$$\begin{aligned} w(y) &= \int_0^l [C^{zz}(y,\eta)Z(\eta) + C^{z\alpha}(y,\eta)\overline{m}(\eta)]\, d\eta \\ w^{'}(y) &= \int_0^l [C^{\alpha z}(y,n)Z(\eta) + C^{\alpha\alpha}(y,n)\overline{m}(\eta)]\, d\eta \end{aligned} \tag{4.24}$$

Where,

$$\begin{aligned} C^{zz}(y,\eta) &= \text{lateral deflection at y due to a unit load at } \eta \\ C^{z\alpha}(y,\eta) &= \text{lateral deflection at y due to a unit moment at } \eta \\ C^{\alpha z}(y,\eta) &= \text{slope at y due to a unit load at } \eta \\ C^{\alpha\alpha}(y,\eta) &= \text{slope at y due to a unit moment at } \eta \\ C^{\alpha z}(y,\eta) &= \frac{\partial C^{zz}(y,\eta)}{\partial y} \\ C^{z\alpha}(y,\eta) &= C^{\alpha z}(y,\eta) = \frac{\partial C^{zz}(y,\eta)}{\partial \eta} \end{aligned} \tag{4.25}$$

The influence functions include deflections in both the bending direction and the shear direction. We express the $Z(y)$ load and the moment of $\overline{m}(y)$ as follows.

$$\begin{aligned} Z(\eta) &= F_z(\eta,t) - m(\eta)\ddot{w}(\eta,t) \\ \overline{m}(\eta) &= -\mu(\eta)\ddot{\alpha}'(\eta,t) \end{aligned} \tag{4.26}$$

If rotary inertia effects are taken into consideration, if we want to obtain the integral equations of restrained beam, we must substitute the equations we found above into equation 4.24. As a result of this process, the following equations are obtained.

$$\begin{aligned} w(y,t) &= \int_0^l \left\{c^{zz}(y,\eta)\left[F_z(\eta,t) - m(\eta)\ddot{w}(\eta,t)\right] - C^{z\alpha}(y,\eta)\mu(\eta)\ddot{\alpha}'(\eta,t)\right\} d\eta \\ w'(y,t) &= \int_0^l \left\{c^{\alpha z}(y,\eta)\left[F_z(\eta,t) - m(\eta)\ddot{w}(\eta,t)\right] - C^{\alpha\alpha}(y,\eta)\mu(\eta)\ddot{\alpha}'(\eta,t)\right\} d\eta \end{aligned} \tag{4.27}$$

Since the unknowns in these equations are used in the integral process, these equations are called integral equations. Where α' is equal to w', the problem can be simplified to a problem that can be solved with a single equation from equation 4.27.So we get the following equation:

$$w(y,t) = \int_0^l \left\{C^{zz}(y,\eta)\left[F_z(\eta,t) - m(\eta)\ddot{w}(\eta,t)\right] - C^{z\alpha}(y,\eta)\mu(\eta)\ddot{w}'(\eta,t)\right\} d\eta \tag{4.28}$$

4.1.2.1 Integral Equation of Free Vibration of a Slender Restrained Beam

In the free vibration of the beam model we mentioned above, we equalize μ and $F_z(y,t)$ to zero to neglect the effects of rotary inertia. As a result, equation 4.28 becomes the following equation.

$$w(y,t) = -\int_0^l C^{zz}(y,\eta)\ddot{w}(\eta,t)m(\eta)\,d\eta \tag{4.29}$$

The separated version of this equation can be used as a solution.

$$w(y,t) = W(y)T(t) \tag{4.30}$$

If we substitute our last equation into equation 4.29, the following equation is obtained.

$$-\frac{T}{\ddot{T}} = \frac{1}{W(y)} \int_0^l C(y,\eta) W(\eta) m(\eta)\, d\eta \tag{4.31}$$

Since the y and t parameters are independent from each other, the following equations are obtained.

$$\ddot{T} + w^2 T = 0 \tag{4.32}$$

$$W(y) = w^2 \int_0^l C(y,\eta) W(\eta) m(\eta)\, d\eta \tag{4.33}$$

4.1.3 Natural Mode Shapes and Frequencies Derived From The Integral Equation

In section 4.2.1.2, we learned that we can obtain the natural mode shapes and natural frequencies of the wing structure or another structure representing the wing structure with the solution of a homogeneous integral. The integral equation of the beam with varying properties in previous sections is given below.

$$W(y) = w^2 \int_0^l C(y,\eta) W(\eta) m(\eta)\, d\eta \tag{4.34}$$

The method applied using the integral equation is more useful than the differential method to obtain natural mode shape and natural frequency. The integration process applied on an existing solution is a more appropriate approach in our problem.

4.1.3.1 The Integral Equation Applied To Concentrated Mass Systems

The method we can use to reach the result by using equation 4.34 is to distribute the mass of the beam to different points. If we apply this approach, the integral operation becomes a addition operation and the set of equations is obtained.

$$W_i = w^2 \sum_{j=1}^{n} C_{ij} M_j W_j, \qquad (i = 1, 2, \ldots\ldots, n) \tag{4.35}$$

We can convert this set of equations into matrix form as shown below.

$$\{W\} = w^2 [C] \begin{bmatrix} \ddots & & \\ & M & \\ & & \ddots \end{bmatrix} \{W\} \tag{4.36}$$

By solving this equation, we get eigenvalue values that enable us to find mode shapes and natural frequencies.

4.2 Modal Analysis by Using 3D Timoshenko Beam Theory and 3D Euler-Bernoulli Beam Theory

4.2.1 3D Timoshenko Beam Theory

Timoshenko beam theory eliminates the assumption that the cross-section plane remains perpendicular to the neutral axis after deformation. In this theory, the result is achieved with high accuracy by taking the shear deformation effects into account. By taking these effects into account, the flexibility of the beam is increased and as a result, lower natural frequency values are obtained compared to other methods that do not take into account these effects.

4.2.1.1 Nodal Coordinates of 3D Timoshenko Beam Theory

Figure 4.5 shows the beam element with a total of 2 nodes with 6 degrees of freedom in each node.

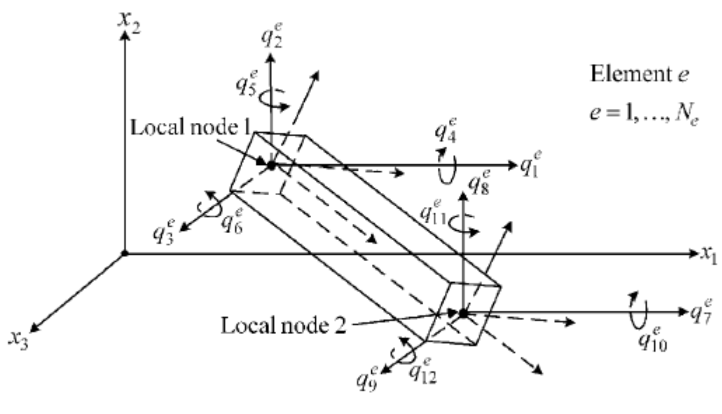

Figure 4.5 : Nodal displacements for beam element e in global coordinates[23].

These 12 degrees of freedom shown in figure 4.37 are in the global x_1, x_2 and x_3 directions. Figure 4.6 shows local degrees of freedom in 3D.

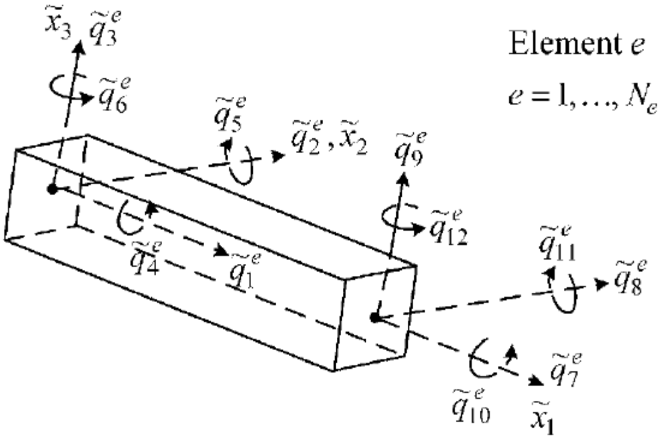

Figure 4.6 : Nodal displacements for 3D beam element e in local coordinates[23].

Figure 4.7 shows the local degrees of freedom in the local coordinate system.

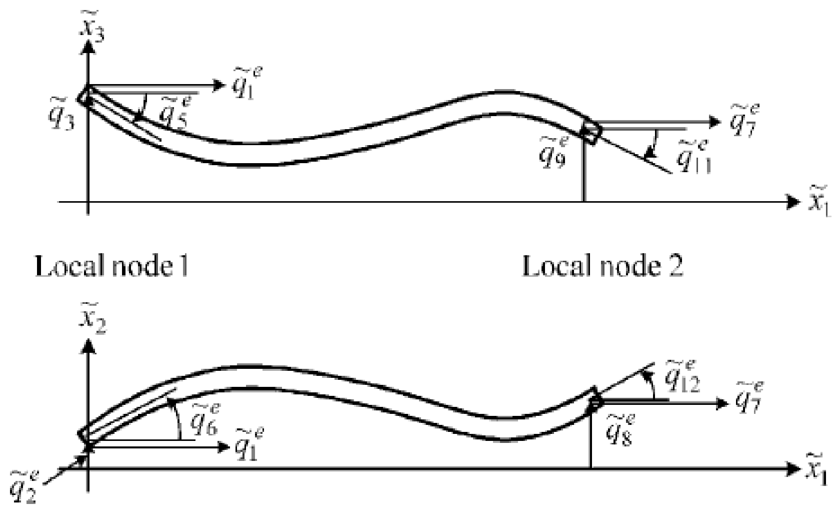

Figure 4.7 : Local degrees of freedom in the local coordinate system[23].

As can be seen from these figures, a total of 12 degrees of freedom of a beam element is expressed in the local coordinate system and the global coordinate system as follows [23] .

In local coordinates:

$$\widetilde{q}_e = (\widetilde{q}_1^e, \widetilde{q}_2^e, \widetilde{q}_3^e, \widetilde{q}_4^e, \widetilde{q}_5^e, \widetilde{q}_6^e, \widetilde{q}_7^e, \widetilde{q}_8^e, \widetilde{q}_9^e, \widetilde{q}_{10}^e, \widetilde{q}_{11}^e, \widetilde{q}_{12}^e)^T \quad (4.37)$$

In global coordinates:

$$q_e = (q_1^e,\ q_2^e,\ q_3^e,\ q_4^e,\ q_5^e,\ q_6^e,\ q_7^e,\ q_8^e,\ q_9^e,\ q_{10}^e,\ q_{11}^e,\ q_{12}^e)^T \tag{4.38}$$

Generally, displacement on both the local coordinate system and the global coordinate system is used in the vibration analysis of the structure. Displacements in the local coordinate system are used to calculate stress and reaction forces. The displacements in the global coordinate system are used to observe the general movement of the structure. We use the coordinate transformation matrix, which provides the transformation between the local coordinate system and the global coordinate system, to obtain the element stiffness matrix and the mass matrix. To better see the relationship between these two coordinate systems, the displacement vector $\vec{V}$ given in figure 4.8 is considered.

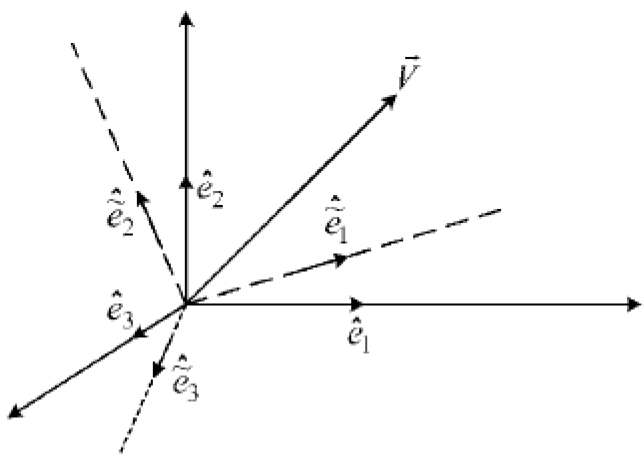

Figure 4.8 : Vector $\vec{V}$ and the local and global coordinate system unit vectors[23].

We can express this displacement vector in both coordinate systems as follows.

$$\vec{V} = V_1\hat{e}_1 + V_2\hat{e}_2 + V_3\hat{e}_3 = \widetilde{V}_1\hat{\tilde{e}}_1 + \widetilde{V}_2\hat{\tilde{e}}_2 + \widetilde{V}_3\hat{\tilde{e}}_3 \tag{4.39}$$

The transformation of the displacement vectors in these two coordinate systems between themselves is shown below.

$$\begin{Bmatrix} \widetilde{V}_1 \\ \widetilde{V}_2 \\ \widetilde{V}_3 \end{Bmatrix} = \begin{bmatrix} C_{11} & C_{12} & C_{13} \\ C_{21} & C_{22} & C_{23} \\ C_{31} & C_{32} & C_{33} \end{bmatrix} \begin{Bmatrix} V_1 \\ V_2 \\ V_3 \end{Bmatrix}, \qquad C_{ij} = cos(\angle \hat{\tilde{e}}_i, \hat{e}_j) \tag{4.40}$$

In figure 4.9 below, the rotational and translational degrees of freedom of the beam element in both the local coordinate system and the global coordinate system are shown.

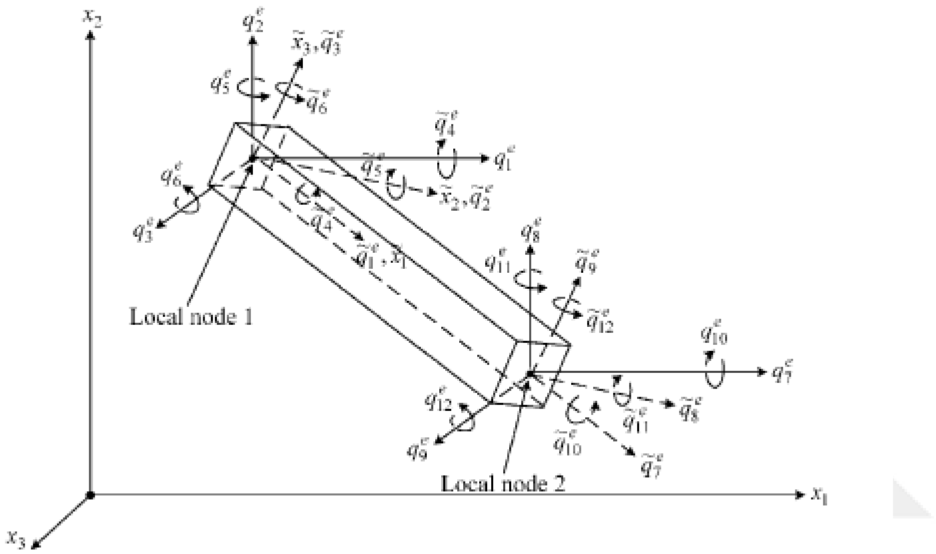

Figure 4.9 : The 12 local and 12 global displacements at nodes 1 and 2 of element[23].

The expression of the vectors shown in figure 4.10, both on the local coordinate axis and on the global coordinate axis:

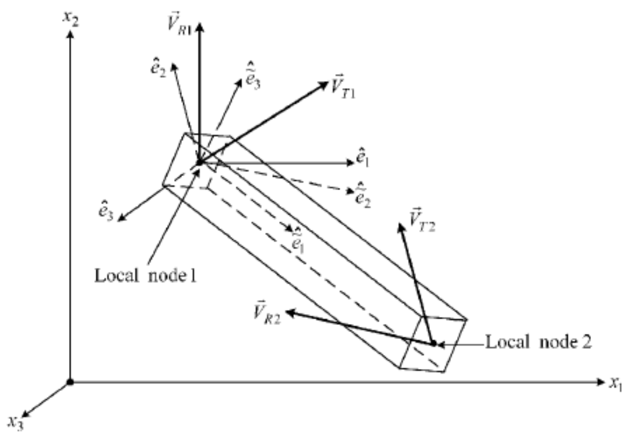

Figure 4.10 : The two nodal translation and two nodal rotation vectors of element e[23].

$$\vec{V}_{T1} = q_1^e \hat{e}_1 + q_2^e \hat{e}_2 + q_3^e \hat{e}_3 = \widetilde{q}_1^e \hat{\widetilde{e}}_1 + \widetilde{q}_2^e \hat{\widetilde{e}}_2 + \widetilde{q}_3^e \hat{\widetilde{e}}_3 = \text{translation vector at local node 1}$$

$$\vec{V}_{R1} = q_4^e \hat{e}_1 + q_5^e \hat{e}_2 + q_6^e \hat{e}_3 = \widetilde{q}_4^e \hat{\widetilde{e}}_1 + \widetilde{q}_5^e \hat{\widetilde{e}}_2 + \widetilde{q}_6^e \hat{\widetilde{e}}_3 = \text{rotation vector at local node 1}$$

$$\vec{V}_{T2} = q_7^e \hat{e}_1 + q_8^e \hat{e}_2 + q_9^e \hat{e}_3 = \widetilde{q}_7^e \hat{\widetilde{e}}_1 + \widetilde{q}_8^e \hat{\widetilde{e}}_2 + \widetilde{q}_9^e \hat{\widetilde{e}}_3 = \text{translation vector at local node 2}$$

$$\vec{V}_{R2} = q_{10}^e \hat{e}_1 + q_{11}^e \hat{e}_2 + q_{12}^e \hat{e}_3 = \widetilde{q}_{10}^e \hat{\widetilde{e}}_1 + \widetilde{q}_{11}^e \hat{\widetilde{e}}_2 + \widetilde{q}_{12}^e \hat{\widetilde{e}}_3 = \text{rotation vector at local node 2} \tag{4.41}$$

Thus, the transformation of the displacement of a 3-dimensional beam element between its coordinate axes can be expressed as follows.

$$\begin{Bmatrix} \widetilde{q}_1^e \\ \widetilde{q}_2^e \\ \widetilde{q}_3^e \\ \widetilde{q}_4^e \\ \widetilde{q}_5^e \\ \widetilde{q}_6^e \\ \widetilde{q}_7^e \\ \widetilde{q}_8^e \\ \widetilde{q}_9^e \\ \widetilde{q}_{10}^e \\ \widetilde{q}_{11}^e \\ \widetilde{q}_{12}^e \end{Bmatrix} = \begin{bmatrix} \lambda & 0 & 0 & 0 \\ 0 & \lambda & 0 & 0 \\ 0 & 0 & \lambda & 0 \\ 0 & 0 & 0 & \lambda \end{bmatrix} \begin{Bmatrix} q_1^e \\ q_2^e \\ q_3^e \\ q_4^e \\ q_5^e \\ q_6^e \\ q_7^e \\ q_8^e \\ q_9^e \\ q_{10}^e \\ q_{11}^e \\ q_{12}^e \end{Bmatrix} \tag{4.42}$$

$$\widetilde{q}_e = \widetilde{T}_e \times q_e \tag{4.43}$$

Where,

$$\lambda = \begin{bmatrix} C_{11}^e & C_{12}^e & C_{13}^e \\ C_{21}^e & C_{22}^e & C_{23}^e \\ C_{31}^e & C_{32}^e & C_{33}^e \end{bmatrix}$$

$\widetilde{q}_e$ = nodal displacement in local coordinates

$\widetilde{T}_e$ = transformation matrix

q_e = nodal displacement in global coordinates

The terms C_{11}^e, C_{12}^e and C_{13}^e in this transformation matrix are the cosine value of the angle between the local $\widetilde{x}$ axis and the global x, y, and z axes, respectively. Similarly, the terms C_{21}^e, C_{22}^e and C_{23}^e are the cosine value of the angle between the local $\widetilde{y}$ axis and the global x, y, and z axes, respectively.Likewise, the terms C_{31}^e, C_{32}^e and C_{33}^e are the cosine value of the angle between the local $\widetilde{z}$ axis and the global x, y, and z axes, respectively.

4.2.1.2 Shape Functions, Element Stiffness, and Mass Matrices

Euler-Bernoulli shape functions are used in 3D timoshenko beam theory to find the element mass matrix. This method evaluates the kinetic energy of the element in determining the mass matrix. In this method, the same shape functions are used to obtain the mass matrix and stiffness matrix of the element. Therefore, a consistent mass matrix is obtained for the element. Strain displacement relation, which is different from strain displacement relation used for Euler-Bernoulli, in equations of motion of 3D Timoshenko beam theory is used. The kinematic assumptions used in the Euleri-Bernoulli beam theory are given below.

- Cross-section planes remains plane
- cross-section planes are always perpendicular to the neutral axis before and after deformation.

These assumptions generate the following equation.

$$\widetilde{\varepsilon}_{Bx3} = -\widetilde{x}_2 \frac{\partial}{\partial \widetilde{x}_1} \left(\frac{\partial \widetilde{u}_2}{\partial \widetilde{x}_1} \right) \tag{4.44}$$

The $\widetilde{u}_2$ parameter used in this equation represents the displacement of the neutral axis in the $x2$ direction. The coordinates where the element is exposed to deformation are shown in figure 4.11.

The assumption that the cross-section planes used in the euler-bernoulli 3D beam theory will always be perpendicular to the neutral axis before and after deformation, disappears in the 3D Timoshenko's beam theory. Timoshenko beam theory includes extra displacement that is not in the Euler-Bernoulli beam theory. As shown in figure 4.11, point a moves to point a'' instead of point a' after deformation. As can be noticed from the figure, the plane $b-a'$ is perpendicular to the neutral axis.

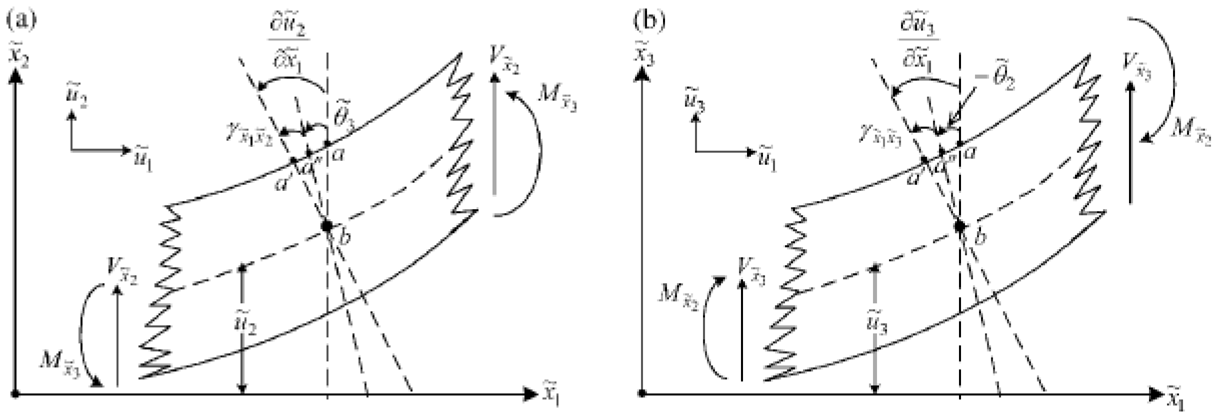

Figure 4.11 : Kinematics for beam deformation in the (a) $\widetilde{x}_1 - \widetilde{x}_2$ and (b) $\widetilde{x}_1 - \widetilde{x}_3$ planes[23].

Strain–Displacement Relations and Shear Form Factors

The neutral axis slope $\dfrac{\partial \widetilde{u}_2}{\partial \widetilde{x}_1}$ in equation 4.14 is removed from the equation and the parameter $\widetilde{\theta}_3$ is replaced.

$$\widetilde{\varepsilon}_{Bx3} = -\widetilde{x}_2 \frac{\partial \widetilde{\theta}_3}{\partial \widetilde{x}_1} \tag{4.45}$$

Similarly, the equation on the $x1 - x3$ plane is obtained as follows.

$$\widetilde{\varepsilon}_{Bx2} = -\widetilde{x}_3 \frac{\partial}{\partial \widetilde{x}_1}\left(-\widetilde{\theta}_2\right) = \widetilde{x}_3 \frac{\partial \widetilde{\theta}_2}{\partial \widetilde{x}_1} \tag{4.46}$$

Shear strain equations for $x1 - x2$ plane and $x1 - x3$ plane are obtained as follows.

$$\gamma_{\widetilde{x}_1,\widetilde{x}_2} = \frac{\partial \widetilde{u}_1}{\partial \widetilde{x}_2} + \frac{\partial \widetilde{u}_2}{\partial \widetilde{x}_1}, \quad \gamma_{\widetilde{x}_1,\widetilde{x}_3} = \frac{\partial \widetilde{u}_1}{\partial \widetilde{x}_3} + \frac{\partial \widetilde{u}_3}{\partial \widetilde{x}_1} \tag{4.47}$$

As shown in figure 4.11, the parameters of $\widetilde{\theta}_3$ and $\widetilde{\theta}_2$ can be expressed as follows.

$$\widetilde{\theta}_3 = -\frac{\partial \widetilde{u}_1}{\partial \widetilde{x}_2}, \quad \widetilde{\theta}_2 = \frac{\partial \widetilde{u}_1}{\partial \widetilde{x}_3} \tag{4.48}$$

Therefore, equation 8 can be written as follows.

$$\gamma_{\widetilde{x}_1,\widetilde{x}_2} = -\widetilde{\theta}_3 + \frac{\partial \widetilde{u}_2}{\partial \widetilde{x}_1}, \quad \gamma_{\widetilde{x}_1,\widetilde{x}_3} = \widetilde{\theta}_2 + \frac{\partial \widetilde{u}_3}{\partial \widetilde{x}_1} \tag{4.49}$$

While obtaining shear stress equations, the equation changes according to the deformation of the cross section and the position of the cross-section on the beam.

$$\tau_{\widetilde{x}_1,\widetilde{x}_2} = G\gamma_{\widetilde{x}_1,\widetilde{x}_2}(\widetilde{x}_1,\widetilde{x}_2,\widetilde{x}_3), \quad \tau_{\widetilde{x}_1,\widetilde{x}_3} = G\gamma_{\widetilde{x}_1,\widetilde{x}_3}(\widetilde{x}_1,\widetilde{x}_2,\widetilde{x}_3) \tag{4.50}$$

The G parameter in this equation represents the shear modulus of elasticity. Shear forces are obtained as follows.

$$V_{\widetilde{x}_2} = \int_{A(\widetilde{x}_1)} \tau_{\widetilde{x}_1,\widetilde{x}_2}\, dA = \tau^{ave}_{\widetilde{x}_1,\widetilde{x}_2} A, \quad V_{\widetilde{x}_2} = \int_{A(\widetilde{x}_1)} \tau_{\widetilde{x}_1,\widetilde{x}_3}\, dA = \tau^{ave}_{\widetilde{x}_1,\widetilde{x}_3} A \tag{4.51}$$

The ave in equation 4.51 represents the average value across the cross-section. As can be seen from figure 4.11, the shear strain changes only depending on the position on the x1 axis. So we get the effective shear stress equations as follows.

$$\widetilde{\tau}_{\widetilde{x}_1,\widetilde{x}_2}(\widetilde{x}_1) = G\gamma_{\widetilde{x}_1,\widetilde{x}_2}(\widetilde{\widetilde{x}}_1) \quad \text{and} \quad \widetilde{\tau}_{\widetilde{x}_1,\widetilde{x}_3}(\widetilde{x}_1) = G\gamma_{\widetilde{x}_1,\widetilde{x}_3}(\widetilde{\widetilde{x}}_1) \tag{4.52}$$

As can be understood from equation 14.52, effective shear stress values change only depending on the position on the x1 axis. Below are also average shear stress equations.

$$\tau^{ave}_{\widetilde{x}_1,\widetilde{x}_2} = k_2\widetilde{\tau}_{\widetilde{x}_1,\widetilde{x}_2}(\widetilde{x}_1) = k_2G\widetilde{\gamma}_{\widetilde{x}_1,\widetilde{x}_2}(\widetilde{x}_1), \quad \tau^{ave}_{\widetilde{x}_1,\widetilde{x}_3} = k_3\widetilde{\tau}_{\widetilde{x}_1,\widetilde{x}_3}(\widetilde{x}_1) = k_3G\widetilde{\gamma}_{\widetilde{x}_1,\widetilde{x}_3}(\widetilde{x}_1) \tag{4.53}$$

We get shear forces from equations 4.51, 4.52 and 4.53 as follows:

$$V_{\widetilde{x}_2} = k_2AG\gamma_{\widetilde{x}_1,\widetilde{x}_2}, \quad V_{\widetilde{x}_3} = k_3AG\gamma_{\widetilde{x}_1,\widetilde{x}_3} \tag{4.54}$$

From this equation, we can rewrite the effective shear stresses given in equation 4.52 in the form below.

$$\widetilde{\tau}_{\widetilde{x}_1,\widetilde{x}_2} = \frac{\tau^{ave}_{\widetilde{x}_1,\widetilde{x}_2}}{k_2} = \frac{V_{\widetilde{x}_2}}{k_2A}, \quad \widetilde{\tau}_{\widetilde{x}_1,\widetilde{x}_3} = \frac{\tau^{ave}_{\widetilde{x}_1,\widetilde{x}_3}}{k_3} = \frac{V_{\widetilde{x}_3}}{k_3A} \tag{4.55}$$

The k parameters in these equations represent shear form factor values. As will be seen in the cases we will apply later, shear form factor is obtained as follows in beam models representing the wing structure with rectangular cross-section.

$$k = \frac{10(1+\nu)}{12+11\nu} \tag{4.56}$$

ν in this equation represents the poisson ratio value. In figure 4.12, shear form factor equations are given for different cross-sections. [24]

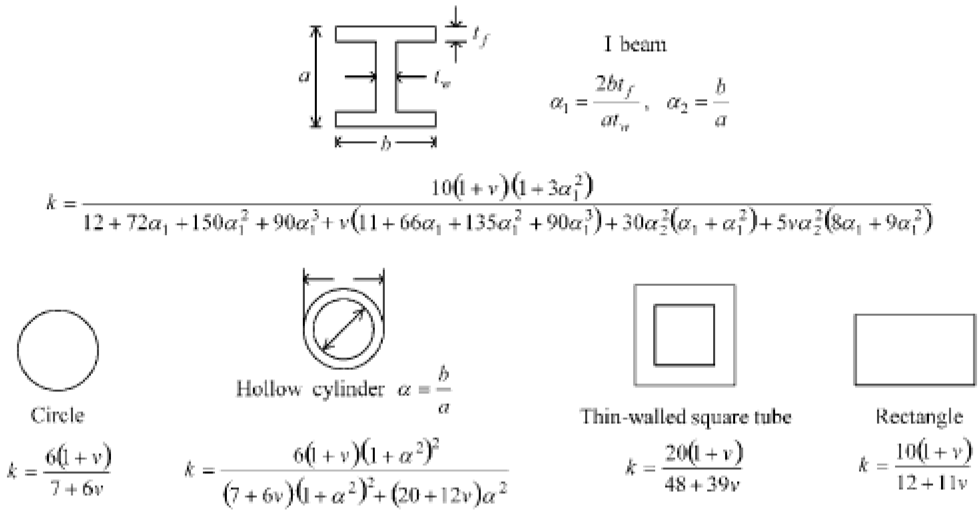

Figure 4.12 : Shear form factors for some common cross sections (ν = Poisson ratio)[23].

$\widetilde{x}_1 - \widetilde{x}_2$ Plane, Translational Differential Equations, Shape Functions, and Stiffness and Mass Matrices

The figure 4.13 below shows the strain distribution due to axial force $P_{\widetilde{x}_1}$ and bending moment $M_{\widetilde{x}_3}$.

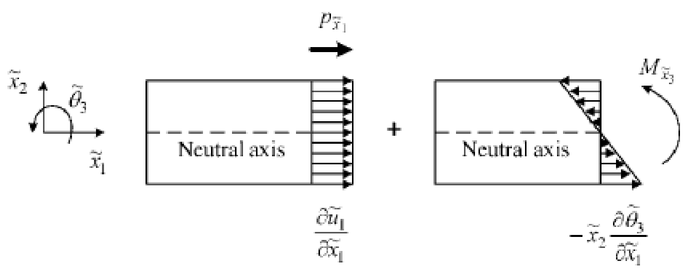

Figure 4.13 : Axial strain distribution for x1 - x2 plane deformation[23].

Strain and stress equations :

$$\varepsilon_{\widetilde{x}_1,\widetilde{x}_2} = \frac{\partial \widetilde{u}_1}{\partial \widetilde{x}_1} - \widetilde{x}_2 \frac{\partial \widetilde{\theta}_3}{\partial \widetilde{x}_1} \rightarrow \sigma_{\widetilde{x}_1,\widetilde{x}_2} = E\varepsilon_{\widetilde{x}_1,\widetilde{x}_2} = E\frac{\partial \widetilde{u}_1}{\partial \widetilde{x}_1} - E\widetilde{x}_2 \frac{\partial \widetilde{\theta}_3}{\partial \widetilde{x}_1} \tag{4.57}$$

Bending moment:

$$M_{\widetilde{x}_3} = \int_A \widetilde{x}_2(-\sigma_{\widetilde{x}_1,\widetilde{x}_2} dA) = -E\frac{\partial \widetilde{u}_1}{\partial \widetilde{x}_1}\int_A \widetilde{x}_2\, dA + E\frac{\partial \widetilde{\theta}_3}{\partial \widetilde{x}_1}\int_A \widetilde{x}_2^2\, dA \tag{4.58}$$

If the cross-section is symmetrical about the neutral axis, the bending moment will change to the form below.

$$M_{\widetilde{x}_3} = EI_{\widetilde{x}_3}\frac{\partial \widetilde{\theta}_3}{\partial \widetilde{x}_1} \tag{4.59}$$

By looking at the figure 4.14 showing the free-body diagram below, we get the following equation from the moment equilibrium.

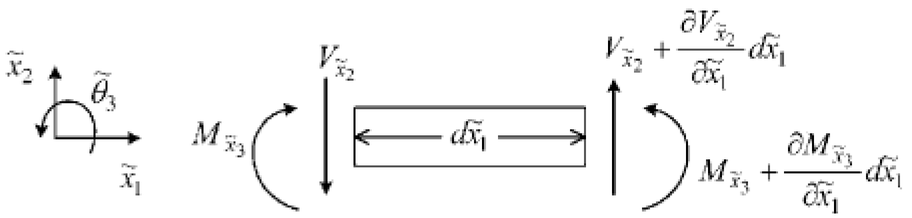

Figure 4.14 : Free body diagram of a differential beam in the x1 x2 plane[23].

$$M_{\widetilde{x}_3} + \frac{\partial M_{\widetilde{x}_3}}{\partial \widetilde{x}_1} d\widetilde{x}_1 + d\widetilde{x}_1\left(V_{\widetilde{x}_2} + \frac{\partial V_{\widetilde{x}_2}}{\partial \widetilde{x}_1} d\widetilde{x}_1\right) - M_{\widetilde{x}_3} = 0 \tag{4.60}$$

If we delete the quadratic terms in equation 4.60, we get the following equation.

$$\frac{\partial M_{\widetilde{x}_3}}{\partial \widetilde{x}_1} + V_{\widetilde{x}_2} = 0 \tag{4.61}$$

The following equation is obtained from the sum of the shear forces on the free-body diagram.

$$-V_{\widetilde{x}_2}+V_{\widetilde{x}_2}+\frac{\partial V_{\widetilde{x}_2}}{\partial \widetilde{x}_1}\,d\widetilde{x}_1=0\rightarrow\frac{\partial V_{\widetilde{x}_2}}{\partial \widetilde{x}_1}=0 \tag{4.62}$$

If we rethink equation 4.18 and equation 4.54:

$$V_{\widetilde{x}_2}=k_2AG\gamma_{\widetilde{x}_1,\widetilde{x}_2}=k_2AG\left(-\widetilde{\theta}_3+\frac{\partial \widetilde{u}_2}{\partial \widetilde{x}_1}\right) \tag{4.63}$$

Governing equation in the $\widetilde{x}_1-\widetilde{x}_2$ plane:

$$\frac{dz^{12}}{d\widetilde{x}_1}=G^{12}z^{12}\quad(4\times 1) \tag{4.64}$$

Where,

$$z^{12}=\begin{Bmatrix}\underset{2\times1}{D^{12}}\\----\\\underset{2\times1}{F^{12}}\end{Bmatrix}=\begin{Bmatrix}\widetilde{u}_2\\\widetilde{\theta}_3\\--\\V_{\widetilde{x}_2}\\M_{\widetilde{x}_3}\end{Bmatrix},\; G_{12}=\begin{bmatrix}0&1&a_{12}&0\\1&0&0&b_{12}\\0&0&0&0\\0&0&-1&0\end{bmatrix},\; a_{12}=\frac{1}{k_2AG},\; b_{12}=\frac{1}{EI_{\widetilde{x}_3}} \tag{4.65}$$

Symbolic solution of equation 4.64:

$$z^{12}(\widetilde{x}_1)=\begin{Bmatrix}\underset{2\times1}{D^{12}}\\----\\\underset{2\times1}{F^{12}}\end{Bmatrix}_{(\widetilde{x}_1)}=\begin{Bmatrix}\widetilde{u}_2\\\widetilde{\theta}_3\\--\\V_{\widetilde{x}_2}\\M_{\widetilde{x}_3}\end{Bmatrix}_{(\widetilde{x}_1)}=\begin{bmatrix}\underset{2\times2}{A_{11}}&\underset{2\times2}{A_{12}}\\\underset{2\times2}{A_{21}}&\underset{2\times2}{A_{22}}\end{bmatrix}\begin{Bmatrix}\widetilde{u}_{20}\\\widetilde{\theta}_{30}\\--\\-V_{\widetilde{x}_2 0}\\-M_{\widetilde{x}_3 0}\end{Bmatrix} \tag{4.66}$$

$$D_{2\times1}(\widetilde{x}_1)=\begin{Bmatrix}\widetilde{u}_2(\widetilde{x}_1)\\\widetilde{\theta}_3(\widetilde{x}_1)\end{Bmatrix}=N^{12}_{2\times4}(\widetilde{x}_1)\begin{Bmatrix}\underset{2\times1}{D_0}\\---\\\underset{2\times1}{D_L}\end{Bmatrix}=N^{12}_{2\times4}(\widetilde{x}_1)\begin{Bmatrix}\widetilde{u}_2(0)\\\widetilde{\theta}_3(0)\\\widetilde{u}_2(L)\\\widetilde{\theta}_3(L)\end{Bmatrix} \tag{4.67}$$

$$F^{12}=\begin{Bmatrix}\underset{2\times1}{F_0}\\----\\\underset{2\times1}{F_L}\end{Bmatrix}=\begin{bmatrix}\underset{2\times2}{K^{12}_{11}}&\underset{2\times2}{K^{12}_{12}}\\\underset{2\times2}{K^{12}_{21}}&\underset{2\times2}{K^{12}_{22}}\end{bmatrix}\begin{Bmatrix}\underset{2\times1}{D_0}\\----\\\underset{2\times1}{D_L}\end{Bmatrix}=\widetilde{K}^{12}D^{12} \tag{4.68}$$

Where,

$$N^{12}(\widetilde{x}_1) = \begin{bmatrix} N_{11}^{12}(\widetilde{x}_1) & N_{12}^{12}(\widetilde{x}_1) & N_{13}^{12}(\widetilde{x}_1) & N_{14}^{12}(\widetilde{x}_1) \\ N_{21}^{12}(\widetilde{x}_1) & N_{22}^{12}(\widetilde{x}_1) & N_{23}^{12}(\widetilde{x}_1) & N_{24}^{12}(\widetilde{x}_1) \end{bmatrix} \tag{4.69}$$

$$\begin{aligned}
N_{11}^{12} &= \gamma_1^{12}(L^3 + 2\widetilde{x}_1^3 - 3\widetilde{x}_1^2 L) + 12\gamma_2^{12}(L - \widetilde{x}_1) \\
N_{12}^{12} &= \gamma_1^{12}(\widetilde{x}_1 L^3 + \widetilde{x}_1^3 L - 2\widetilde{x}_1^2 L^2) + 6\gamma_2^{12}\widetilde{x}_1(L - \widetilde{x}_1) \\
N_{13}^{12} &= -\gamma_1^{12}(2\widetilde{x}_1^3 - 3\widetilde{x}_1^2 L) + \gamma_2^{12}(12\widetilde{x}_1) \\
N_{14}^{12} &= \gamma_1^{12}(\widetilde{x}_1^3 L - \widetilde{x}_1^2 L^2) + 6\gamma_2^{12}\widetilde{x}_1(\widetilde{x}_1 - L) \\
N_{21}^{12} &= 6\gamma_1^{12}\widetilde{x}_1(\widetilde{x}_1 - L) \\
N_{22}^{12} &= \gamma_1^{12}(L^3 + 3\widetilde{x}_1^2 L - 4\widetilde{x}_1 L^2) + 12\gamma_2^{12}(L - \widetilde{x}_1) \\
N_{23}^{12} &= -6\gamma_1^{12}\widetilde{x}_1(\widetilde{x}_1 - L) \\
N_{24}^{12} &= \gamma_1^{12}\widetilde{x}_1(3\widetilde{x}_1 L - 2L^2) + 12\gamma_2^{12}\widetilde{x}_1
\end{aligned} \tag{4.70}$$

$$\begin{gathered}
\widetilde{K}_{11}^{12} = A_{12}^{-1}(L)A_{11}(L),\ \widetilde{K}_{12}^{12} = -A_{12}^{-1}(L) \\
\widetilde{K}_{12}^{12} = A_{12}(L) - A_{22}(L)A_{12}^{-1}(L)A_{11}(L),\ \widetilde{K}_{22}^{12} = A_{22}(L)A_{12}^{-1}(L)
\end{gathered} \tag{4.71}$$

$$A_{11} = \begin{bmatrix} 1 & \widetilde{x}_1 \\ 0 & 1 \end{bmatrix},\ A_{12} = \begin{bmatrix} -\dfrac{b_{12}}{6}\widetilde{x}_1^3 + a_{12}\widetilde{x}_1 & \dfrac{b_{12}}{2}\widetilde{x}_1^2 \\ -\dfrac{b_{12}}{2}\widetilde{x}_1^2 & b_{12}\widetilde{x}_1 \end{bmatrix},\ A_{21} = \begin{bmatrix} 0 & 0 \\ 0 & 0 \end{bmatrix},\ A_{22} = \begin{bmatrix} 1 & 0 \\ -\widetilde{x}_1 & 1 \end{bmatrix} \tag{4.72}$$

Where,

$$\Phi_{12} = \frac{12EI_{\widetilde{x}_3}}{k_2 AGL^2} = \frac{24I_{\widetilde{x}_3}(1+\nu)}{k_2 AL^2},\ \gamma_1^{12} = \frac{1}{L^3(1+\Phi_{12})},\ \gamma_2^{12} = \frac{1}{12L(1+\Phi_{12}^{-1})} \tag{4.73}$$

Finally stiffness matris for the $x1 - x2$ plane :

$$\widetilde{K}^{12} = \begin{bmatrix} \frac{12EI_{\widetilde{x}_3}}{L^3(1+\Phi_{12})} & \frac{6EI_{\widetilde{x}_3}}{L^2(1+\Phi_{12})} & \frac{-12EI_{\widetilde{x}_3}}{L^3(1+\Phi_{12})} & \frac{6EI_{\widetilde{x}_3}}{L^2(1+\Phi_{12})} \\ \frac{6EI_{\widetilde{x}_3}}{L^2(1+\Phi_{12})} & \frac{EI_{\widetilde{x}_3(4+\Phi_{12})}}{L(1+\Phi_{12})} & \frac{-6EI_{\widetilde{x}_3}}{L^2(1+\Phi_{12})} & \frac{EI_{\widetilde{x}_3(2-\Phi_{12})}}{L(1+\Phi_{12})} \\ \frac{-12EI_{\widetilde{x}_3}}{L^3(1+\Phi_{12})} & \frac{-6EI_{\widetilde{x}_3}}{L^2(1+\Phi_{12})} & \frac{12EI_{\widetilde{x}_3}}{L^3(1+\Phi_{12})} & \frac{-6EI_{\widetilde{x}_3}}{L^2(1+\Phi_{12})} \\ \frac{6EI_{\widetilde{x}_3}}{L^2(1+\Phi_{12})} & \frac{EI_{\widetilde{x}_3(2-\Phi_{12})}}{L(1+\Phi_{12})} & \frac{-6EI_{\widetilde{x}_3}}{L^2(1+\Phi_{12})} & \frac{EI_{\widetilde{x}_3(4+\Phi_{12})}}{L(1+\Phi_{12})} \end{bmatrix} \tag{4.74}$$

where,

$$\begin{aligned} I_{\widetilde{x}_2} &= \int_A \widetilde{x}_3^2\, dA = \text{area moment of inertia about the } \widetilde{x}_2 \text{ axis} \\ I_{\widetilde{x}_3} &= \int_A \widetilde{x}_2^2\, dA = \text{area moment of inertia about the } \widetilde{x}_3 \text{ axis} \\ J_P &= \int_A \left(\widetilde{x}_2^2 + \widetilde{x}_3^2\right) dA = I_{\widetilde{x}_2} + I_{\widetilde{x}_3} = \text{area polar moment of inertia} \end{aligned} \tag{4.75}$$

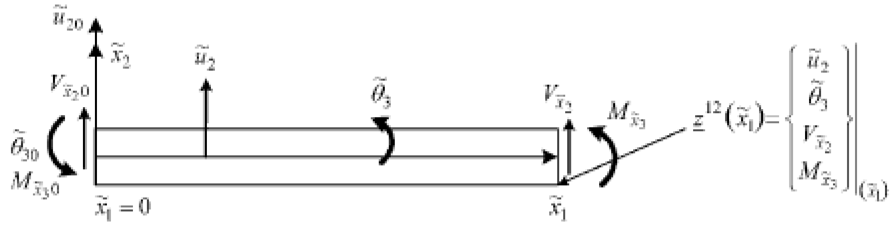

Figure 4.15 : Free body diagram of a beam in the x1 x2 plane[23].

Below is the equation that allows us to obtain the translation mass matrix and the rotary mass matrix.

$$\widetilde{M}_{12u} = \rho A \int_0^L N_{12u}^T N_{12u}\, d\widetilde{x}_1,\ \widetilde{M}_{12\theta} = \rho I_{\widetilde{x}_3} \int_0^L N_{12\theta}^T N_{12\theta}\, d\widetilde{x}_1 \tag{4.76}$$

The translation mass matrix and rotary mass matrix in degrees of freedom u1, theta1, u2 and theta2 are given below.

$$\widetilde{M}_{12u} = \frac{\rho A L}{420 \times (b_{12}L^2 + 12a_{12})^2} \begin{bmatrix} a_1^{12u} & & & \\ a_2^{12u} & a_5^{12u} & \text{symmetric} & \\ a_3^{12u} & -a_4^{12u} & a_1^{12u} & \\ a_4^{12u} & a_6^{12u} & -a_2^{12u} & a_5^{12u} \end{bmatrix} \tag{4.77}$$

Where,

$$
\begin{aligned}
a_1^{12u} &= 156b_{12}^2L^4 + 3528a_{12}b_{12}L^2 + 20160a_{12}^2 \\
a_2^{12u} &= 2L(11b_{12}^2L^4 + 231a_{12}b_{12}L^2 + 1260a_{12}^2) \\
a_3^{12u} &= 54b_{12}^2L^4 + 1512a_{12}b_{12}L^2 + 10080a_{12}^2 \\
a_4^{12u} &= -L(13b_{12}^2L^4 + 378b_{12}b_{12}L^2 + 2520a_{12}^2) \\
a_5^{12u} &= L^2(4b_{12}^2L^4 + 84b_{12}b_{12})L^2 + 504a_{12}^2 \\
a_6^{12u} &= -3L^2(b_{12}^2L^4 + 28b_{12}b_{12}L^2 + 168a_{12}^2)
\end{aligned}
\tag{4.78}
$$

$$
\widetilde{M}_{12\theta} = \frac{\rho I_{\widetilde{x}_3}L}{30 \times (b_{12}L^2 + 12a_{12})^2}
\begin{bmatrix}
a_1^{12\theta} & & & \\
a_2^{12\theta} & a_3^{12\theta} & \text{symmetric} & \\
-a_1^{12\theta} & -a_2^{12\theta} & a_1^{12\theta} & \\
a_2^{12\theta} & a_4^{12\theta} & -a_2^{12\theta} & a_3^{12\theta}
\end{bmatrix}
\tag{4.79}
$$

Where,

$$
\begin{aligned}
a_1^{12\theta} &= 36b_{12}^2L^2 \\
a_2^{12\theta} &= -3Lb_{12}(-b_{12}L^2 + 60a_{12}) \\
a_3^{12\theta} &= 4b_{12}^2L^4 + 60a_{12}b_{12}L^2 + 1440a_{12}^2 \\
a_4^{12\theta} &= -b_{12}^2L^4 - 60a_{12}b_{12}L^2 + 720a_{12}^2
\end{aligned}
\tag{4.80}
$$

$\widetilde{x}_1 - \widetilde{x}_3$ Plane, Translational Differential Equations, Shape Functions, and Stiffness and Mass Matrices

The figure 4.16 below shows the strain distribution in the $X1 - X3$ plane due to axial force $P_{\widetilde{x}_1}$ and bending moment $M_{\widetilde{x}_3}$.

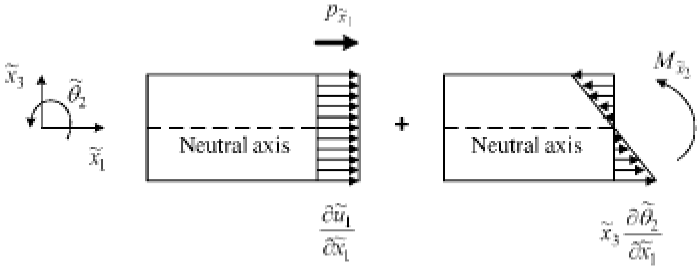

Figure 4.16 : Axial strain distribution for x1 x3 plane deformation[23].

Strain ve stress equations :

$$\varepsilon_{\tilde{x}_1,\tilde{x}_2} = \frac{\partial \tilde{u}_1}{\partial \tilde{x}_1} + \tilde{x}_3 \frac{\partial \tilde{\theta}_2}{\partial \tilde{x}_1} \rightarrow \sigma_{\tilde{x}_1,\tilde{x}_2} = E\varepsilon_{\tilde{x}_1,\tilde{x}_2} = E\frac{\partial \tilde{u}_1}{\partial \tilde{x}_1} + E\tilde{x}_3 \frac{\partial \tilde{\theta}_2}{\partial \tilde{x}_1} \tag{4.81}$$

Bending moment:

$$M_{\tilde{x}_2} = \int_A \tilde{x}_3(-\sigma_{\tilde{x}_1,\tilde{x}_2} dA) = -E\frac{\partial \tilde{u}_1}{\partial \tilde{x}_1}\int_A \tilde{x}_3\, dA + E\frac{\partial \tilde{\theta}_2}{\partial \tilde{x}_1}\int_A \tilde{x}_3^2\, dA \tag{4.82}$$

If the cross-section is symmetrical about the neutral axis, the bending moment will change to the form below.

$$M_{\tilde{x}_2} = EI_{\tilde{x}_2}\frac{\partial \tilde{\theta}_2}{\partial \tilde{x}_1} \tag{4.83}$$

By looking at the figure 4.17 showing the free-body diagram below, we get the following equation from the moment equilibrium.

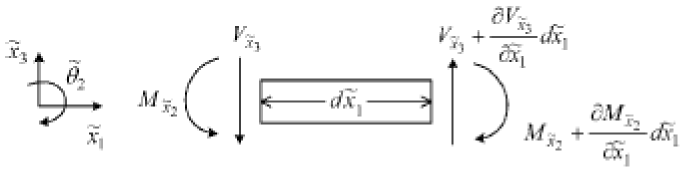

Figure 4.17 : Free body diagram of a differential beam in the x1 x3 plane[23].

$$M_{\tilde{x}_2} + \frac{\partial M_{\tilde{x}_2}}{\partial \tilde{x}_1} d\tilde{x}\_d\tilde{x}_1 \left(V_{\tilde{x}_3} + \frac{\partial V_{\tilde{x}_3}}{\partial \tilde{x}_1} d\tilde{x}_1\right) - M_{\tilde{x}_2} = 0 \tag{4.84}$$

If we delete the quadratic terms in equation 4.84, we get the following equation.

$$\frac{\partial M_{\tilde{x}_2}}{\partial \tilde{x}_1} - V_{\tilde{x}_3} = 0 \tag{4.85}$$

The following equation is obtained from the sum of the shear forces on the free-body diagram.

$$-V_{\tilde{x}_3} + V_{\tilde{x}_3} + \frac{\partial V_{\tilde{x}_3}}{\partial \tilde{x}_1} d\tilde{x}_1 = 0 \rightarrow \frac{\partial V_{\tilde{x}_3}}{\partial \tilde{x}_1} = 0 \tag{4.86}$$

If we rethink equation 4.18 and equation 4.54:

$$V_{\tilde{x}_3} = k_3 AG\gamma_{\tilde{x}_1,\tilde{x}_3} = k_3 AG\left(\tilde{\theta}_2 + \frac{\partial \tilde{u}_3}{\partial \tilde{x}_1}\right) \tag{4.87}$$

Governing equation in the $\tilde{x}_1 - \tilde{x}_3$ plane:

$$\frac{dz^{13}}{d\tilde{x}_1} = G^{13} z^{13} \quad (4\times 1) \tag{4.88}$$

Where,

$$z^{13} = \begin{Bmatrix} \underset{2\times 1}{D^{13}} \\ ----- \\ \underset{2\times 1}{F^{13}} \end{Bmatrix} = \begin{Bmatrix} \tilde{u}_3 \\ \tilde{\theta}_2 \\ -- \\ V_{\tilde{x}_3} \\ M_{\tilde{x}_2} \end{Bmatrix},\ G_{13} = \begin{bmatrix} 0 & 1 & a_{13} & 0 \\ 0 & 0 & 0 & b_{13} \\ 0 & 0 & 0 & 0 \\ 0 & 0 & 1 & 0 \end{bmatrix},\ a_{13} = \frac{1}{k_3 AG},\ b_{13} = \frac{1}{EI_{\tilde{x}_2}} \tag{4.89}$$

Symbolic solution of equation 4.64:

$$z^{13}(\tilde{x}_1) = \begin{Bmatrix} \underset{2\times 1}{D^{13}} \\ ----- \\ \underset{2\times 1}{F^{13}} \end{Bmatrix}_{(\tilde{x}_1)} = \begin{Bmatrix} \tilde{u}_3 \\ \tilde{\theta}_2 \\ -- \\ V_{\tilde{x}_3} \\ M_{\tilde{x}_2} \end{Bmatrix}_{(\tilde{x}_1)} = \begin{bmatrix} \underset{2\times 2}{\hat{A}_{11}} & \underset{2\times 2}{\hat{A}_{12}} \\ \underset{2\times 2}{\hat{A}_{21}} & \underset{2\times 2}{\hat{A}_{22}} \end{bmatrix} \begin{Bmatrix} \tilde{u}_{30} \\ \tilde{\theta}_{20} \\ -- \\ -V_{\tilde{x}_3 0} \\ -M_{\tilde{x}_2 0} \end{Bmatrix} \tag{4.90}$$

$$D_{2\times 1}(\tilde{x}_1) = \begin{Bmatrix} \tilde{u}_3(\tilde{x}_1) \\ \tilde{\theta}_2(\tilde{x}_1) \end{Bmatrix} = N^{13}_{2\times 4}(\tilde{x}_1) \begin{Bmatrix} \underset{2\times 1}{\hat{D}_0} \\ ---- \\ \underset{2\times 1}{\hat{D}_L} \end{Bmatrix} = N^{13}_{2\times 4}(\tilde{x}_1) \begin{Bmatrix} \tilde{u}_3(0) \\ \tilde{\theta}_2(0) \\ \tilde{u}_3(L) \\ \tilde{\theta}_2(L) \end{Bmatrix} \tag{4.91}$$

$$F^{13} = \begin{Bmatrix} \underset{2\times 1}{F_0} \\ ----- \\ \underset{2\times 1}{F_L} \end{Bmatrix} = \begin{bmatrix} \underset{2\times 2}{K^{13}_{11}} & \underset{2\times 2}{K^{13}_{12}} \\ \underset{2\times 2}{K^{13}_{21}} & \underset{2\times 2}{K^{13}_{22}} \end{bmatrix} \begin{Bmatrix} \underset{2\times 1}{D_0} \\ ----- \\ \underset{2\times 1}{D_L} \end{Bmatrix} = \tilde{K}^{13} D^{13} \tag{4.92}$$

Where,

$$N^{13}(\widetilde{x}_1) = \begin{bmatrix} N_{11}^{13}(\widetilde{x}_1) & N_{12}^{13}(\widetilde{x}_1) & N_{13}^{13}(\widetilde{x}_1) & N_{14}^{13}(\widetilde{x}_1) \\ N_{21}^{13}(\widetilde{x}_1) & N_{22}^{13}(\widetilde{x}_1) & N_{23}^{13}(\widetilde{x}_1) & N_{24}^{13}(\widetilde{x}_1) \end{bmatrix} \tag{4.93}$$

$$\begin{aligned}
N_{11}^{13} &= \gamma_1^{13}(L^3 + 2\widetilde{x}_1^3 - 3\widetilde{x}_1^2 L) + 12\gamma_2^{13}(L - \widetilde{x}_1) \\
N_{12}^{13} &= -\gamma_1^{13}(\widetilde{x}_1 L^3 + \widetilde{x}_1^3 L - 2\widetilde{x}_1^2 L^2) - 6\gamma_2^{13}\widetilde{x}_1(L - \widetilde{x}_1) \\
N_{13}^{13} &= -\gamma_1^{13}(2\widetilde{x}_1^3 - 3\widetilde{x}_1^2 L) + \gamma_2^{13}(12\widetilde{x}_1) \\
N_{14}^{13} &= -\gamma_1^{13}(\widetilde{x}_1^3 L - \widetilde{x}_1^2 L^2) - 6\gamma_2^{13}\widetilde{x}_1(\widetilde{x}_1 - L) \\
N_{21}^{13} &= -6\gamma_1^{13}\widetilde{x}_1(\widetilde{x}_1 - L) \\
N_{22}^{13} &= \gamma_1^{13}(L^3 + 3\widetilde{x}_1^2 L - 4\widetilde{x}_1 L^2) + 12\gamma_2^{13}(L - \widetilde{x}_1) \\
N_{23}^{13} &= 6\gamma_1^{13}\widetilde{x}_1(\widetilde{x}_1 - L) \\
N_{24}^{12} &= \gamma_1^{13}\widetilde{x}_1(3\widetilde{x}_1 L - 2L^2) + 12\gamma_2^{13}\widetilde{x}_1
\end{aligned} \tag{4.94}$$

$$D_0 = \begin{Bmatrix} \widetilde{u}_{30} \\ \widetilde{\theta}_{20} \end{Bmatrix},\ D_L = \begin{Bmatrix} \widetilde{u}_{3L} \\ \widetilde{\theta}_{2L} \end{Bmatrix},\ F_0 = \begin{Bmatrix} V_{\widetilde{x}_3 0} \\ M_{\widetilde{x}_2 0} \end{Bmatrix},\ F_L = \begin{Bmatrix} V_{\widetilde{x}_3 L} \\ M_{\widetilde{x}_2 L} \end{Bmatrix} \tag{4.95}$$

$$\hat{A}_{11} = \begin{bmatrix} 1 & -\widetilde{x}_1 \\ 0 & 1 \end{bmatrix},\ \hat{A}_{12} = \begin{bmatrix} -\frac{b_{13}}{6}\widetilde{x}_1^3 + a_{13}\widetilde{x}_1 & -\frac{b_{13}}{2}\widetilde{x}_1^2 \\ \frac{b_{13}}{2}\widetilde{x}_1^2 & b_{13}\widetilde{x}_1 \end{bmatrix},\ \hat{A}_{21} = \begin{bmatrix} 0 & 0 \\ 0 & 0 \end{bmatrix},\ \hat{A}_{22} = \begin{bmatrix} 1 & 0 \\ \widetilde{x}_1 & 1 \end{bmatrix} \tag{4.96}$$

Where,

$$\Phi_{13} = \frac{12EI_{\widetilde{x}_2}}{k_{13}AGL^2} = \frac{24I_{\widetilde{x}_2}(1+\nu)}{k_{13}AL^2},\ \gamma_2^{13} = \frac{\gamma_{13}}{12L(1+\Phi_{13})} = \frac{1}{12L(1+\Phi_{13}^{-1})} \tag{4.97}$$

Finally stiffness matris for the $x1 - x3$ plane :

$$\widetilde{K}^{13} = \begin{bmatrix} \frac{12EI_{\widetilde{x}_3}}{L^3(1+\Phi_{13})} & \frac{-6EI_{\widetilde{x}_2}}{L^2(1+\Phi_{13})} & \frac{-12EI_{\widetilde{x}_2}}{L^3(1+\Phi_{13})} & \frac{-6EI_{\widetilde{x}_2}}{L^2(1+\Phi_{13})} \\ \frac{-6EI_{\widetilde{x}_2}}{L^2(1+\Phi_{13})} & \frac{EI_{\widetilde{x}_2(4+\Phi_{13})}}{L(1+\Phi_{13})} & \frac{6EI_{\widetilde{x}_2}}{L^2(1+\Phi_{13})} & \frac{EI_{\widetilde{x}_2(2-\Phi_{13})}}{L(1+\Phi_{13})} \\ \frac{-12EI_{\widetilde{x}_2}}{L^3(1+\Phi_{13})} & \frac{6EI_{\widetilde{x}_2}}{L^2(1+\Phi_{13})} & \frac{12EI_{\widetilde{x}_2}}{L^3(1+\Phi_{13})} & \frac{6EI_{\widetilde{x}_2}}{L^2(1+\Phi_{13})} \\ \frac{-6EI_{\widetilde{x}_2}}{L^2(1+\Phi_{13})} & \frac{EI_{\widetilde{x}_2(2-\Phi_{13})}}{L(1+\Phi_{13})} & \frac{6EI_{\widetilde{x}_2}}{L^2(1+\Phi_{13})} & \frac{EI_{\widetilde{x}_2(4+\Phi_{13})}}{L(1+\Phi_{13})} \end{bmatrix} \tag{4.98}$$

The numbers on the top and side of this matrix represent degrees of freedom. These degrees of freedom are $\widetilde{q}_3$, $\widetilde{q}_5$, $\widetilde{q}_9$ and $\widetilde{q}_1 1$, respectively. These degrees of freedom represent $\widetilde{u}_{30}$, $\widetilde{\theta}_{20}$, $\widetilde{u}_{3L}$ and $\widetilde{\theta}_{2L}$, respectively. Below is the equation that allows us to obtain the translation mass matrix and the rotary mass matrix.

$$\widetilde{M}_{13u} = \rho A \int_0^L N_{13u}^T N_{13u}\, d\widetilde{x}_1,\ \widetilde{M}_{13\theta} = \rho I_{\widetilde{x}_2} \int_0^L N_{13\theta}^T N_{13\theta}\, d\widetilde{x}_1 \tag{4.99}$$

The translation mass matrix and rotary mass matrix in degrees of freedom $\widetilde{u}_{30}$, $\widetilde{\theta}_{20}$, $\widetilde{u}_{3L}$ and $\widetilde{\theta}_{2L}$ are given below.

$$\widetilde{M}_{13u} = \frac{\rho A L}{420 \times (b_{13}L^2 + 12a_{13})^2} \begin{bmatrix} a_1^{13u} & & & \\ a_2^{13u} & a_5^{13u} & \text{symmetric} & \\ a_3^{13u} & -a_4^{13u} & a_1^{13u} & \\ a_4^{13u} & a_6^{13u} & -a_2^{13u} & a_5^{13u} \end{bmatrix} \tag{4.100}$$

Where,

$$\begin{aligned} a_1^{13u} &= 156b_{13}^2L^4 + 3528a_{13}b_{13}L^2 + 20160a_{13}^2 \\ a_2^{13u} &= -2L(11b_{13}^2L^4 + 231a_{13}b_{13}L^2 + 1260a_{13}^2) \\ a_3^{13u} &= 54b_{13}^2L^4 + 1512a_{13}b_{13}L^2 + 10080a_{13}^2 \\ a_4^{13u} &= L(13b_{13}^2L^4 + 378b_{13}b_{13}L^2 + 2520a_{13}^2) \\ a_5^{13u} &= L^2(4b_{13}^2L^4 + 84b_{13}b_{13})L^2 + 504a_{13}^2 \\ a_6^{13u} &= -3L^2(b_{13}^2L^4 + 28b_{13}b_{13}L^2 + 168a_{13}^2) \end{aligned} \tag{4.101}$$

$$\widetilde{M}_{13\theta} = \frac{\rho I_{\widetilde{x}_2} L}{30 \times (b_{13}L^2 + 12a_{13})^2} \begin{bmatrix} a_1^{13\theta} & & & \\ a_2^{13\theta} & a_3^{13\theta} & \text{symmetric} & \\ -a_1^{13\theta} & -a_2^{13\theta} & a_1^{13\theta} & \\ a_2^{13\theta} & a_4^{13\theta} & -a_2^{13\theta} & a_3^{13\theta} \end{bmatrix} \tag{4.102}$$

Where,

$$\begin{aligned} a_1^{13\theta} &= 36b_{13}^2L^2 \\ a_2^{13\theta} &= -3Lb_{13}^{(} - b_{13}L^2 + 60a_{13}) \\ a_3^{13\theta} &= 4b_{13}^2L^4 + 60a_{13}b_{13}L^2 + 1440a_{13}^2 \\ a_4^{13\theta} &= -b_{13}^2L^4 - 60a_{13}b_{13}L^2 + 720a_{13}^2 \end{aligned} \tag{4.103}$$

Axial (Longitudinal) $\widetilde{x}_1$ Differential Equation, Shape Functions, and Stiffness and Mass Matrices

The figure 4.18 below shows normal stress applied to the cross-section of the beam structure.

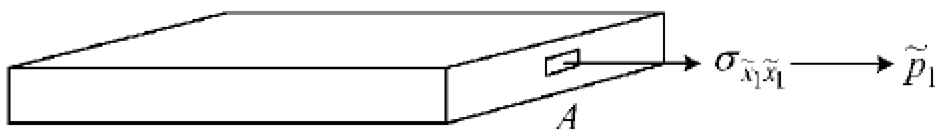

Figure 4.18 : Axial stress acting on a beam cross section[23].

As can be seen in figure 4.19, in the case of static equilibrium, $\widetilde{F}_{10}$ is equal to the size of $\widetilde{F}_{11}$ but in the opposite direction.

Figure 4.19 : Axial nodal forces on a beam element[23].

$$\begin{Bmatrix} \widetilde{F}_{10} \\ \widetilde{F}_{1L} \end{Bmatrix} = \begin{bmatrix} \frac{EA}{L} & -\frac{EA}{L} \\ -\frac{EA}{L} & \frac{EA}{L} \end{bmatrix} \begin{Bmatrix} \widetilde{u}_{10} \\ \widetilde{u}_{1L} \end{Bmatrix} \tag{4.104}$$

As a result, the axial stiffness matrix is obtained as follows.

$$\widetilde{K}_{11} = \begin{bmatrix} \frac{EA}{L} & -\frac{EA}{L} \\ -\frac{EA}{L} & \frac{EA}{L} \end{bmatrix} \tag{4.105}$$

Below is the equation that allows us to obtain the mass matrix.

$$\widetilde{M}_{ax} = \rho A \int_0^L \begin{bmatrix} N_1^{11} N_1^{11} & N_1^{11} N_2^{11} \\ N_2^{11} N_1^{11} & N_2^{11} N_2^{11} \end{bmatrix} d\widetilde{x}_1 = \rho A \int_0^L N_{ax}^T N_{ax} \, d\widetilde{x}_1 \tag{4.106}$$

where,

$$N_1^{11} = 1 - \frac{\widetilde{x}_1}{L},\ N_2^{11} = \frac{\widetilde{x}_1}{L} \tag{4.107}$$

The mass matrix in the degrees of freedom $\widetilde{u}_{10}$ and $\widetilde{u}_{1L}$ is given below.

$$N_1^{11} = 1 - \frac{\widetilde{x}_1}{L},\ N_2^{11} = \frac{\widetilde{x}_1}{L} \tag{4.108}$$

$$\widetilde{M}_{axial} = \rho AL \begin{bmatrix} \frac{1}{3} & \frac{1}{6} \\ \frac{1}{6} & \frac{1}{3} \end{bmatrix} \tag{4.109}$$

Torsional $\widetilde{\theta}_1$ Differential Equation, Shape Functions, and Stiffness and Mass Matrices

As can be seen in figure 4.20, in the case of static equilibrium, the $\widetilde{M}_{10}$ is equal to $\widetilde{M}_{1L}$ but in the opposite direction.

Figure 4.20 : Twist torques at nodes of a beam[23].

As a result, the torsional stiffness matrix is obtained as follows.

$$\widetilde{K}_{torsional} = \begin{bmatrix} \frac{GJ}{L} & -\frac{GJ}{L} \\ -\frac{GJ}{L} & \frac{GJ}{L} \end{bmatrix} \tag{4.110}$$

Below is the equation that allows us to obtain the mass matrix.

$$\widetilde{M}_{tor} = \rho\, j_P \int_0^L \begin{bmatrix} N_{\theta 1}^{11} N_{\theta 1}^{11} & N_{\theta 1}^{11} N_{\theta 2}^{11} \\ N_{\theta 2}^{11} N_{\theta 1}^{11} & N_{\theta 2}^{11} N_{\theta 2}^{11} \end{bmatrix} d\widetilde{x}_1 = \rho\, j_P \int_0^L N_{\theta 1}^T N_{\theta 1}\, d\widetilde{x}_1 \tag{4.111}$$

where,

$$N_{\theta 1}^{11} = 1 - \frac{\widetilde{x}_1}{L}, \; N_{\theta 2}^{11} = \frac{\widetilde{x}_1}{L} \tag{4.112}$$

The mass matrix in the degrees of freedom of $\widetilde{\theta}_{10}$ and $\widetilde{\theta}_{1L}$ is given below.

$$\widetilde{M}_{tosional} = \rho J_P L \begin{bmatrix} \frac{1}{3} & \frac{1}{6} \\ \frac{1}{6} & \frac{1}{3} \end{bmatrix} \tag{4.113}$$

Twelve-Dof Element Stiffness Matrix and Mass Matrix in Timoshenko's Beam Theory

The figure below shows the displacements, rotations, moments, and forces in the local coordinates of the element.

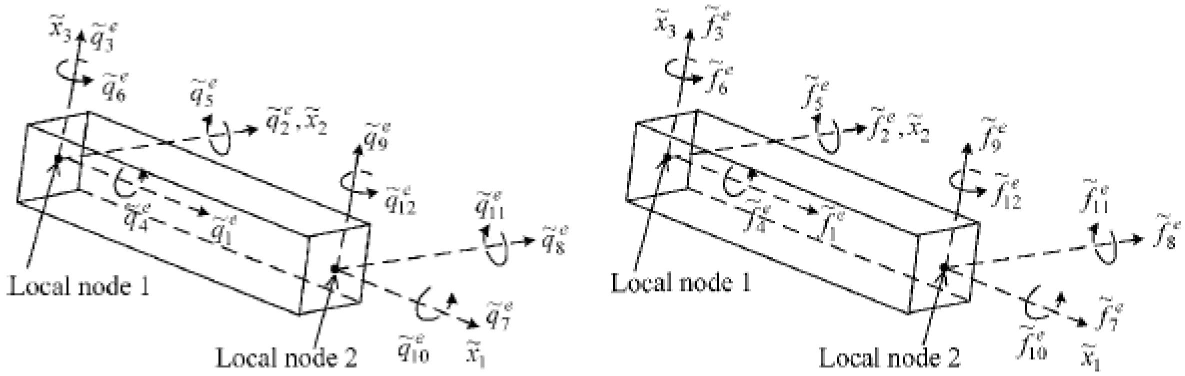

Figure 4.21 : Nodal displacements and forces in local coordinates[23].

Finally, we get the following equation which contains the stiffness matrix of the element.

$$
\begin{Bmatrix} \widetilde{f}_1 \\ \widetilde{f}_2 \\ \widetilde{f}_3 \\ \widetilde{f}_4 \\ \widetilde{f}_5 \\ \widetilde{f}_6 \\ \widetilde{f}_7 \\ \widetilde{f}_8 \\ \widetilde{f}_9 \\ \widetilde{f}_{10} \\ \widetilde{f}_{11} \\ \widetilde{f}_{12} \end{Bmatrix} = \begin{bmatrix}
\frac{EA}{L} & & & & & & & & & & & \\
0 & \frac{12\beta_{12}^a}{L^3} & & & & & & & & & & \\
0 & 0 & \frac{12\beta_{13}^a}{L^3} & & & & & & & & & \\
0 & 0 & 0 & \frac{GJ}{L} & & & & \text{symmetric} & & & & \\
0 & 0 & \frac{-6\beta_{13}^a}{L^2} & 0 & \frac{\beta_{13}^b}{L} & & & & & & & \\
0 & \frac{6\beta_{12}^a}{L^2} & 0 & 0 & 0 & \frac{\beta_{13}^b}{L} & & & & & & \\
\frac{-EA}{L} & 0 & 0 & 0 & 0 & 0 & \frac{EA}{L} & & & & & \\
0 & \frac{-12\beta_{12}^a}{L^3} & 0 & 0 & 0 & \frac{-6\beta_{12}^a}{L^2} & 0 & \frac{12\beta_{12}^a}{L^3} & & & & \\
0 & 0 & \frac{-12\beta_{13}^a}{L^3} & 0 & \frac{6\beta_{13}^a}{L^2} & 0 & 0 & 0 & \frac{12\beta_{13}^a}{L^3} & & & \\
0 & 0 & 0 & \frac{-GJ}{L} & 0 & 0 & 0 & 0 & 0 & \frac{GJ}{L} & & \\
0 & 0 & \frac{-6\beta_{13}^a}{L^2} & 0 & \frac{\beta_{13}^c}{L} & 0 & 0 & 0 & \frac{6\beta_{13}^a}{L^2} & 0 & \frac{6\beta_{13}^b}{L} & \\
0 & \frac{6\beta_{12}^a}{L^2} & 0 & 0 & 0 & \frac{\beta_{12}^c}{L} & 0 & \frac{-6\beta_{12}^a}{L^2} & 0 & 0 & 0 & \frac{\beta_{12}^b}{L}
\end{bmatrix} \begin{Bmatrix} \widetilde{q}_1 \\ \widetilde{q}_2 \\ \widetilde{q}_3 \\ \widetilde{q}_4 \\ \widetilde{q}_5 \\ \widetilde{q}_6 \\ \widetilde{q}_7 \\ \widetilde{q}_8 \\ \widetilde{q}_9 \\ \widetilde{q}_{10} \\ \widetilde{q}_{11} \\ \widetilde{q}_{12} \end{Bmatrix} \tag{4.114}
$$

We can briefly express the equation as follows:

$$\widetilde{F} = \widetilde{K}_e * \widetilde{q} \tag{4.115}$$

where

$$
\begin{aligned}
\beta_{12}^a &= \frac{EI_{\widetilde{x}_3}}{1+\Phi_{12}} & \beta_{13}^a &= \frac{EI_{\widetilde{x}_2}}{1+\Phi_{13}} \\
\beta_{12}^b &= (4+\Phi_{12})\beta_{12}^a & \beta_{13}^b &= (4+\Phi_{13})\beta_{13}^a \\
\beta_{12}^c &= (2-\Phi_{12})\beta_{12}^a & \beta_{13}^c &= (2-\Phi_{13})\beta_{13}^a \\
\Phi_{12} &= \frac{12EI_{\widetilde{x}_3}}{k_2AGL^2} = \frac{24I_{\widetilde{x}_3}(1+\nu)}{k_2AL^2} & \Phi_{13} &= \frac{12EI_{\widetilde{x}_2}}{k_3AGL^2} = \frac{24I_{\widetilde{x}_2}(1+\nu)}{k_3AL^2}
\end{aligned}
$$

The consistent mass matrix $\widetilde{M}_e^T$ elements, including rotary inertia and shear deformation effects, is given in table 4.1.

The negative sign used in parentheses of the matrix terms indicates that the corresponding value's negative will be used. Consistent mass matrix is a symmetric matrix ($\widetilde{M}_e^T = \widetilde{M}_e$). Undefined terms in this consistent mass matrix are zero. Two parameters used to find consistent mass matrix elements are given below.

$$\gamma_{m12} = \frac{\rho L}{(b_{12}L^2+12a_{12})^2}, \quad \gamma_{m13} = \frac{\rho L}{(b_{13}L^2+12a_{13})^2}$$

Table 4.1 : Consistent Mass Matrix Elements in Timoshenko's Beam Theory.

Term	**Entry**	**Term**	**Entry**
(4,4), (10,10)	$\frac{\rho J_P L}{3}$	(1,1), (7,7)	$\frac{\rho A L}{3}$
(10,4)	$\frac{\rho J_P L}{6}$	(7,1)	$\frac{\rho A L}{6}$
(2,2), (8,8)	$\gamma_{m12}\left(\frac{Aa_1^{12u}}{420}+\frac{I_{\tilde{x}_3}a_1^{12\theta}}{30}\right)$	(3,3), (9,9)	$\gamma_{m13}\left(\frac{Aa_1^{13u}}{420}+\frac{I_{\tilde{x}_2}a_1^{13\theta}}{30}\right)$
(6,2), (-12,-8)	$\gamma_{m12}\left(\frac{Aa_2^{12u}}{420}+\frac{I_{\tilde{x}_3}a_2^{12\theta}}{30}\right)$	(5,3), (-11,-9)	$\gamma_{m13}\left(\frac{Aa_2^{13u}}{420}+\frac{I_{\tilde{x}_2}a_2^{13\theta}}{30}\right)$
(8,2)	$\gamma_{m12}\left(\frac{Aa_3^{12u}}{420}-\frac{I_{\tilde{x}_3}a_2^{12\theta}}{30}\right)$	(9,3)	$\gamma_{m13}\left(\frac{Aa_3^{13u}}{420}-\frac{I_{\tilde{x}_2}a_1^{13\theta}}{30}\right)$
(12,2), (-8,-6)	$\gamma_{m12}\left(\frac{Aa_4^{12u}}{420}+\frac{I_{\tilde{x}_3}a_2^{12\theta}}{30}\right)$	(11,3), (-9,-5)	$\gamma_{m13}\left(\frac{Aa_4^{13u}}{420}+\frac{I_{\tilde{x}_2}a_2^{13\theta}}{30}\right)$
(6,6), (12,12)	$\gamma_{m12}\left(\frac{Aa_5^{12u}}{420}+\frac{I_{\tilde{x}_3}a_3^{12\theta}}{30}\right)$	(5,5), (11,11)	$\gamma_{m13}\left(\frac{Aa_5^{13u}}{420}+\frac{I_{\tilde{x}_2}a_3^{13\theta}}{30}\right)$
(12,6)	$\gamma_{m12}\left(\frac{Aa_6^{12u}}{420}+\frac{I_{\tilde{x}_3}a_4^{12\theta}}{30}\right)$	(11,5)	$\gamma_{m13}\left(\frac{Aa_6^{13u}}{420}+\frac{I_{\tilde{x}_2}a_4^{13\theta}}{30}\right)$

4.2.2 3D Euler-Bernoulli Beam Theory

In Timoshenko's beam theory, effects from shear force were included in the beam model, which represents the wing structure. For timoshenko beam theory, the effect from the shear forces was always taken into account to obtain the element stiffness matrix and the element mass matrix in the local coordinate system. For the Euler-Bernoulli beam theory, the effects from these shear forces are neglected. As will be shown in the next section, while finding stiffness matrix and mass matrix, shear deformation effects are neglected as mentioned above.

4.2.2.1 Twelve-Dof Element Stiffness Matrix and Mass Matrix in Euler-Bernoulli Beam Theory

Equation 4.116 which contains the stiffness matrix of the element is obtained using same steps as in the Timoshenko's beam theory but neglecting shear deformation effects. Below is the equation that contains the stiffness matrix of the element in local coordinate system.

$$
\begin{Bmatrix} \widetilde{f}_1 \\ \widetilde{f}_2 \\ \widetilde{f}_3 \\ \widetilde{f}_4 \\ \widetilde{f}_5 \\ \widetilde{f}_6 \\ \widetilde{f}_7 \\ \widetilde{f}_8 \\ \widetilde{f}_9 \\ \widetilde{f}_{10} \\ \widetilde{f}_{11} \\ \widetilde{f}_{12} \end{Bmatrix} =
\begin{bmatrix}
\frac{EA}{L} &&&&&&&&&&& \\
0 & \frac{12EI_{\widetilde{x}_3}}{L^3} &&&&&&&&&& \\
0 & 0 & \frac{12EI_{\widetilde{x}_2}}{L^3} &&&&&&&&& \\
0 & 0 & 0 & \frac{GJ}{L} &&&& \text{symmetric} &&&& \\
0 & 0 & \frac{-6EI_{\widetilde{x}_2}}{L^2} & 0 & \frac{4EI_{\widetilde{x}_2}}{L} &&&&&&& \\
0 & \frac{6EI_{\widetilde{x}_3}}{L^2} & 0 & 0 & 0 & \frac{4EI_{\widetilde{x}_3}}{L} &&&&&& \\
\frac{-EA}{L} & 0 & 0 & 0 & 0 & 0 & \frac{EA}{L} &&&&& \\
0 & \frac{-12EI_{\widetilde{x}_3}}{L^3} & 0 & 0 & 0 & \frac{-6EI_{\widetilde{x}_3}}{L^2} & 0 & \frac{12EI_{\widetilde{x}_3}}{L^3} &&&& \\
0 & 0 & \frac{-12EI_{\widetilde{x}_2}}{L^3} & 0 & \frac{6EI_{\widetilde{x}_2}}{L^2} & 0 & 0 & 0 & \frac{12EI_{\widetilde{x}_2}}{L^3} &&& \\
0 & 0 & 0 & \frac{-GJ}{L} & 0 & 0 & 0 & 0 & 0 & \frac{GJ}{L} && \\
0 & 0 & \frac{-6EI_{\widetilde{x}_2}}{L^2} & 0 & \frac{2EI_{\widetilde{x}_2}}{L} & 0 & 0 & 0 & \frac{6EI_{\widetilde{x}_2}}{L^2} & 0 & \frac{4EI_{\widetilde{x}_2}}{L} & \\
0 & \frac{6EI_{\widetilde{x}_3}}{L^2} & 0 & 0 & 0 & \frac{2EI_{\widetilde{x}_3}}{L} & 0 & \frac{-6EI_{\widetilde{x}_3}}{L^2} & 0 & 0 & 0 & \frac{4EI_{\widetilde{x}_3}}{L}
\end{bmatrix}
\begin{Bmatrix} \widetilde{q}_1 \\ \widetilde{q}_2 \\ \widetilde{q}_3 \\ \widetilde{q}_4 \\ \widetilde{q}_5 \\ \widetilde{q}_6 \\ \widetilde{q}_7 \\ \widetilde{q}_8 \\ \widetilde{q}_9 \\ \widetilde{q}_{10} \\ \widetilde{q}_{11} \\ \widetilde{q}_{12} \end{Bmatrix}
\tag{4.116}
$$

We can briefly express the equation as follows:

$$\widetilde{F} = \widetilde{K}_e * \widetilde{q} \tag{4.117}$$

The consistent mass matrix elements of the Euler-Bernoulli beam element is given in table 4.2.

The negative sign used in parentheses of the matrix terms indicates that the corresponding value's negative will be used. Consistent mass matrix is a symmetric matrix ($\widetilde{M}_e^T = \widetilde{M}_e$). Undefined terms in this consistent mass matrix are zero. Parameters used to find consistent mass matrix elements are given below.

$$\gamma_{m12}^{u} = \frac{\rho AL}{420}, \;\; \gamma_{m12}^{\theta} = \frac{\rho I_{\widetilde{x}_3}}{30L}, \;\; \gamma_{m13}^{u} = \frac{\rho AL}{420}, \;\; \gamma_{m13}^{\theta} = \frac{\rho I_{\widetilde{x}_2}}{30L}$$

Table 4.2 : Consistent Mass Matrix Elements in Euler-Bernoulli Beam Theory.

Term	Entry	Term	Entry
(1,1), (7,7)	$\frac{\rho AL}{3}$	(7,1)	$\frac{\rho AL}{6}$
(4,4), (10,10)	$\frac{\rho J_P L}{3}$	(10,4)	$\frac{\rho J_P L}{6}$
(2,2), (8,8)	$\gamma^u_{m12}*156+\gamma^\theta_{m12}*36$	(3,3), (9,9)	$\gamma^u_{m13}*156+\gamma^\theta_{m13}*36$
(6,2), (-12,-8)	$\gamma^u_{m12}*22L+\gamma^\theta_{m12}*3L$	(5,3), (-11,-9)	$\gamma^u_{m13}*(-22L)+\gamma^\theta_{m13}*(-3L)$
(6,6), (12,12)	$\gamma^u_{m12}*4L^2+\gamma^\theta_{m12}*4L^2$	(5,5), (11,11)	$\gamma^u_{m13}*4L^2+\gamma^\theta_{m13}*4L^2$
(8,2)	$\gamma^u_{m12}*54+\gamma^\theta_{m12}*(-36)$	(9,3)	$\gamma^u_{m13}*54+\gamma^\theta_{m13}*(-36)$
(8,6), (-12,-2)	$\gamma^u_{m12}*13L+\gamma^\theta_{m12}*(-3L)$	(9,5), (-11,-3)	$\gamma^u_{m13}*(-13L)+\gamma^\theta_{m13}*3L$
(12,6)	$\gamma^u_{m12}*(-3L^2)+\gamma^\theta_{m12}*(-L^2)$	(11,5)	$\gamma^u_{m13}*(-3L^2)+\gamma^\theta_{m13}*(-L^2)$

4.3 Using PATRAN/NASTRAN to Find Flutter Speed of the Weakened AGARD 445.6 Wing

In this section, the commercial program PATRAN / NASTRAN, which uses double lattice method, will be used to calculate aerodynamic loads. Double lattice method is an aerodynamic tool used worldwide to calculate the flutter speed of planes. double lattice method Models the lifting surface of a aircraft performing simple harmonic motion under the subsonic flow using the finite element method. As a result of this modeling, aerodynamic loads on the control surfaces and the reaction of the structure against these loads are found. Double lattice method is reduced to vortex lattice method at zero reduced frequency value. The number of elements created in this method largely depends on the aspect ratio and reduced frequency. Finite elements created at high reduced frequency values should have a low chordwise size. In fact, having a high reduced frequency value creates a requirement in the finite number of elements required for good aerodynamic modeling. The application of this method in complex geometries is achieved by eliminating singularities in lift along lines where normal speed is discontinuous. In this method, the normal speed caused by the unit force is defined by an integral of the subsonic kernel function. By providing normal speed limit conditions at certain points on the lifting surface, the load on each finite element can be calculated. By providing normal velocity boundary conditions at certain points on the lifting surface, the load on each finite element can be calculated. The validity of the double lattice method will be discussed by comparing the actual flutter speed results obtained from the experiments of a structure with the flutter speed results obtained from the commercial program PATRAN / NASTRAN. Weakened AGARD 445.6 wing is a widely used model to understand the accuracy of a flutter analysis program developed. By comparing the experimental data obtained from tests of AGARD 445.6 wing in Langley dynamic tunnel and the data obtained by using any commercial software program, it can be concluded about the accuracy of this commercial program. AGARD 445.6 wing is a wing structure with NACA 65A004 airfoil section a, 1.6525 aspect ratio, 0.6576 taper ratio and 45 degree quarter chord swept angle. Holes are available at various locations on this experimental wing structure to reduce the stiffness value. These holes are filled with a lower stiffness material to protect the aerodynamic surface. In the figure 4.22, the dimensions of the weakened AGARD 445.6 wing are given.

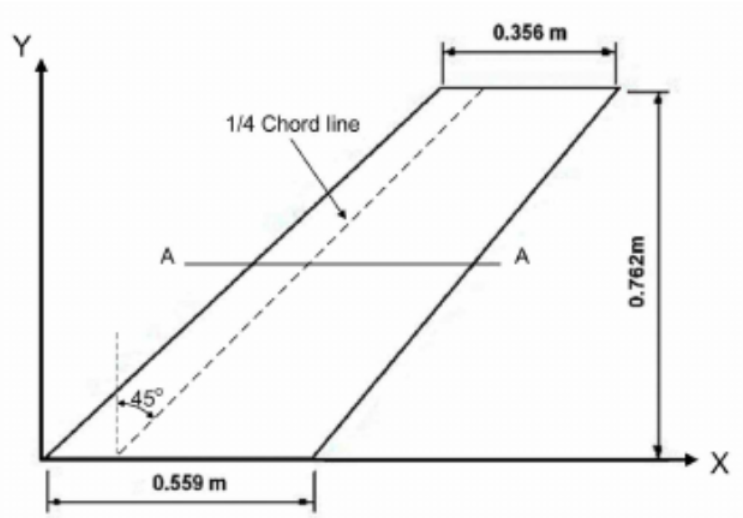

Figure 4.22 : AGARD 445.6 wing geometry.

Material properties of AGARD 445.6 wing is given below [25].

$$
\begin{aligned}
E_{11} &= 3.1511 \times 10^9 \ Pa, \\
E_{22} &= 0.4162 \times 10^9 \ Pa, \\
\nu &= 0.31, \\
G &= 0.4392 \times 10^9 \ Pa, \\
\rho(\text{density}) &= 381.98 \ kg/m^3
\end{aligned}
$$

Natural frequencies of the AGARD 445.6 wing are found in NASTRAN 103 module by modal analysis. These results are compared with the test results in table 4.3.

Table 4.3 : Natural Frequencies of Weakened AGARD 445.6.

	NASTRAN (hz)	**Experiment(hz)[25]**
Mode 1	9.56	9.6
Mode 2	39.91	38.1
Mode 3	50.1	50.7
Mode 4	96.2	98.5

Finally, using the NASTRAN aeroelasticity module, flutter speed and flutter frequency are obtained. These results are compared with the experimental results in table 4.4.

Table 4.4 : Flutter Speed and Flutter Frequency from NASTRAN Aeroelasticity Module and Experiment[25].

	NASTRAN	**Experiment[25]**
Flutter speed (m/s)	302.1	296.7
Flutter frequency(Hz)	16.02	16.09

As can be seen in the table above, the results obtained using PATRAN/NASTRAN and the results of the experiment are very close. This proves that NASTRAN commercial software using double lattice method gives reliable results.

4.4 Comparison of finite Elements Based 3D Flutter Analysis With Analytical 3D Flutter Analysis

In this section, we will compare the flutter speeds obtained by using the PATRAN/NASTRAN commercial program with the flutter speeds found by using the mode shape and frequency data obtained from different modal analysis methods in 3D analytical flutter analysis. In the previous section, we used the PATRAN / NASTRAN commercial program to calculate the flutter speed of the Agard 445.6 wing and it was found to be perfectly close to the test results. The flutter speed of uniform beam and double tapered beam structures will be calculated and the speeds obtained from these different methods will be compared. As a result of these comparisons, MATLAB codes will be validated for the developed 3D analytical flutter analysis. The different cases where these comparisons are made are given below.

4.4.1 Case 1

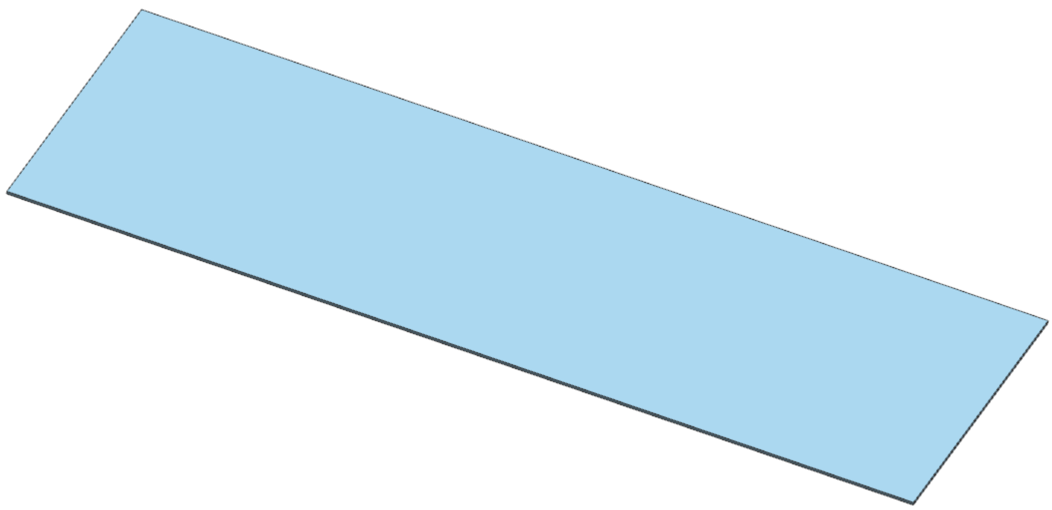

Figure 4.23 : Uniform beam.

In this case, uncoupled bending frequency, uncoupled torsion frequency, bending mode shape function and torsion mode shape function required for 3D analytical flutter analysis will be found in 3 different methods described in previous sections. Using these methods in equations 3.55 and 3.56, flutter speed will be calculated. Finally, using the PATRAN / NASTRAN commercial analysis program, flutter analysis of the uniform beam will be performed and the result will be compared with the results of 3 different analytical flutter analysis. The uniform beam structure consists of aluminum and the material properties are given below.

$$\begin{aligned}
E(\text{elasticity modulus}) &= 70 \times 10^{9}\ Pa,\\
\nu(\text{poisson ratio}) &= 0.35,\\
G(\text{shear modulus}) &= \frac{E}{2(1+\nu)} = 25925925925.9259\ Pa,\\
\rho(\text{density}) &= 2700\ kg/m^{3}
\end{aligned}$$

Sizes of the uniform beam are given in figure 4.24 and figure 4.25.

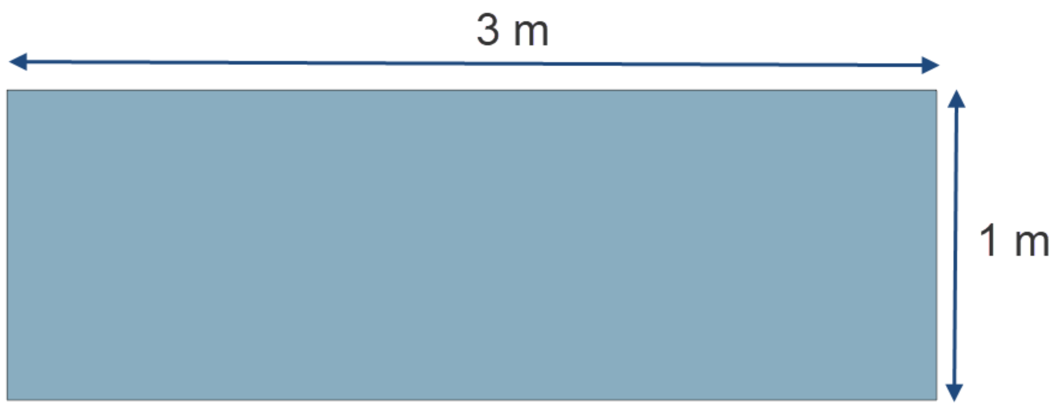

Figure 4.24 : Top view of uniform beam.

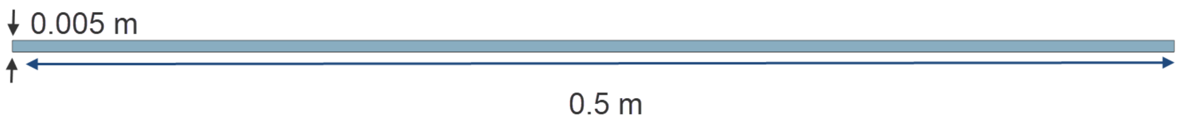

Figure 4.25 : Rectangular cross section of uniform beam.

Static unbalance parameter (x_{α}) is 0 because the beam has symmetrical cross-section.

4.4.1.1 Modal Analysis by Using Concentrated Mass Systems

Modal analysis of the uniform beam shown above will be performed using the concentrated mass system method. The uniform beam structure is divided into 10 different parts of the same length. Then the mass matrix and the influence coefficient matrix are found using the generated MATLAB code. Then, using equation 4.36, uncoupled bending frequency (w_w), uncoupled torsion frequency (w_θ), bending mode shape function (f_w) and torsion mode shape function (f_θ) are found. These values we find as a result of modal analysis are given below.

$w_w = 5.7954$ rad/sn.

$w_\theta = 32.2409$ rad/sn.

$f_w = 0,002617(y^*)^4 - 0,0443(y^*)^3 + 0,2401(y^*)^2 - 0,006866(y^*) - 0,001169$

$f_\theta = 0,0022054(y^*)^4 - 0,02994(y^*)^3 + 0,00684(y^*)^2 + 0,5265(y^*) + 5,9425 \times 10^{-4}$

Finally, using the equation 3.66, the flutter speed is obtained. All these steps were done using the MATLAB code. The U-g graph that gives the flutter speed of the uniform beam structure, which we analyze by using the concentrated mass system, is given in figure 4.26 and figure 4.27.

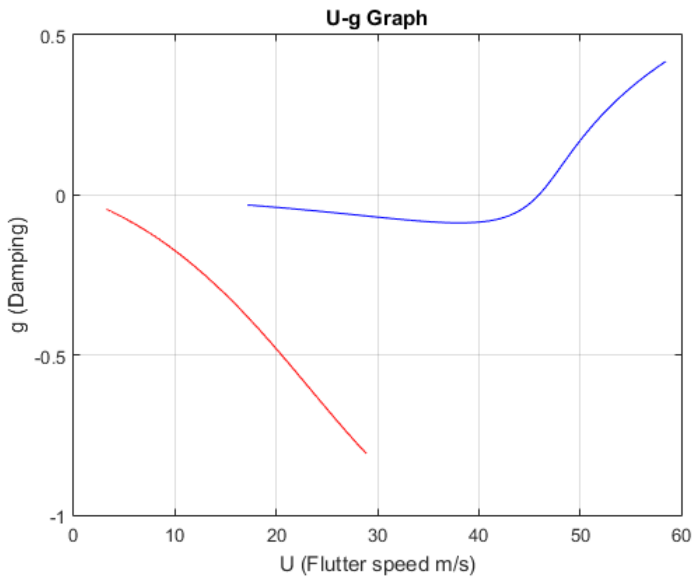

Figure 4.26 : U-g graphic of uniform beam.

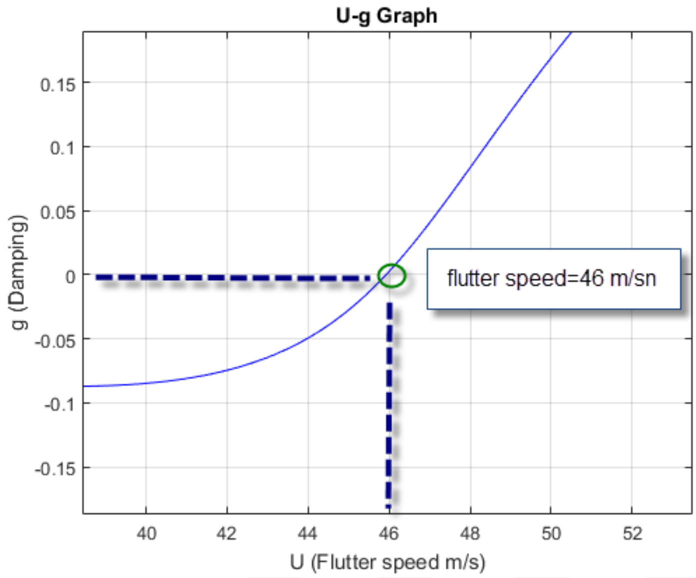

Figure 4.27 : Flutter speed of uniform beam.

4.4.1.2 Modal Analysis by Using Timoshenko's Beam Theory

Modal analysis of the uniform beam shown above will be performed using the Timoshenko's beam theory. The uniform beam structure is divided into 200 different parts of the same length. Then the mass matrix and the stiffness matrix are found using the generated MATLAB code. Then, uncoupled bending frequency (w_w), uncoupled torsion frequency (w_θ), bending mode shape function (f_w) and torsion mode shape function (f_θ) are found. These values we find as a result of modal analysis are given below.

$w_w = 5.7422$ rad/sn.

$w_\theta = 35.9840$ rad/sn.

$f_w = 0,18206(y^*)^4 - 1,01273(y^*)^3 + 1,8422(y^*)^2 - 0,01247(y^*) + 4,1307 \times 10^{-4}$

$f_\theta = 2,3479(y^*)^4 - 4,2898(y^*)^3 + 1,326(y^*)^2 + 1,6377(y^*) + 0,002941$

Using the equation 3.66, the flutter speed is obtained. All these steps were done using the MATLAB code. The U-g graph that gives the flutter speed of the uniform beam structure, which we analyze by using the Timoshenko's beam theory, is given in figure 4.28 and figure 4.29.

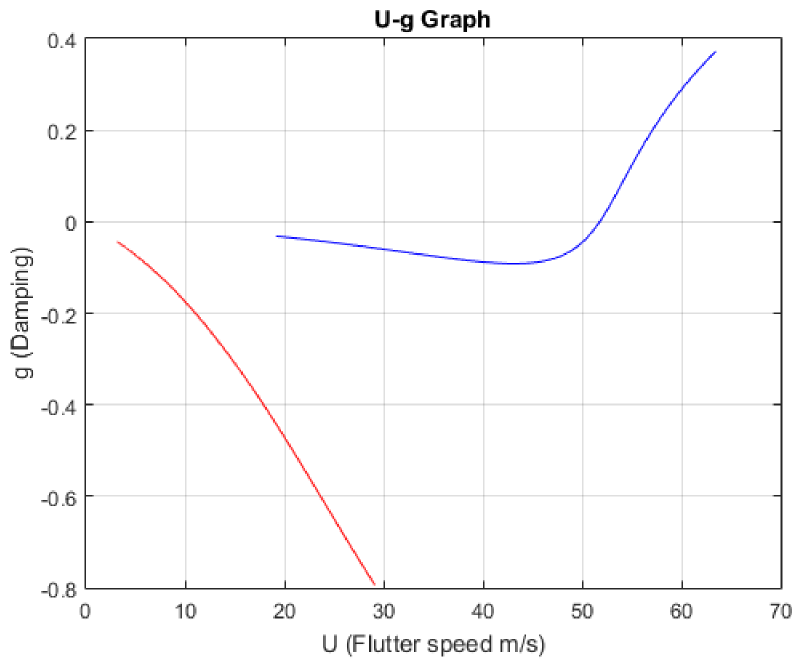

Figure 4.28 : U-g graphic of uniform beam.

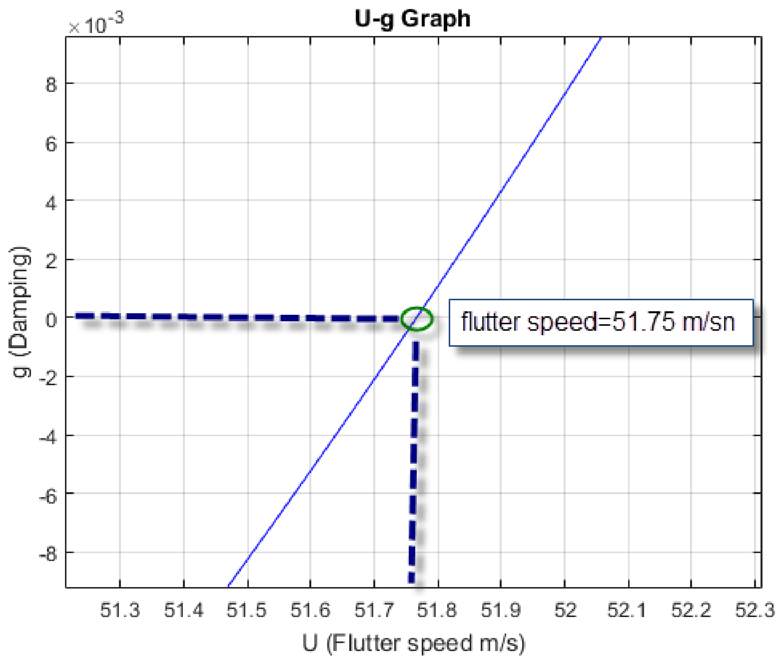

Figure 4.29 : Flutter speed of uniform beam.

4.4.1.3 Modal Analysis by Using Euler-Bernoulli Beam Theory

Modal analysis of the uniform beam shown above will be performed using the Euler-Bernoulli beam theory. The uniform beam structure is divided into 200 different parts of the same length. Then the mass matrix and the stiffness matrix are found using the generated MATLAB code. Then, uncoupled bending frequency (w_w), uncoupled torsion frequency (w_θ), bending mode shape function (f_w) and torsion mode shape function (f_θ) are found. These values we find as a result of modal analysis are given.

$$w_w = 5.8219 \text{ rad/sn.}$$

$$w_\theta = 35.8737 \text{ rad/sn.}$$

$$f_w = 0,18742(y^*)^4 - 1,02669(y^*)^3 + 1,8512(y^*)^2 - 0,01284(y^*) + 4,24723 \times 10^{-4}$$

$$f_\theta = 0,1764(y^*)^4 - 0,7937(y^*)^3 + 0,053022(y^*)^2 + 1,56382(y^*) + 2,3239 \times 10^{-4}$$

Finally, using the equation 3.66, the flutter speed is obtained. All these steps were done using the MATLAB code. The U-g graph that gives the flutter speed of the uniform beam structure, which we analyze by using the Euler-Bernoulli beam theory, is given in figure 4.30 and figure 4.31.

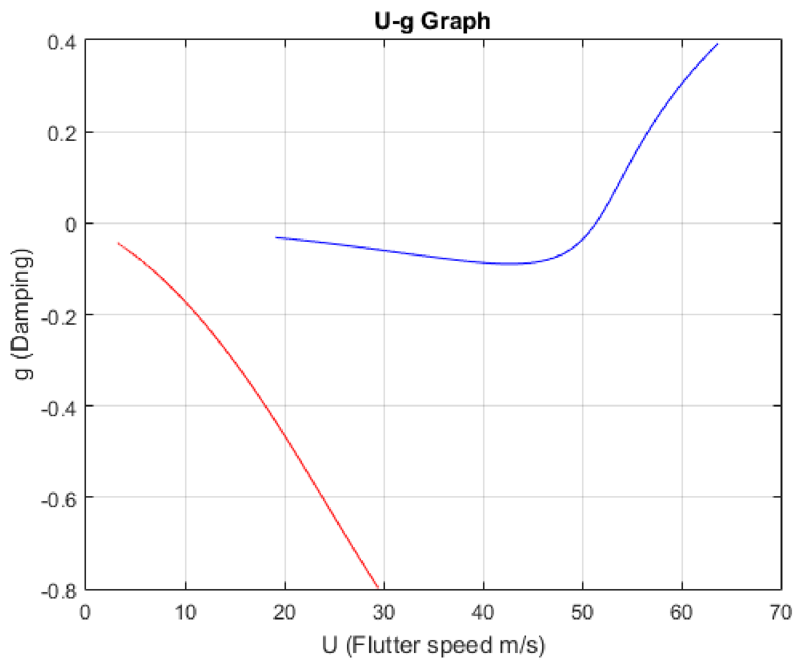

Figure 4.30 : U-g graphic of uniform beam.

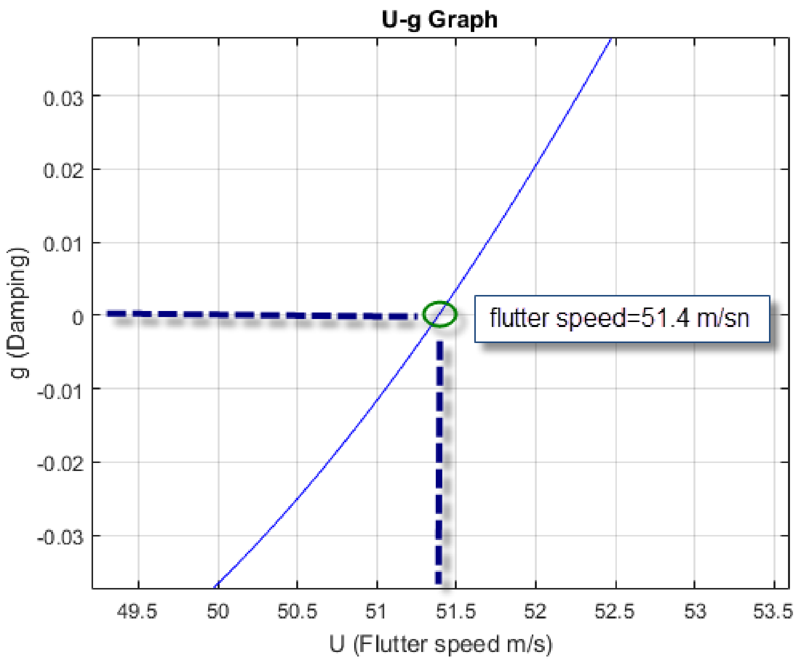

Figure 4.31 : Flutter speed of uniform beam.

4.4.1.4 Modal Analysis by Using MSC PATRAN/NASTRAN

The aeroelastic analysis of the uniform beam structure has been done using the commercial program MSC PATRAN / NASTRAN. As mentioned earlier in this commercial software program, aerodynamic loads are calculated using the double lattice method. Uniform beam structure is modeled using the finite element method for use in analysis. This model is created by using meshnig tool in MSC PATRAN / NASTRAN program. FEM model consists of TET10 solid mesh elements. The FEM model created using the geometry of the uniform beam is shown in the figure 4.32.

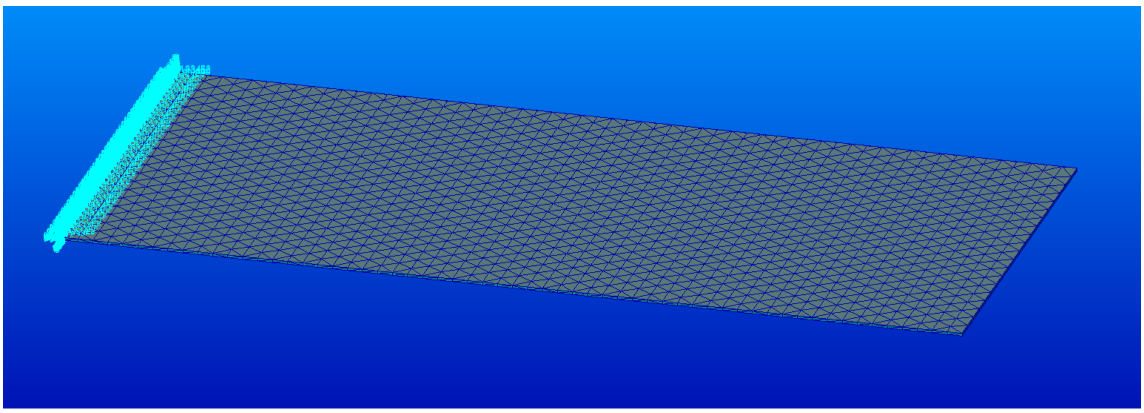

Figure 4.32 : FEM model of uniform beam.

This FEM model is fixed from the root of the uniform beam at 6 degrees of freedom and solved in MSC NASTRAN modal analysis solver, and first bending frequency, first torsion frequency, pure bending mode shape and pure torsion mode shapes are obtained. MSC NASTRAN modal analysis results are given in the figures 4.33 and 4.34.

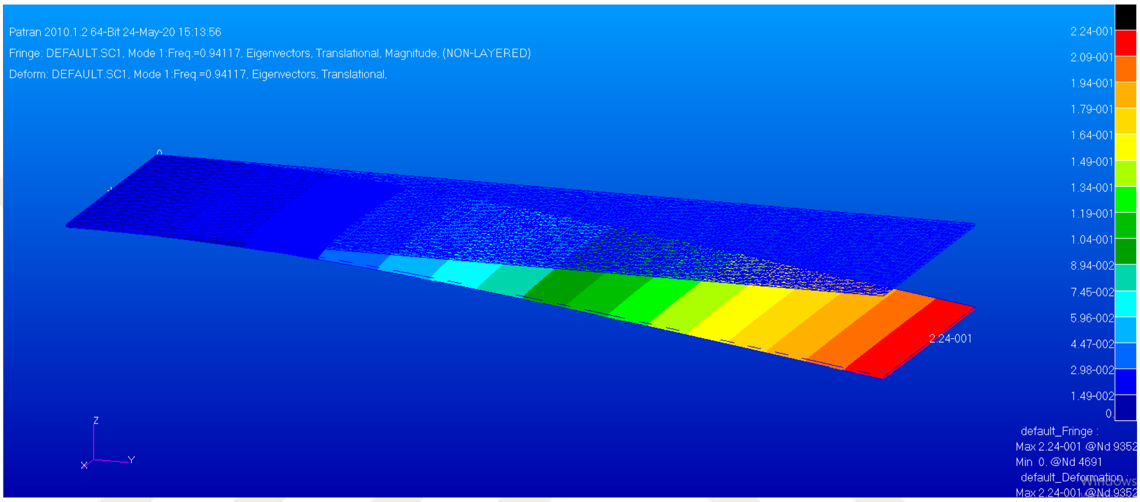

Figure 4.33 : First bending mode shape of uniform beam.

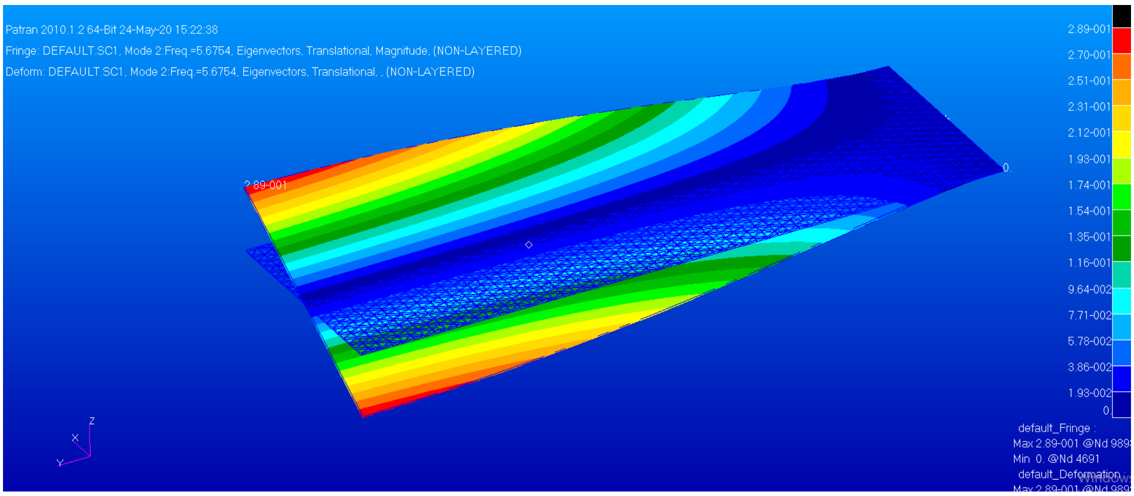

Figure 4.34 : First torsion mode shape of uniform beam.

First bending natural frequency and first torsion natural frequency from MSC NASTRAN:

$$w_w = 0.94117 \text{ Hz} = 5.9135 \text{ rad/sn.}$$

$$w_\theta = 5.6754 \text{ Hz} = 35.6595 \text{ rad/sn.}$$

Aeroelastic analysis of uniform beam structure shown in Figure 4.23 was performed in MSC FlightLoads and Dynamics Module. In this module, a flat plate aerodynamic model has been created. lifting surface has been created and this lifting surface is meshed. Splines were created between the previously created FEM model and the mesh elements created on the lifting surface. In addition, Mach number-reduced frequency pairs were created. P-k method was chosen as the analysis method in MSC FlightLoads and Dynamics Module. result datas given in figure 4.35 are obtained in the final report given at the end of the analysis in MSC®FlightLoads and Dynamics Module.

KFREQ	1./KFREQ	VELOCITY	DAMPING	FREQUENCY	COMPLEX	EIGENVALUE
3.5498	2.8170460E-01	5.0000000E+00	-3.5665494E-03	5.6497102E+00	-6.3303001E-02	3.5498177E+01
1.7606	5.6797719E-01	1.0000000E+01	-1.3581536E-02	5.6042719E+00	-2.3912114E-01	3.5212681E+01
1.1602	8.6189342E-01	1.5000000E+01	-2.3877064E-02	5.5397196E+00	-4.1554552E-01	3.4807087E+01
0.8569	1.1669871E+00	2.0000000E+01	-3.4315117E-02	5.4552426E+00	-5.8809763E-01	3.4276302E+01
0.6715	1.4891347E+00	2.5000000E+01	-4.5777608E-02	5.3438735E+00	-7.6852703E-01	3.3576550E+01
0.5447	1.8360257E+00	3.0000000E+01	-5.8315597E-02	5.2010689E+00	-9.5285583E-01	3.2679279E+01
0.4508	2.2182567E+00	3.5000000E+01	-7.1601763E-02	5.0223427E+00	-1.1297437E+00	3.1556311E+01
0.3771	2.6515799E+00	4.0000000E+01	-8.4805131E-02	4.8018146E+00	-1.2793148E+00	3.0170692E+01
0.3163	3.1611123E+00	4.5000000E+01	-9.6420921E-02	4.5312986E+00	-1.3725996E+00	2.8470991E+01
0.2639	3.7889717E+00	5.0000000E+01	-1.0125787E-01	4.2004786E+00	-1.3362184E+00	2.6392385E+01
0.2171	4.6071987E+00	5.5000000E+01	-8.4386110E-02	3.7999322E+00	-1.0073879E+00	2.3875679E+01
0.1749	5.7161946E+00	6.0000000E+01	-8.2102418E-03	3.3411372E+00	-8.6178742E-02	2.0992985E+01
0.1405	7.1150088E+00	6.5000000E+01	1.7669740E-01	2.9079573E+00	1.6142398E+00	1.8271235E+01
0.1154	8.6688414E+00	7.0000000E+01	4.4223794E-01	2.5703194E+00	3.5710258E+00	1.6149794E+01
0.0955	1.0466882E+01	7.5000000E+01	7.4433732E-01	2.2808359E+00	5.3335171E+00	1.4330914E+01
0.0780	1.2825094E+01	8.0000000E+01	1.0979669E+00	1.9855441E+00	6.8488665E+00	1.2475542E+01
0.0606	1.6494602E+01	8.5000000E+01	1.5767974E+00	1.6403147E+00	8.1255531E+00	1.0306401E+01
0.0405	2.4676041E+01	9.0000000E+01	2.4873090E+00	1.1609596E+00	9.0718679E+00	7.2945247E+00
0.0000	9.9999996E+24	9.5000000E+01	2.0016289E-01	0.0000000E+00	1.3180386E+01	0.0000000E+00
0.0000	9.9999996E+24	1.0000000E+02	2.7777433E-01	0.0000000E+00	1.9253649E+01	0.0000000E+00

Figure 4.35 : Result datas from MSC FlightLoads and Dynamics Module.

The velocity value that corresponds to the zero value where the damping value takes from the negative value to the positive value gives the flutter speed. If the U-g graph is drawn from these result values, the flutter speed is found more comfortable. U-g graphic is given in figure 4.36 and figure 4.37.

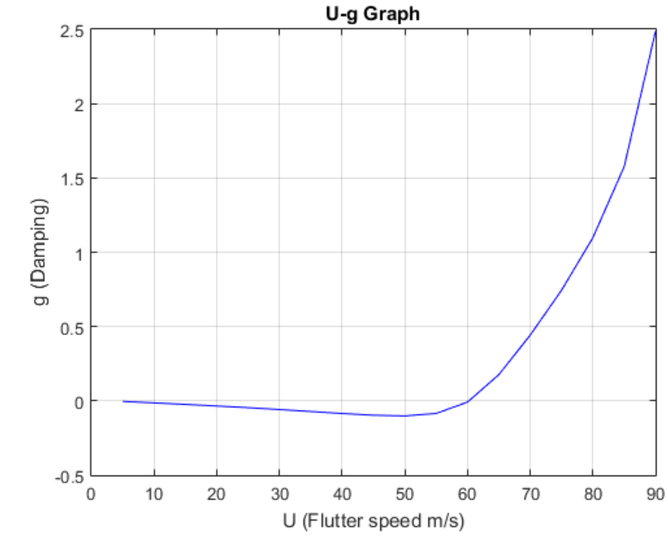

Figure 4.36 : U-g graph created by datas from MSC FlightLoads and Dynamics Module.

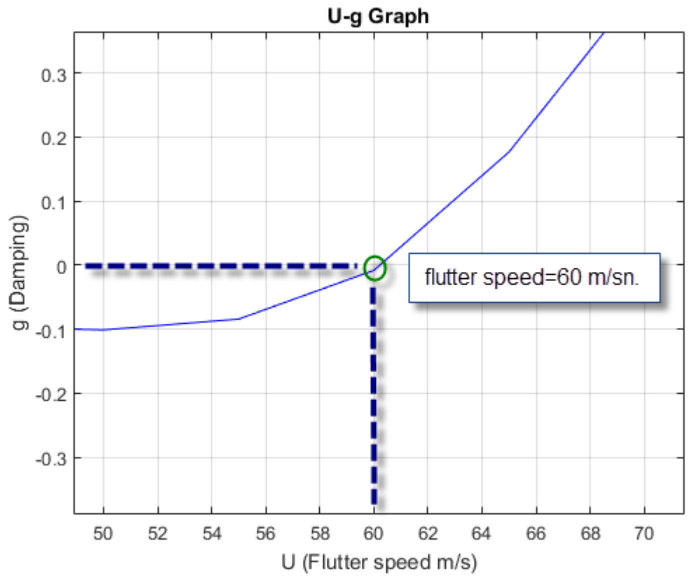

Figure 4.37 : U-g graph created by datas from MSC FlightLoads and Dynamics Module.

4.4.2 Case 2

In this case,In this case, the steps for case 1 will be applied in the same way, but this time our model is not uniform beam but taper beam. uncoupled bending frequency, uncoupled torsion frequency, bending mode shape function and torsion mode shape function required for 3D analytical flutter analysis will be found in 3 different methods described in previous sections. Using these methods in equations 3.55 and 3.56,

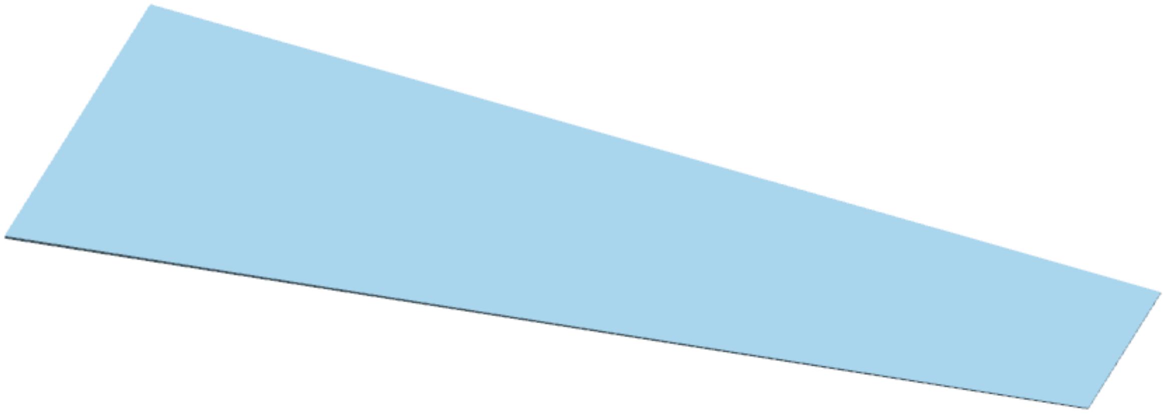

Figure 4.38 : Double tapered beam

flutter speed will be calculated. Finally, using the PATRAN / NASTRAN commercial analysis program, flutter analysis of the tapered beam will be performed and the result will be compared with the results of 3 different analytical flutter analysis. The double tapered beam structure consists of aluminum as like case 1 so the material properties are same.

Sizes of the double tapered beam are given in figure 4.38, figure 4.39, and figure 4.41.

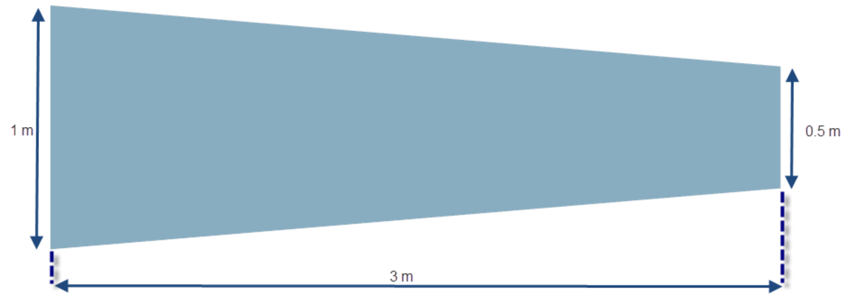

Figure 4.39 : Top view of double tapered beam.

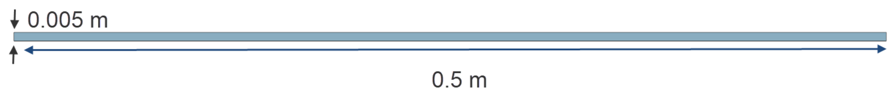

Figure 4.40 : Rectangular tip cross section of double tapered beam.

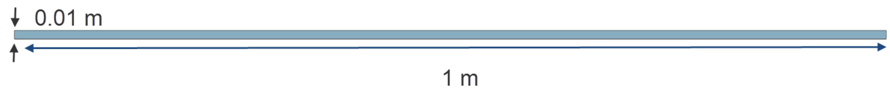

Figure 4.41 : Rectangular root cross section of double tapered beam.

Static unbalance parameter (x_α) is 0 because the beam has symmetrical cross-section.

4.4.2.1 Modal Analysis by Using Concentrated Mass Systems

Modal analysis of the double tapered beam shown above will be performed using the concentrated mass system method. The double tapered beam structure is divided into 10 different parts of the same length. Then the mass matrix and the influence coefficient matrix are found using the generated MATLAB code. Then, using equation 4.36, uncoupled bending frequency (w_w), uncoupled torsion frequency (w_θ), bending mode shape function (f_w) and torsion mode shape function (f_θ) are found. These values we find as a result of modal analysis are given below.

$w_w = 7.6707$ rad/sn.

$w_\theta = 51.7801$ rad/sn.

$f_w = -0,0071803(y^*)^4 + 0,02461(y^*)^3 + 0,121124(y^*)^2 + 0,01015(y^*) - 0,0016462$

$f_\theta = -0,005037(y^*)^4 - 0,00943(y^*)^3 + 0,09797(y^*)^2 + 0,27486(y^*) + 6,1549 \times 10^{-4}$

where;

$$y^* = \frac{y}{l} \qquad \text{which is the reduced spanwise variable}$$

Finally, using the equation 3.66, the flutter speed is obtained. All these steps were done using the MATLAB code. The U-g graph that gives the flutter speed of the double tapered beam structure, which we analyze by using the concentrated mass system, is given in figure 4.42 and figure 4.43.

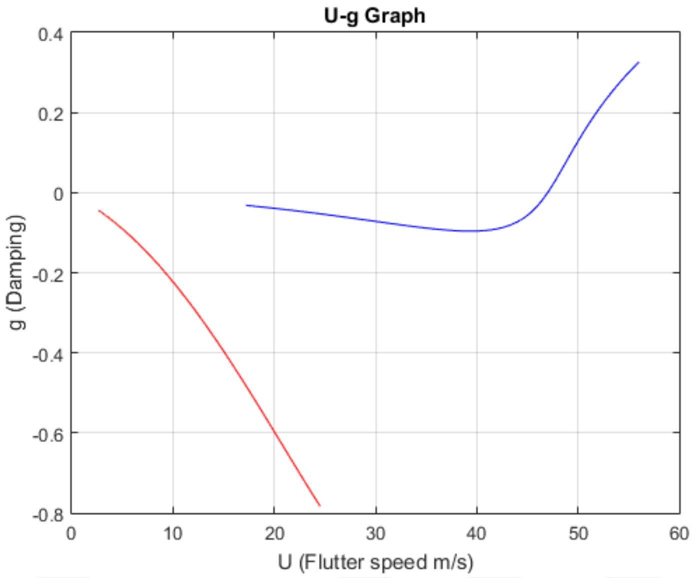

Figure 4.42 : U-g graphic of double tapered beam.

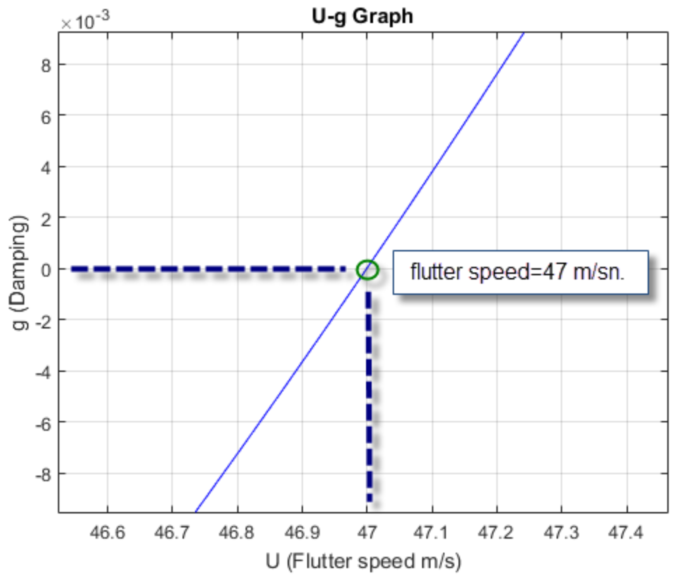

Figure 4.43 : Flutter speed of double tapered beam.

4.4.2.2 Modal Analysis by Using Timoshenko's Beam Theory

Modal analysis of the double tapered beam shown above will be performed using the Timoshenko's beam theory. The double tapered beam structure is divided into 200 different parts of the same length. Then the mass matrix and the stiffness matrix are found using the generated MATLAB code. Then, uncoupled bending frequency (w_w), uncoupled torsion frequency (w_θ), bending mode shape function (f_w) and torsion mode shape function (f_θ) are found. These values we find as a result of modal analysis are given below.

$w_w = 7.5535$ rad/sn.

$w_\theta = 52.0238$ rad/sn.

$f_w = -0,43007(y^*)^4 + 0,47582(y^*)^3 + 0,94248(y^*)^2 + 0,01187(y^*) - 3,31658 \times 10^{-4}$

$f_\theta = -0,643425(y^*)^4 + 0,16807(y^*)^3 + 0,6467(y^*)^2 + 0,83106(y^*) + 8,935 \times 10^{-4}$

Finally, using the equation 3.66, the flutter speed is obtained. All these steps were done using the MATLAB code. The U-g graph that gives the flutter speed of the double tapered beam structure, which we analyze by using the Timoshenko's beam theory, is given in figure 4.44 and figure 4.45.

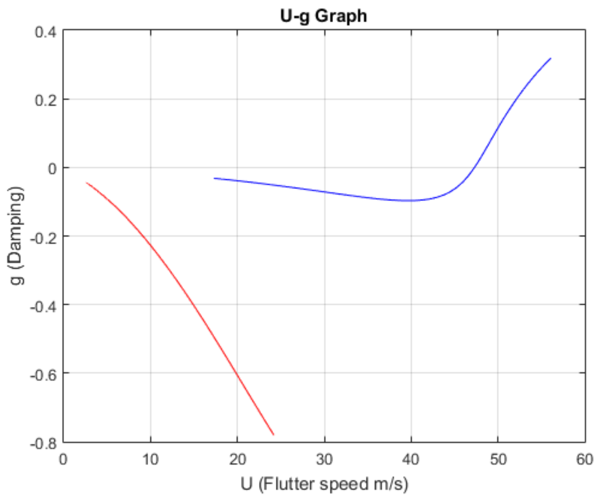

Figure 4.44 : U-g graphic of double tapered beam.

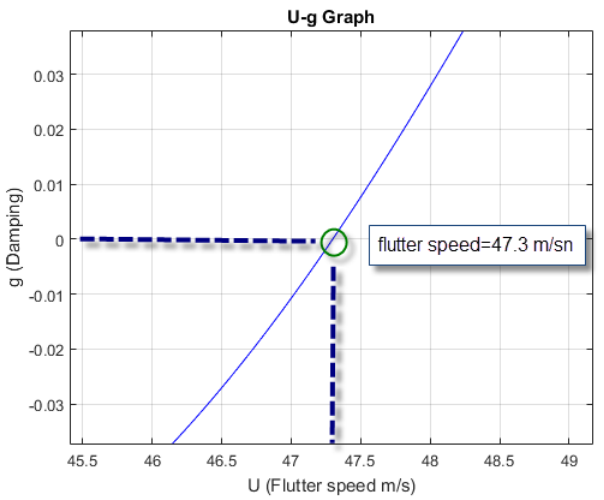

Figure 4.45 : Flutter speed of double tapered beam.

4.4.2.3 Modal Analysis by Using Euler-Bernoulli Beam Theory

Modal analysis of the double tapered beam shown above will be performed using the Euler-Bernoulli beam theory. The double tapered beam structure is divided into 200 different parts of the same length. Then the mass matrix and the stiffness matrix are found using the generated MATLAB code. Then, uncoupled bending frequency (w_w), uncoupled torsion frequency (w_θ), bending mode shape function (f_w) and torsion mode shape function (f_θ) are found. These values we find as a result of modal analysis are given below.

$w_w = 7.5159$ rad/sn.

$w_\theta = 52.0227$ rad/sn.

$f_w = -0,432057(y^*)^4 + 0,48315(y^*)^3 + 0,93662(y^*)^2 + 0,01245(y^*) - 3,53144 \times 10^{-4}$

$f_\theta = -0,6435(y^*)^4 + 0,16836(y^*)^3 + 0,64653(y^*)^2 + 0,83104(y^*) + 8,9441 \times 10^{-4}$

Finally, using the equation 3.66, the flutter speed is obtained. All these steps were done using the MATLAB code. The U-g graph that gives the flutter speed of the double tapered beam structure, which we analyze by using the Euler-Bernoulli beam theory, is given in figure 4.46 and figure 4.47.

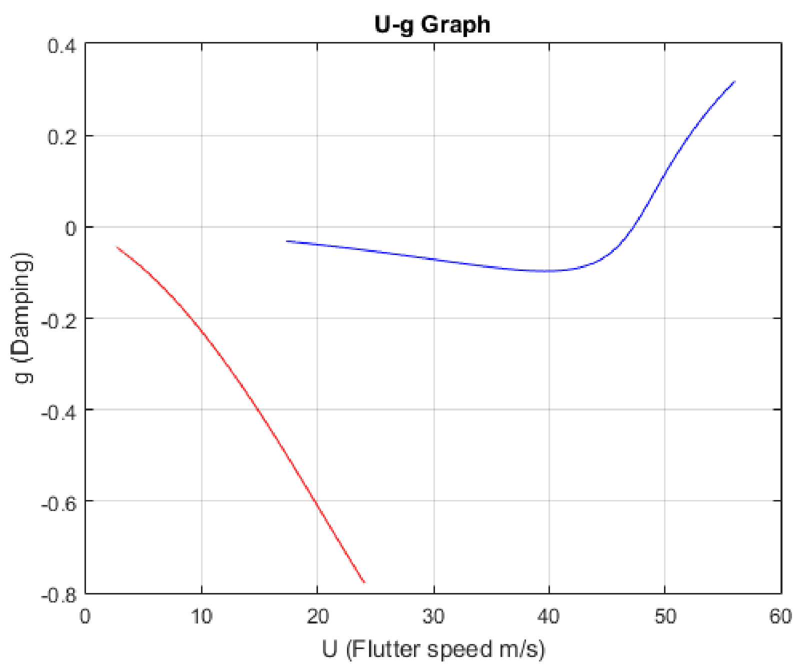

Figure 4.46 : U-g graphic of double tapered beam.

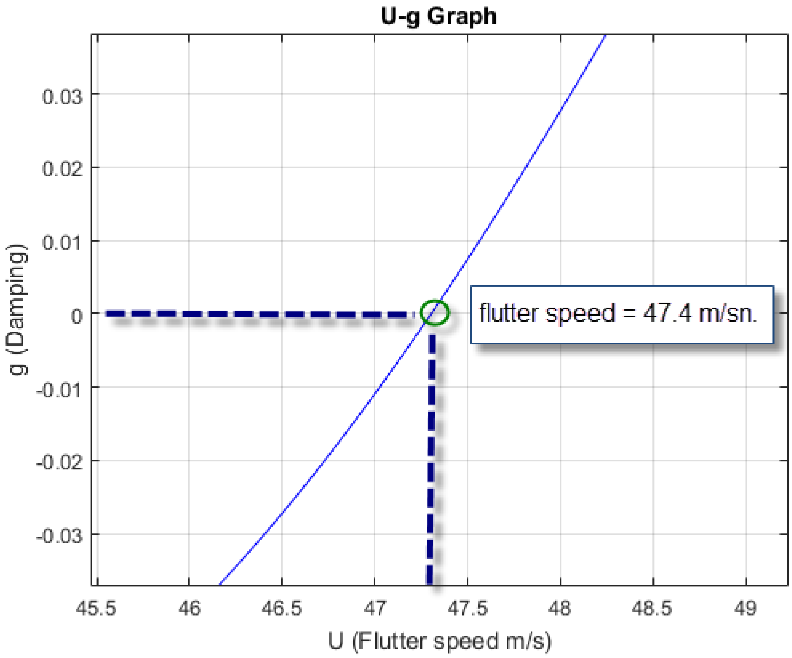

Figure 4.47 : Flutter speed of double tapered beam.

4.4.2.4 Modal Analysis by Using MSC PATRAN/NASTRAN

The aeroelastic analysis of the double tapered beam structure has been done using the commercial program MSC PATRAN / NASTRAN. Double tapered beam structure is modeled using the finite element method for use in analysis. This model is created by using meshnig tool in MSC PATRAN / NASTRAN program. FEM model consists of TET10 solid mesh elements. The FEM model created using the geometry of the double tapered beam is shown in the figure 4.48.

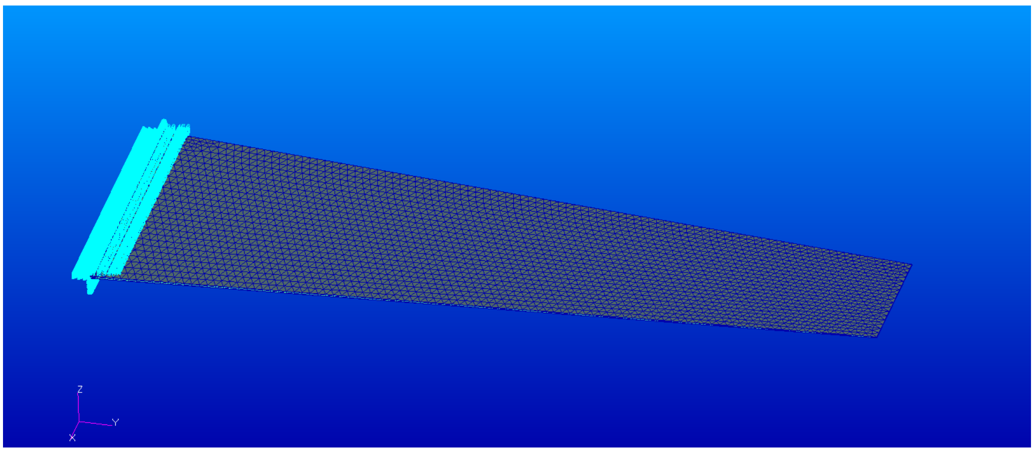

Figure 4.48 : FEM model of double tapered beam.

This FEM model is fixed from the root of the double tapered beam at 6 degrees of freedom and solved in MSC NASTRAN modal analysis solver, and first bending frequency, first torsion frequency, pure bending mode shape and pure torsion mode shapes are obtained. MSC NASTRAN modal analysis results are given in the figures 4.49 and 4.50.

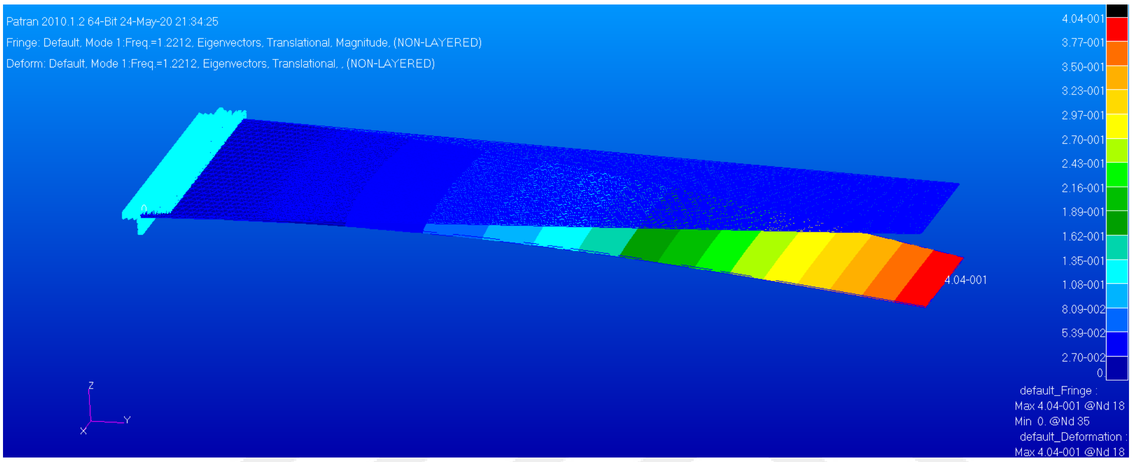

Figure 4.49 : First bending mode shape of double tapered beam.

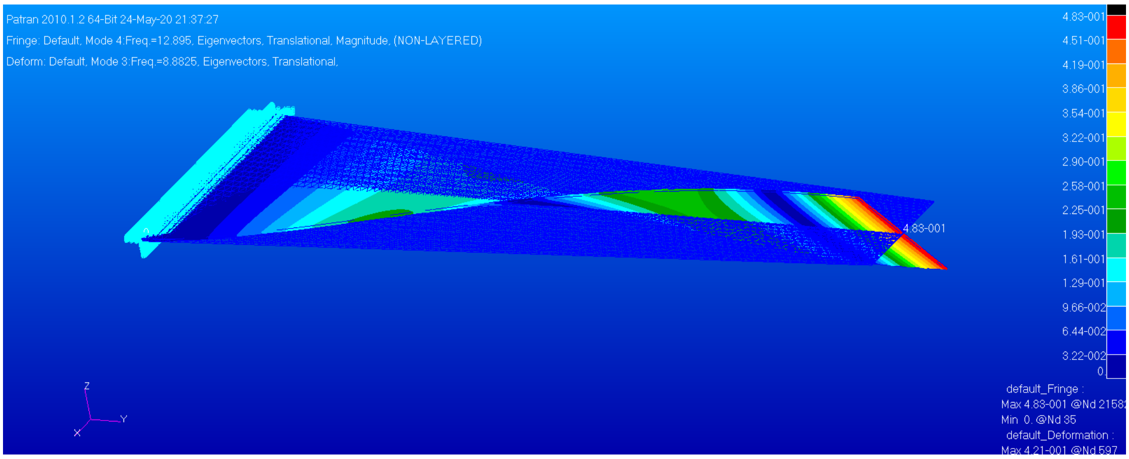

Figure 4.50 : First torsion mode shape of double tapered beam.

First bending natural frequency and first torsion natural frequency from MSC NASTRAN:

$$w_w = 1.2212 \text{ Hz} = 7.6730 \text{ rad/sn.}$$

$$w_\theta = 8.8825 \text{ Hz} = 55.8103 \text{ rad/sn.}$$

Aeroelastic analysis of double tapered beam structure shown in Figure 4.38 was performed in MSC FlightLoads and Dynamics Module. In this module, a flat plate aerodynamic model has been created. lifting surface has been created and this lifting surface is meshed. Splines were created between the previously created FEM model and the mesh elements created on the lifting surface. In addition, Mach number-reduced frequency pairs were created. P-k method was chosen as the analysis method in MSC FlightLoads and Dynamics Module. result datas given in figure 4.51 are obtained in the final report given at the end of the analysis in MSC FlightLoads and Dynamics Module.

KFREQ	1./KFREQ	VELOCITY	DAMPING	FREQUENCY	COMPLEX	EIGENVALUE
3.4718	2.8803542E-01	5.0000000E+00	-2.8472359E-03	8.8408537E+00	-7.9080164E-02	5.5548725E+01
1.7216	5.8084607E-01	1.0000000E+01	-1.3354203E-02	8.7681713E+00	-3.6785519E-01	5.5092049E+01
1.1341	8.8179100E-01	1.5000000E+01	-2.3576850E-02	8.6635456E+00	-6.4169896E-01	5.4434666E+01
0.8368	1.1949887E+00	2.0000000E+01	-3.3411097E-02	8.5238600E+00	-8.9469892E-01	5.3556992E+01
0.6547	1.5273370E+00	2.5000000E+01	-4.3945063E-02	8.3363371E+00	-1.1508937E+00	5.2378750E+01
0.5297	1.8878584E+00	3.0000000E+01	-5.4999910E-02	8.0932312E+00	-1.3984077E+00	5.0851273E+01
0.4368	2.2893889E+00	3.5000000E+01	-6.5455601E-02	7.7860742E+00	-1.6010880E+00	4.8921349E+01
0.3635	2.7512956E+00	4.0000000E+01	-7.3117822E-02	7.4044504E+00	-1.7008498E+00	4.6523537E+01
0.3027	3.3037045E+00	4.5000000E+01	-7.2083928E-02	6.9371552E+00	-1.5709766E+00	4.3587433E+01
0.2509	3.9859202E+00	5.0000000E+01	-4.7134034E-02	6.3886857E+00	-9.4601059E-01	4.0141296E+01
0.2087	4.7926655E+00	5.5000000E+01	1.7293151E-02	5.8446116E+00	3.1752628E-01	3.6722778E+01
0.1736	5.7609682E+00	6.0000000E+01	6.0181480E-02	5.3042727E+00	1.0028560E+00	3.3327728E+01
0.1336	7.4845786E+00	6.5000000E+01	2.8822896E-01	4.4229913E+00	4.0050097E+00	2.7790474E+01
0.1119	8.9366703E+00	7.0000000E+01	5.8634418E-01	3.9892604E+00	7.3484359E+00	2.5065264E+01
0.0942	1.0615358E+01	7.5000000E+01	8.9667088E-01	3.5982940E+00	1.0136304E+01	2.2608749E+01
0.0783	1.2772102E+01	8.0000000E+01	1.2527521E+00	3.1900516E+00	1.2554884E+01	2.0043686E+01
0.0629	1.5894870E+01	8.5000000E+01	1.7154205E+00	2.7235293E+00	1.4677515E+01	1.7112440E+01
0.0467	2.1414152E+01	9.0000000E+01	2.4552646E+00	2.1404827E+00	1.6510489E+01	1.3449050E+01
0.0261	3.8372292E+01	9.5000000E+01	4.5407820E+00	1.2608864E+00	1.7986908E+01	7.9223833E+00
0.0000	9.9999996E+24	1.0000000E+02	2.4377446E-01	0.0000000E+00	2.7035172E+01	0.0000000E+00

Figure 4.51 : Result datas from MSC FlightLoads and Dynamics Module.

The velocity value that corresponds to the zero value where the damping value takes from the negative value to the positive value gives the flutter speed. If the U-g graph is drawn from these result values, the flutter speed is found more comfortable. U-g graphic is given in figure 4.52, and figure 4.53.

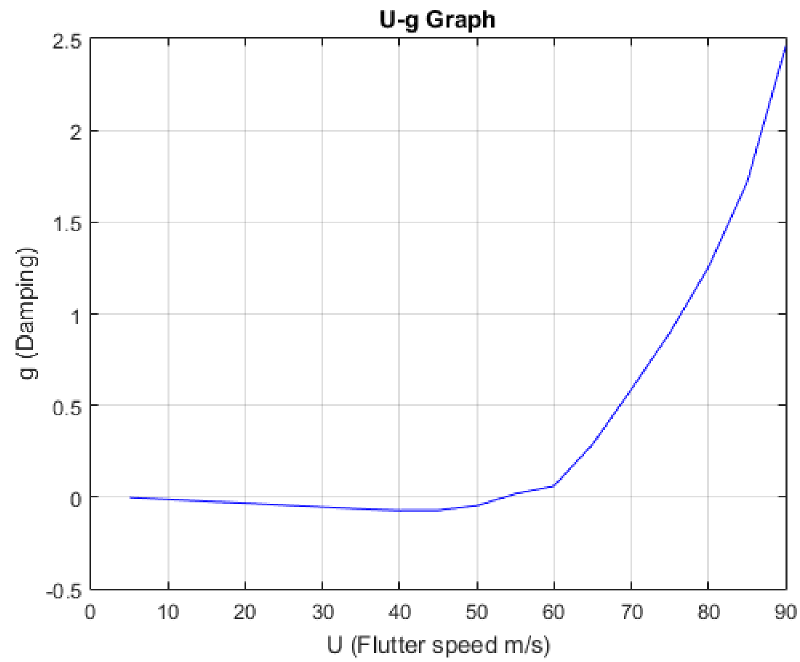

Figure 4.52 : U-g graph created by datas from MSC FlightLoads and Dynamics Module.

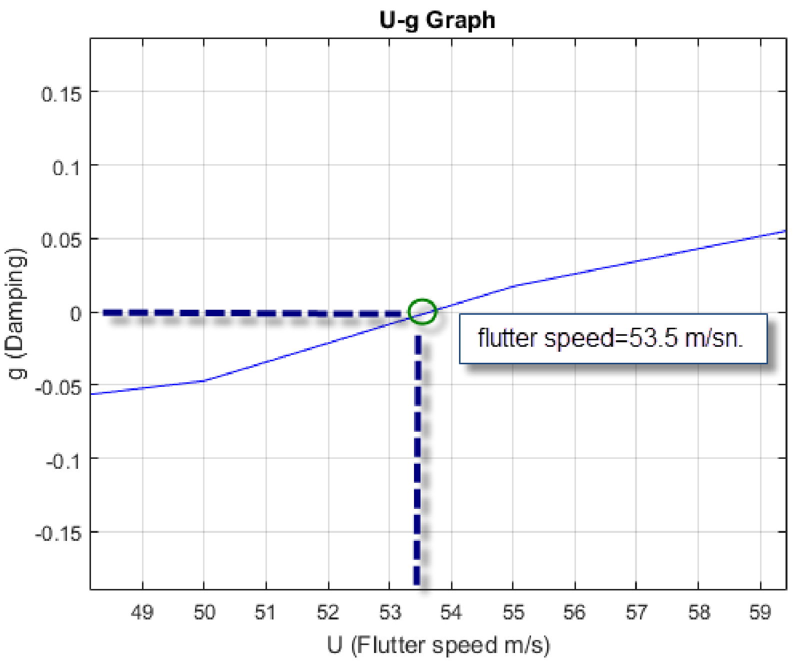

Figure 4.53 : U-g graph created by datas from MSC FlightLoads and Dynamics Module.

4.5 Conclusion

Three different methods are explained for the modal analysis of the structure, which is required to be used in the three-dimensional analytical aeroelastic analysis method. Aeroelastic analysis of the weakened AGARD 445.6 wing model was made using the MSC FlightLoads and Dynamics module and MSC NASTRAN commercial software programs. This commercial software program uses double lattice method to calculate aerodynamic loads. The results obtained by using commercial software were compared with the test results of the AGARD 445.6 wing model in the wind tunnel. The results were observed to be very close to each other. As a result, the results obtained from MSC FlightLoads and Dynamics module and MSC NASTRAN commercial software program have been proved to be consistent with real results. Different modal analysis methods are applied on the structure with a constant cross section and the structure where both the height and width of the cross section change with linear ratio. These data are used in MATLAB codes developed for three-dimensional aeroelastic analysis and the flutter speeds of these two different structures were obtained. By using MSC FlightLoads and Dynamics module and MSC NASTRAN commercial software program, the flutter speeds of these two different structures were obtained. The results obtained from MATLAB codes and the commercial software program were compared. As a result of the comparison, it was observed that the flutter speeds obtained from MATLAB codes were lower than the flutter speeds obtained from commercial software. As a result, it was seen that the MATLAB code using the standard strip theory gives more conservative results than the real values. Flutter speed results obtained by using the mode analysis results made by using Euler-Bernoulli beam theory and Tymoshenko beam theory in MATLAB code. These results were found to be more consistent than the results of the flutter speeds obtained by using the mode analysis results using the discrete mass system method in the MATLAB code.

5. CONCLUSIONS AND RECOMMENDATIONS

In the first stage of the thesis, a tool was prepared using the methods taken from the literature in MATLAB code to find the flutter speed of two dimensional, two degree of freedom and two dimensional, three degree of freedom structures. The purpose of these tools is to save time in advanced design processes by being used in the preliminary design phase. The results were obtained by applying these MATLAB codes prepared on the problems obtained from the literature. These results are compared with the proven results in the literature and the consistency of MATLAB codes has been proved. As a result of these operations, the flutter speed of a two-dimensional model known as cross section can be calculated. Thus, the design process can be continued reliably by calculating the flutter speed before a detailed design process.

In the second stage of the thesis, the method developed for the calculation of the flutter speed of three-dimensional structures was obtained from the literature and examined in detail at this stage of the thesis.MATLAB code has been generated using this method to calculate the flutter speed of models of different sizes from the literature. The modal analysis method used to obtain the model's natural frequency values and mode shapes were analyzed by taking the source of the literature from which we took the problem. The aerodynamic loads used in the three-dimensional flutter calculation we used in the MATLAB tool were calculated using the functions developed by Theodorsen. Standard strip theory is used in these functions of Theodorsen. In the literature resource we used for validation, two different methods were investigated to be used in the flutter calculation of the models. These methods are standard strip theory and double lattice method. These two methods are used in the calculation of aerodynamic loads. The generated MATLAB tool was applied on models of different sizes and compared with the results of the literature. However, it is understood that the results obtained from MATLAB code and the literature results using the double lattice method are different. These results proved that the developed MATLAB tool is consistent. However, the effect of the methods used in the calculation of aerodynamic loads on the result of flutter speed was seriously observed.

In the last stage of the thesis, different modal analysis methods that will be integrated into the method investigated in the previous stage of the thesis are used to use in calculating the flutter speed of three-dimensional structures. Flutter speed of weakened AGARD 445.6 wing model was calculated by using MSC PATRAN / NASTRAN software, which is a commercial analysis program widely used in industry. The commercial software MSC PATRAN / NASTRAN uses the double lattice method to calculate aerodynamic loads. The results obtained from commercial software of MSC PATRAN / NASTRAN and the results of the tests performed in the wind tunnel of the same model in the literature are very close to each other. Thus, the flutter speed obtained from MSC PATRAN / NASTRAN commercial software using double lattice method has been proved to be consistent. The different modal analysis methods investigated in this section in the thesis are integrated into the MATLAB code developed for three-dimensional flutter speed calculation. For these three modal analysis methods, flutter speed was calculated on two different models. At the same time, the flutter speed of these two different models was calculated using MSC PATRAN / NASTRAN commercial software, which has been demonstrated to be consistent with actual results. Analysis results obtained using MATLAB code were compared with analysis results obtained using MSC PATRAN / NASTRAN commercial software. As a result of this comparison, it was observed that the flutter speeds obtained using the MATLAB code were lower than the flutter speeds obtained using the commercial software MSC PATRAN / NASTRAN. It was understood that the analysis made using the standard strip theory was more conservative than the double lattice method. If the results obtained by using three different modal analysis methods are compared within themselves, it was observed that the results obtained by using Timoshenko's beam theory and Euler-Bernoulli beam theory gave more realistic results than the results obtained by using discrete mass system.

REFERENCES

[1] **Wagner, H.U.** (1925). H. Uber die Entstenhung des Dynamischen Auftriebes von Tragflugeln, *Z. Angew. Math. Mech.*, *5*(1), 17–35.

[2] **Jones, R.T.**, (1940), The unsteady lift of a finite wing of finite aspect ratio (Report No. 681). Washington : National Advisory Committee for Aeronautics.

[3] **Lomax, H.**, **Heaslet, F.B. and Sluder, L.**, (1952), Two and Three Dimensional Unsteady Lift Problems in High Speed Flight(Report No. 1077).Washington : National Advisory Committee for Aeronautics.

[4] **Theodorsen, T.**, (1934), General Theory of Aerodynamic Instability and the Mechanism of Flutter(Report No. 496).Washington : National Advisory Committee for Aeronautics.

[5] **Watkins, C.E., W.D. and Cunningham, H.**, (1959), A Systematic Kernel Function Procedure for Determining Aerodynamic Forces on Oscillating or Steady Finite Wings at Subsonic Speeds(Report No. 48).Washington : National Advisory Committee for Aeronautics.

[6] **Rowe, W. S., W.B.A. and Redman, M.C.** (1974). Unsteady Subsonic Aerodynamic Loading Caused by Control Surface Motion, *Journal of Aircraft*, *11*(1), 45–53.

[7] **Rodden, W.P. and Albano, E.** (1969). A Doublet-Lattice Method for Calculating Lift Distributions on Oscillating Surfaces in Subsonic Flows, *American Institute of Aeronautics and Astronautics*, *7*(2), 279–285.

[8] **Theodorsen, T. and Garrick, I.E.**, (1940), Mechanism of flutter a Theoretical and Experimental Investigation of The Flutter Problem (Report No. 685).Washington : National Advisory Committee for Aeronautics.

[9] **Smilg, B. and Wasserman, L.S.**, (1942), Application of Three-Dimensional Flutter Theory to Aircraft Structures, (Report No. 4798). American Air Force.

[10] **Richardson, J.** (1965). A More Realistic Method for Routine Flutter Calculations, *Symposium on Structural Dynamics and Aeroelasticity*, Boston,MA,U.S.A.

[11] **Hassig, H.J.** (1971). An Approximate True Damping Solution of the Flutter Equation by Determinant Iteration, *Journal of Aircraft*, *8*(11), 885–889.

[12] **Goland, M. and Luke, Y.L.** (1949). A Study of the Bending-Torsion Aeroelastic Modes for Aircraft Wings, *Journal of The Aeronautical Sciences*, *16*(7), 389–396.

[13] **Scanlan, R.H. and Rosenbaum, R.**, (1951). *Introduction to the Study of Aircraft Vibration and Flutter,*, The MacMillan Co, Cambridge.

[14] **Seber, G., L. and Sakarya, E.** (2009). Flutter Characteristic of A Typical Section Model With A Trailing Edge Control Surface, *5. Ankara International Aerospace Conference*, METU, Ankara - TURKEY.

[15] **Fung, Y.**, (1993). *An Introduction to the Theory of Aeroelasticity*, Dover Publications, New York.

[16] **Bryson, A.E.**, (1994). *Control of Spacecraft and Aircraft*, Princeton University Press, Princeton, New Jersey.

[17] **Myklestad, N.**, (1944). *Vibration Analysis*, McGraw-Hill Book Company, Inc.,, New York.

[18] **Goland, M. and Luke, Y.** (1945). The Flutter of a Uniform Cantilever Wing, *Journal of Applied Mechanics*, *12*(4), 197–208.

[19] **Berci, M. and Cavallaro, R.** (2018). A Hybrid Reduced-Order Model for the Aeroelastic Analysis of Flexible Subsonic Wings—A Parametric Assessment, *Aerospace*, *5*(76).

[20] **Young, W. C.; Budynas, R.G.**, (2012). *Roark's Formulas for Stress and Strain,*, McGraw-Hill,, New York, 8 edition.

[21] **Hodges, D.H. and Pierce, G.A.**, (2011). *Introduction to Structural Dynamics and Aeroelasticity*, Cambridge University Press, Cambridge, 2 edition.

[22] **Bisplinghoff, R. L., H.A. and Halfman, R.L.**, (1955). *Aeroelasticity,*, Addison-Wesley Publishing Co., Inc.,, Mineola, New York.

[23] **Palazzolo, A.B.**, (2016). *Vibration Theory and Applications with Finite Elements and Active Vibration Control,*, John Wiley Sons, Ltd,,, West Sussex, United Kingdom, 8 edition.

[24] **Cowper, G.R.** (1966). The Shear Coefficient in Timoshenko's Beam Theory, *Journal of Applied Mechanics,*, *33*(2), 335–340.

[25] **Kolonay, R.M. and Yamg, H.T.Y.** (1998). Unsteady Aeroelastic Optimization in the Transonic Regime,, *Journal of Aircraft,*, *35*(1), 60–68.

CURRICULUM VITAE

Name Surname: Bilgehan ŞEREF

Place and Date of Birth: Antalya / 15.01.1990

E-Mail: bilgehanseref@hotmail.com

EDUCATION:

- **B.Sc.:** 2015, ITU, Faculty of Aeronautics and Astronautics, Aeronautical Engineering
- **M.Sc.:** 2020, ITU, Faculty of Aeronautics and Astronautics, Aeronautical and Astronautical Engineering Programme

PROFESSIONAL EXPERIENCE AND REWARDS:

- Structural Analysts in Turkish Aerospace Industries (Started in May 2018)